AFOSR-TR- 93 0692

FIRST ANNUAL TECHNICAL REPORT FOR THE PROJECT

"Development of a Technique to Determine the Morphology and Dynamics of Agglomerates in Chemically Reacting Flows"

Submitted to the

DEPARTMENT OF THE AIR FORCE
AIR FORCE OFFICE OF SCIENTIFIC RESEARCH

Project Manager: Dr. Julian Tishkoff

Grant No: F49620-92-J-0447

Prepared by:

Dr. T. Charalampopoulos
Associate Professor of Mechanical Engineering
Mechanical Engineering
LSU, Baton Rouge, LA 70803
Tel. (504) 388-5894

CONTENTS

I. REPORT DOCUMENTATION PAGE

Form Approved
OMB No. 0704-0188

1. AGENCY USE ONLY (Leave blank)	2. REPORT DATE	3. REPORT TYPE AND DATES COVERED
	8/1/1993	1st Ann. Tech. Report 8/1/92-8/1/93

4. TITLE AND SUBTITLE (U) Development of a Technique to Determine the Morphology and Dynamics of Agglomerates in Chemically Reacting Flows

5. FUNDING NUMBERS

PE - 61102F
PR - 2308
SA - BS
G - F49620-92-J-0447

6. AUTHOR(S)

Tryfon Charalampopoulos

7. PERFORMING ORGANIZATION NAME(S) AND ADDRESS(ES)

Louisiana State University
Mechanical Engineering Department
Baton Rouge, LA 70803

8. PERFORMING ORGANIZATION REPORT NUMBER

9. SPONSORING/MONITORING AGENCY NAME(S) AND ADDRESS(ES)

AFOSR/NA
110 Duncan Avenue, Suite B115
Bolling AFB DC 20332-0001

10. SPONSORING/MONITORING AGENCY REPORT NUMBER

11. SUPPLEMENTARY NOTES

12a. DISTRIBUTION/AVAILABILITY STATEMENT

Approved for public release; distribution is unlimited

12b. DISTRIBUTION CODE

13. ABSTRACT (Maximum 200 words)

Analytical and experimental studies for the morphology and dynamics of agglomerated particulates in combustion systems were carried out. The analytical studies entailed the investigation of the validity of the approximate relations for scattering and absorption characteristics as well as predictions of the depolarized light scattering intensities for the agglomerates as functions of primary particle diameter, primary particle number density, scattering angle and optical properties of the particles. The approximate relations were found to be accurate to within 20% or better for agglomerates consisting of Rayleigh size primary particles and with optical properties typical of flame soot. It was found that the agglomerate structures encountered in typical flame systems and other agglomerates composed of metallic or dielectric spheres the reciprocity relations do not hold. Experiments were carried out utilizing latex spheres dispersions in distilled water. The results indicate that multiple scattering within the agglomerate may be the cause for the significant difference (up to 30% or more) of the depolarization ratio from the expected value of 1.0.

14. SUBJECT TERMS Soot Formation, Particle Sizing, Agglomerate Characterization, Depolarized Light Scattering, Reciprocity Relations.

15. NUMBER OF PAGES 131

16. PRICE CODE

17. SECURITY CLASSIFICATION OF REPORT	18. SECURITY CLASSIFICATION OF THIS PAGE	19. SECURITY CLASSIFICATION OF ABSTRACT	20. LIMITATION OF ABSTRACT
Unclassified	Unclassified	Unclassified	UL

II. SUMMARY OF THE RESEARCH PROGRESS FOR THE REPORTING PERIOD

Overview

Agglomerated particulate structures of variable degree of complexity occur in many environments such as combustion systems, atmospheric dispersions and colloidal dispersions to mention a few. Knowledge of the morphological characteristics of agglomerated structures in combustion systems is important for accurate prediction of radiative transfer in dense and dilute absorbing and scattering media, surface growth of particulates as well as in the quality control of material synthesis through the aerosol route. This part of the work focuses on the analytical and experimental investigation of agglomerated flame particulates utilizing the conventional absorption and scattering properties of these structures. It is found that the existing approximate relations for the absorption/scattering cross section of the agglomerates are accurate to within 20% or less for all typical values of refractive indices, number of primary particles and diameters typically encountered in flame systems. On the other hand it is demonstrated that the reciprocity relations are not satisfied for the type of carbonaceous agglomerated structures studied in this work. To the contrary these structures appear to be strongly depended on the agglomerate parameters and the type of agglomerate considered.

In order to elucidate the cause of this anomaly scattering and transmission measurements in dilute and dense polystyrene suspensions were carried out. The depolarized components of the scattered light are seen to be strongly dependent on the degree of particle concentrations. This result indicates that the failure of the agglomerated structures to satisfy the reciprocity relations identically may be due to multiple scattering occurring within agglomerated structures. In addition the present results indicate that further exploratory work is required to better understand the interaction of electromagnetic radiation with agglomerated structures and dense media, and to investigate the potential of the anisotropy characteristics as morphology diagnostic tool in reacting systems.

Introduction

Combustion generated particulates such as soot have wide ramifications in radiative transfer, pollution studies and material synthesis through the climate control. Some applications seek to enhance soot productions since the high emissivity results in increased radiative heat transfer rates. Other applications seek to reduce soot output; for example, soot emissions can lead to air pollution and can block exit ports of jet engines.

There are two methods for the study of soot characteristics: ex-situ and in-situ. In the first method the particles are collected from the flame using sampling probes. Size and shape information can subsequently be obtained using electron microscopy. In the second method a coherent light beam of moderate power is used and the amount of light energy scattered and absorbed by the particles is monitored by appropriate combination of light detectors. The ex-situ method, although simple to use, possesses disadvantages because the sampling process perturbs the flow field and as a result both the actual size and shape of the particles may be altered. The in-situ technique though complex from an experimental standpoint, can yield unambiguous information about the size and shape of the particles. More importantly the in-situ approach possesses the potential to yield real time information about size and shape of combustion particulates which can be very valuable in product quality control and in the area of combustion synthesis.

During soot formation small primary particles coalesce into larger agglomerates. These agglomerates of cluster, chains and random shapes no longer obey the theory for spherical particles. Jones [1, 2] has developed rigorous theory for agglomerates consisting of assemblies of small spheres with size parameters in the Rayleigh limit.

Nevertheless, several questions remain unresolved for a complete understanding of the scattering characteristics of agglomerates and their implications on the interpretation of conventional light scattering measurements and radiative transfer predictions. Such questions include but are not limited to: (i) Optical and geometrical anisotropy, (ii) Particle size and size distribution of primary particles within a given agglomerate, (iii) Multiple scattering between the primary particles of the same agglomerate, (iv) Multiple scattering with different agglomerates of dense med and (v) Determination of the optical properties of the agglomerate and of the ..nary particle as function of the temperature and chemical composition for conditions reflecting practical applications.

This part of the work will focus on the analytical investigation of the anisotropic characteristics of the agglomerates and on the analytical and experimental aspects of the multiple scattering effects for this type of agglomerated structures. The analytical investigation of the anisotropic characteristics is based on scattering, dissymetry and special extinction measurements from sooting flames [3, 4, 5, 6] and on the modified analytical expression for the extinction behavior of agglomerated structures [7]. On the other hand the multiple scattering portion of the study is based on the measured scattering and absorption characteristics from variable concentration of polystyrene spheres suspended in water. Specifics are given in the following section.

Scattering Models for Agglomerates

Electron micrographs of soot samples collected from flames demonstrate clearly the existence of agglomerated soot structures. Jones and Wong [8] determined the presence of soot agglomerates in flames from direct optical evidence. So it was concluded that soot particles in their early stages of formation are nearly spherical, but beyond a certain point in their evolution grow by agglomeration, forming chain or random like structures composed of essentially spherical subunits. In situ laser scattering is usually employed to obtain the soot characteristics of a system [9].

Several investigators have dealt with the development of theoretical model for the predictions of the absorption and scattering cross section of the agglomerated structures composed of two or more spherical subunits. Levine and Olaofe [10] developed expressions for the scattering intensities of two particles for particular orientations relative to a plane polarized incident electromagnetic wave. However for an agglomerate these intensities should be averaged over all possible orientations of the line of centers joining the two particles. Lips and Levine [11] examined theoretically the scattering of electromagnetic waves from two identical, rigid, non-absorbing neighboring particles. They determined the four scattering amplitude coefficients, which completely describe the scattering of the incident wave for two Rayleigh particles by making use of the results of Levine and Olaofe [10]. Ravey [12] calculated the components of light scattered by suspensions of aggregates of small dielectric or absorbing spheres and obtained some analytical relations for the depolarization ratio. The main advantage of the proposed method is that it can be applied to aggregates which possess more than two spheres, dielectric or absorbing. Later Ravey [13] performed computer simulation of aggregation of spherical particles and evaluated mean values of the morphological and optical properties. Specifically the dimensions of the ellipsoid were calculated that give a dynamically equivalent aggregate sphere.

More recently, Jones [1, 2] developed an analytical model using the integral equation formulation for the scattering and absorption efficiencies of agglomerates consisting of spherical subunits with size parameter in the Rayleigh regime. The expressions for the extinction efficiencies were recently modified by introducing a correction factor [7]. Since the expressions given in the Jones' formulation are computationally intensive other investigators [14, 15] sought the development of more simplified expressions for the scattering and absorption cross sections of the agglomerate. Apart from the theoretical and analytical studies experimental work has also been carried out in the area of agglomerate characterization under flame conditions. Ulrich and Subramanian [16] derived a growth rate expression of carbon particles in flames considering both collision and coalescence phenomena. For silica aggregates the value of N_p was estimated using electron micrographs. According to Lahaye and Prado [17] soot and carbon blacks are identical from the stand point of morphology and microstructure consisting of aggregates of pseudospherical particles. Roessler and coworkers [18] noted that particles produced at high fuel/air ratio are highly agglomerated, consisting mainly of elemental carbon with values of specific optical extinction.

Prado and Lahaye [9] studied the physical mechanisms of soot formation from the first measurable spherical units to the final agglomerates. In the early stages of particle growth, coalescent collisions between particles dominate the process resulting in a decreasing number density of particles of increasing diameter. At a later stage, collisions are no longer coalescent and chain forming collisions become predominant. According to the comprehensive review by Alessio [19] the morphological analysis of soot aggregates with optical techniques depend on the

development of advanced theoretical models for light scattering and extinction by absorbing particles of many different shapes. Prado and coworkers [20] used probe and laser light scattering and absorption techniques in a complementary fashion and measured soot volume fraction, agglomerate mean diameter and number density of agglomerates.

Megaridis and Dobbins [21] studied soot aggregate morphology within a soot emitting coannular ethylene/air diffusion flame of atmospheric pressure using a probe sampling technique. The primary particle diameters were obtained through electron microscope analysis of the soot aggregates collected from the flame environment. The primary particle diameters were combined with laser diagnostic and velocity measurements to calculate soot surface growth rates, soot surface areas and primary particle number densities. Charalampopoulos and Chang [4] inferred the agglomerate parameters i.e. diameter of primary particles, number density of agglomerates and number density of primary particles per agglomerate using in situ laser measurements and the scattering model for agglomerates.

Nevertheless the validity range of the approximate models for the extinction cross section of agglomerates both in terms of the number of primary particles, size parameter and refractive indices is yet to be established. In this part of the study the validity of the approximate expression for the extinction cross section for agglomerates [2] for typical values of refractive indices, size parameter and number of primary particles was assessed. Comparisons with the exact expressions were carried out and conclusions were drawn. The theoretical basis for these calculations is presented in the next section.

Theory

The scattering field for an agglomerate of arbitrary configuration exposed to an *incident radiation field is depicted for convenience pictorially in Figure 1. For* an agglomerate consisting of N_p number of spheres with the same refractive index $m = n + ik$ but different radii R, Jones [1] formulated an approximate solution. The formulation entails the simultaneous solution of a $3N_p$ linear system of equations for the internal field E (r_i) of the ith sphere. The individual spheres (primary particles) were assumed to be sufficiently small ($\pi d_p/\lambda < 0.1$) so that the internal field may be considered constant. In this development the power of the incident wave extinguished is written as

$$P_{ext} = \frac{4\pi}{k} \text{Im}[E_{inc} \cdot A(\theta=0, \phi = 0)] , \tag{1}$$

where $k = 2\pi/\lambda$, with λ being the wavelength of the incident radiation and $E_{inc} = E_o \exp ikz$. Here E_o is the amplitude of the incident radiation and z the direction of propagation of the incident wave. The function $A(\theta,\phi)$, represents the scattering amplitude defined by

$$E_{sca} = A(\theta,\phi) \exp(ikr)/r. \tag{2}$$

Recently [7] it was noted that equation (1) should be written as:

$$P_{ext} = \frac{4\pi}{k} \text{Im}[E_o \cdot A(\theta=0, \phi=0)], \tag{3}$$

where E_o is the amplitude of the incident radiation. The extinction efficiency for the agglomerate is given by [2]:

$$Q_{ext} = \frac{4kR}{3N_p I_o} \text{Im}[(\epsilon - 1) \sum_{j=1}^{N_p} E_o \cdot E(r_j)], \tag{4}$$

where N_p is the number of primary particles in the agglomerate assumed to have the same radius, ϵ is the permittivity of the work space equal to the square of the refractive index ($\epsilon = m^2$) and I_o is the intensity of the incident radiation being equal with the square of the incident field. Utilizing the correct equation for P_{ext} the expression for the extinction efficiency becomes:

$$Q_{ext} = \frac{4kR}{3N_p I_o} \text{Im}[(m^2 - 1) \sum_{j=1}^{N_p} \exp(ikz_j) E_o \cdot E(r_j)] \tag{5}$$

An approximate equation for the extinction cross section of the agglomerate ($C_{e,a}$) as a function of number of primary particles (N_p) and the extinction cross section of a

spherical particle ($C_{e,s}$) of diameter equal to the diameter of the primary particle (d_p) had been originally introduced [2] namely:

$$C_{e,a} = N_p C_{e,s}, \tag{6}$$

where for Rayleigh size particles

$$C_{e,s} = \frac{\pi^2 d_p^3}{\lambda} \text{Im}\left(\frac{m^2-1}{m^2+2}\right)$$

The exact extinction cross section of the agglomerate is given by [2]:

$$C_{e,a} = Q_{ext} N_p \pi d_p^2 / 4 \tag{7}$$

Since the exact expressions are computationally intensive the use of the approximate expressions is more desirable.

Numerical Calculation

As noted earlier Jones' formulation requires that the primary particles be of Rayleigh size ($\pi d_p/\lambda < 0.1$). The solution is obtained by assuming that the individual spheres are sufficiently small that the internal field may be considered constant. Hence for ($\pi d_p/\lambda$) > 0.1 the theory introduces error in the inferred quantities. Normally the refractive index for soot particles lies between ($1.4 + 0.4i$) to ($2.0 + 1.0i$). According to Charalampopoulos and Chang the refractive index lies between $1.6 + 0.53i$ and $1.73 + 0.64i$ for propane oxygen flame system. The validity of approximate relation should be determined for all ranges of refractive index, size parameter, number of primary particles in an agglomerate and types of agglomerate (straight chain, random chain and cluster) in the Rayleigh region. Equation (7) and equation (6) are used to calculate $C_{e,a}$(exact) and $C_{e,a}$(approximate) extinction cross sections and the percentage of error between the approximate expression and the exact equation is determined according to the relation $100(C_{e,a}[\text{Eq.(6)}] - C_{e,a}[\text{Eq.(7)}])/C_{e,a}[\text{Eq.(7)}]$.

The variation of the percentage difference with respect to size parameter (x_p), number of primary particles in an agglomerate (N_p) and refractive index (m = n + ik) may be better assessed by using three dimensional plots. With reference to Figure 2. it may be seen that for N_p = 10, x_p = 0.01 and for all possible ranges of refractive index the percentage of error is within 14.75%. It should be noted that the percentage of error is an increasing function of both real and imaginary part of refractive index. Comparing Figures 2 and 3 the percentage of error is not a strong function of size parameter. On the other hand for m = 2.0 + 1.0i, N_p = 50 and x_p = 0.094 (see Figure 4) the percentage of error is about 18%. It is also noted that the percentage of error decreases with increase in size parameter and increases with increase in number of primary particles in an agglomerate. Thus for straight chain the approximate relation given by (Eq.(6)) can be used for all possible ranges of refractive index (typical of soot particles), number of primary particles in an agglomerate and size parameter in Rayleigh region with an error of less than approximately 20%.

With reference to Figures 5, 6 and 7 it is observed that for clusters the percentage of error is an increasing function of both real and imaginary part of refractive

index. Also the percentage of error is weak function of the number of primary particles in an agglomerate and is below 5% for all possible ranges of refractive index, number of primary particles in an agglomerate and size parameter. For a random chain agglomerate the percentage of error is not a systematic function of size parameter, number of primary particles in an agglomerate and refractive index, whereas the percentage error does not exceed 10% (see Tables 1 and 2).

So, it may be concluded that the approximate relation for extinction cross section can be used with more confidence in the case of clusters and random chain agglomerates than straight chain agglomerates. But the error introduced due to the use of the approximate relation (Eq. 6) does not exceed 20% irrespective of type of agglomerate, refractive index, number of primary particles in an agglomerate and size parameter.

Depolarization of Agglomerates

As noted earlier the effects of agglomeration of flame particulates play an important role on the radiative characteristics of combustion systems [5]. Several theories for scattering and absorption of flame particulates have been proposed. Nevertheless the complete characterization of agglomerates is hindered simply because the number of unknowns are usually more than the number of experimental measurements possible. In a recent publication Charalampopoulos and Chang [4] used the real and imaginary part of refractive index [3] and inferred diameter of primary particle, number of primary particle in an agglomerate and number density of agglomerates. Nevertheless the effects of anisotropy of the particles in the light scattering measurements and data interpretation have not been fully explored. Anisotropic particles such as the agglomerates cause rotation in the plane of polarization of the incident electric field vector unlike the spherical particles due to the geometrical anisotropy. The existence of definite amount of depolarization in light scattered from soot agglomerates has been noted in previous studies [1, 6, 19]. Although systematic studies of the particle anisotropy under flame conditions are not available, several works have been carried out in colloidal systems.

Several investigators [6, 22-25] have studied depolarization of light scattered in colloidal suspensions and agglomerated particulates. According to Krishnan [22] three quantities namely polarization ratio (ρ_u), depolarization ratio in the vertical plane (ρ_v) and depolarization ratio in the horizontal plane (ρ_h) are related to the size, shape and structure of particles contained in the solution. Hence from a knowledge of their magnitudes it is possible to estimate the size, shape and structure of the scattering particles. Recently [6] it was noted that depolarized scattering measurements in sooting flame systems, can yield particle morphology information provided that they are carried out in the ultraviolet wavelength of 0.275 micrometers or even smaller. The depolarization characteristics of particles may be utilized to obtain additional independent equations. So the objective of this part of the work is to further explore the possibility of using depolarization as a means for determining the soot agglomerate characteristics. Thus both Jones' theory [1, 2] and Saxon's reciprocity theorem [26] will be discussed.

Jones used Saxon's integral equation [27] to determine the scattered electric field at any point in space taking multiple scattering into consideration. Referring to Figure 1 the incident field is taken to be associated with an infinite plane wave of the form

$$E_{inc} = E_o \exp(ikz) \tag{8}$$

whereas the scattered electric field at any distance r from the origin is given by:

$$E_{sca}(r) = \frac{1}{3}(m^2 - 1)\frac{\exp(ikr)}{r}\sum_{j=1}^{N_p} k^2 R_j^3 \exp(-ikrj\cos\beta j)\,(\Theta_j\theta_1 - \Phi_j\phi_1) \tag{9}$$

where θ_1 and ϕ_1 are unit vectors in the θ and ϕ directions and Θ_j, Φ_j are given by:

$$\Theta_j = \cos\theta\cos\phi E_x(r_j) + \cos\theta\sin\phi\, E_y(r_j) - \sin\theta E_z(r_j) \tag{10}$$

$$\Phi_j = \sin\phi\, E_x(r_j) - \cos\phi E_y(r_j) \tag{11}$$

Here E_x, E_y and E_z are the respective component of the electric field vector E. The rectangular field components are determined by solving $3N_p$ linear simultaneous equations given by

$$E(r_l) - \frac{i}{3}\left|\frac{m^2-1}{m^2+2}\right| \sum_{j=1, j\neq l}^{N_p} (kR_j)^3 T_{lj} E(r_j) = \frac{3}{m^2+2} E_{inc}(r_l) \tag{12}$$

$$l = 1,2,3.....N_p$$

According to Figure 8 the scattered intensity is described in the following format. H stands for horizontal and V stands for vertical polarization orientation. Specifically, H_v is the components of the scattered intensity corresponding to the following setting: The polarizer is placed in front of the detector with its axis coinciding with the scattering (measurement) plane whereas the incident electric field vector oscillates perpendicularly to the scattering plane. Similarly V_h is the component of the scattered intensity detected with the polarizer axis oriented perpendicularly on the scattering plane and the incident electric field vector oscillating in the scattering plane. Krishnan [38] stated that reciprocity theorem ($H_v = V_h$) is valid not for a single nonspherical particle, but for a solution containing a large number of particles which have no preferred orientation in the plane of observation. H_v and V_h intensity for an individual particle of arbitrary size and shape oriented in a specific way are not equal to each other. But if an averaging is carried out over all orientations of the particle in the horizontal plane which are similarly situated with respect to a vertical axis the H_v and V_h intensities are equal [24]. Krishnan carried out an experimental investigation to verify the reciprocity theorem. Using double image prism he took photographs of H_v, V_h, V_v and H_h intensity of graphite solution, sulphur suspensions, red gold solutions, bredig's silver solution, stearic acid solutions, dilute milk, dilute toluene emulsions and concentrated toluene emulsions. The quantities H_v and V_h were found to be exactly identical in intensity and color establishing the validity of reciprocity theorem. However no measurements were obtained for H_v and V_h in the multiple scattering region.

Perrin [28] has stated the law of reciprocity more explicitly. According to Perrin if two incident polarized beams have equal intensities, the inverse emerging beams of the same polarization, which are associated with them, also have equal intensities.

Saxon [26] described the scattering of an incoming electromagnetic wave by an unrestricted scattering object in terms of a tensor scattering matrix. Unrestricted scatterer means no restriction on the scatterer. This implies that the reciprocity theorem applies to the assembly of soot aggregates that are dissipative in nature from optical standpoint. The field at large distances from the scattering region has the form:

$$\lim_{r\to\infty} E(nr) = q\ \exp(ikrn_o\cdot n) + Aq(n,n_o)\frac{\exp(ikr)}{r} \tag{13}$$

Where the plane wave is incident along the direction n_0, q is a unit vector in the direction of polarization and $Aq(n,n_0)$ is the amplitude of the wave scattered in the direction n. In the above equation the first term of the right hand side stands for the

incident field and second term of the right hand side represents the field of the scattered wave at large distances from the scattering region. According to Saxon, the reciprocity relation may be written as:

$$q \cdot A_q(n,n_o) = q \cdot A_q(-n_o,-n) \tag{14}$$

This relation implies that the direction of the incident wave and the direction of observation are interchanged, the component of the scattered wave in the direction of polarization remains unchanged. Bayvel and Jones [12] wrote the relationship between incident and scattered waves using a scattering matrix.

$$\begin{pmatrix} E_{h,sca} \\ E_{v,sca} \end{pmatrix} = \begin{pmatrix} S_2 & S_3 \\ S_4 & S_1 \end{pmatrix} \begin{pmatrix} E_{h,inc} \\ E_{v,inc} \end{pmatrix} \exp(ik_o r)/k_o r \tag{15}$$

where $k_o = 2\pi/\lambda_o$ is the wave number in vacuum, λ_o the wavelength in vacuum and S $= \begin{pmatrix} S_2 & S_3 \\ S_4 & S_1 \end{pmatrix}$ is the scattering matrix. If the directions of incidence and scattering are interchanged then a relationship exists between the original scattering matrix and that for reversed situation. Using the reciprocity theorem for the reversed situation Bayvel and Jones wrote that $S = \begin{pmatrix} S_2 & -S_4 \\ -S_3 & S_1 \end{pmatrix}$. Jones [2] plotted the H_v to V_h ratio versus angle for chain of random orientation and observed that the reciprocity theorem was not satisfied. However no explanation was provided for the observed discrepancy. Bayvel and Jones [12] on the other hand pointed out that the violation of reciprocity theorem may be due to an error which is undiscovered or genuine. But it does indicate the need for caution in using this theory. More recently [29] it was pointed out that the observed anomaly was due to an error in the computer program. A graph was presented between the H_v to V_h ratio with respect to scattering angle for straight chain (kr = 0.2, m = 1.6+0.8i, N_p = 10) and concluded that the H_v to V_h ratio is unity to within less than 6%. The deviation was attributed to rounding error and concluded that his theory satisfies the reciprocity theorem. Nevertheless it should be noted that the validity of the theory for agglomerates may not be ascertained by just arbitrarily considering a single set of parameters. To the contrary it appears that a more thorough investigation for a range of refractive indices, size parameters, number of primary particles and type of agglomerate is required. This is accomplished in the next section.

Numerical Calculation for Depolarization Ratios

Making use of Eq. (15) for the forward direction we get $H_v = E_{h,sca} = \exp(ik_o r)$ $S_3 E_{v,inc}/k_o r$ and for the backward direction we get $V_h = E_{v,sca} = -\exp(ik_o r)$ $S_3 E_{h,inc}/k_o r$. For $E_{v,inc} = E_{h,inc}$ we have $H_v = V_h$.

The components of the scattered intensities H_v and V_h may be calculated from Eq. (9) for different agglomerate structures. The reciprocity relation is independent of the nature of scatterer. So any agglomerate can be assumed as a single scatterer and

reciprocity theorem should be valid for agglomerates also. For a check of reciprocity relation we see that $H_v = V_h = 0.0$ for a single isotropic spherical scatterer [8, 9].

According to Perrin [28] the reciprocity relation is true if the optical system is not affected by a reversal of time, so that the sense of propagation of light is immaterial. There must be no movements, no electric currents and no magnetic fields of the optical system. There must be no frequency shifts or, at least, if these occur it should be possible to reverse them. For example, the law of reciprocity is not valid for fluorescence or for Raman effects, in which the change of frequency is irreversible [28].

As a first step towards elucidation of the applicability of the reciprocity theorem for agglomerates calculations were carried out similar to those by Jones [29]. Figure 9 shows the H_v to V_h ratio with respect to scattering angle for straight chain with size parameter (kr = 0.2), refractive index (m = 1.6 + 0.8i) and number of primary particles (N_p = 10). It may be seen that the agreement between the results of the present calculation and those of Jones [29] are quite satisfactory. In order to investigate the applicability of the reciprocity relation to the agglomerated particulate structures in flames numerical calculation were carried out using the experimental results reported recently by Charalampopoulos and Chang [4] (see Table 3).

Charalampopoulos and Chang [3] determined the refractive index of soot particles by assuming that all soot particles are of spherical shape. In their recent publication [4] they have reported diameter of primary particles, number of primary particles in an agglomerate and number density of agglomerates at different flame heights using the refractive index from their previous publication [3]. Here the data from their previous publications i.e. diameter of primary particles, number of primary particles in an agglomerate and refractive index are used to calculate H_v and V_h for cluster, random chain and straight chain agglomerates. The ratio of H_v and V_h are plotted with respect to scattering angle for different flame heights (see Figures 10 and 11).

Agglomerates are assumed to be a combination of small spherical particles [1]. For a spherical particle H_v and V_h intensities are zero. But there are definite H_v and V_h intensities for agglomerates due to multiple scattering between the primary particles. For single primary particle the H_v and V_h intensity should be equal to zero due to the absence of multiple scattering. For a check of the calculation, the H_v and V_h intensities for a single spherical particle were calculated by using our program for both cluster, random chain and straight chain. It was found to be equal to 0.0. Random orientation of agglomerates were considered by calculating the mean scattered intensity over all possible orientations. A ten point Gaussian integration formula was used for integration.

Comparison with Prolate Spheroid

The scattered intensity for different orientations (vertical or horizontal) of polarizer before and after the scatterer were calculated for the straight chain agglomerate and prolate spheroid. The purpose of the calculation is to compare straight chain with prolate spheroid. These calculations were undertaken since the prolate spheroid resembles closely to the straight chain with respect to form anisotropy.

The calculations were done for flame height 6mm and 16mm. Because, for 16mm flame height straight chain violates the reciprocity theorem more compared to 6mm flame height. The prolate spheroid was compared with straight chain according to equivalent length and equivalent volume model. For equivalent length models both the length and diameter of the straight chain and prolate spheroid are the same. For the equivalent volume models the length of prolate spheroid and straight chain are same. But, the radius of prolate spheroid is changed so that the volume of the prolate spheroid and straight chain are the same.

From Figures 12 and 13 it may be seen that H_v and V_h intensity for prolate spheroid is not a function of scattering angle. Additional calculations demonstrated that the nature of variation of H_h intensity for prolate spheroid and straight chain is the same. But V_v intensity for straight chain decreases with respect to scattering angle, while for prolate spheroid it does not vary with respect to scattering angle. It was also observed that the order of magnitude for H_v, V_h, V_v and H_h intensity are the same for both straight chain and prolate spheroid. This behavior suggests that a correction which is a function of scattering angle can be used to model the straight chain with equivalent prolate spheroid according to scattered intensity.

Variation of the Depolarization Ratio with Agglomerate Parameters

With reference to Figure 11 it may be seen that for straight chain there is a systematic variation of H_v to V_h ratio with flame height. Also the H_v to V_h ratio increases with flame height. For 16mm flame height the variation of H_v to V_h ratio with scattering angle lies between -15% to 35%. For cluster agglomerate no systematic variation of H_v to V_h ratio with flame height was found. But the rate of variation is much more compared to the straight chain. The nature of variation is also different from the straight chain. From Figure 10 it can be seen that the variation of H_v to V_h ratio lies between -90% to 400%. Thus the previously inferred conclusion [44] that reciprocity theorem is satisfied within less than about 6% is not correct. It is also noted that the nature of variation of H_v to V_h ratio is a function of type of agglomerate. This dependence suggests that the H_v to V_h ratio for agglomerates (measured and predicted) may be used as an additional independent piece of information for morphology characterization of particulates in flame system.

Since all properties of soot particles vary with flame height the variation of H_v to V_h ratio with respect to individual properties like diameter of primary particles and number of primary particles three dimensional plots were plotted. With reference to Figure 14 and 15 for straight chain there is a systematic increase of H_v to V_h ratio with respect to either diameter or number of primary particles. The variation of H_v/V_h with respect to the primary particle diameter appears to follow the same trends of its variation with respect to the number of primary particles for straight chain. However for the cluster agglomerate the variation of H_v to V_h ratio curve with respect to the number of primary particles is discontinuous and with respect to diameter is continuous (see Figures 16 and 17). In this program the coordinates of the primary particles for clusters are fixed. We know that the H_v and V_h intensities are function of the geometry of the agglomerate. By increasing the number of primary particles the geometry of the cluster is changed in a fixed manner. So, the ratio of H_v to V_h is not a function of the number of primary particles alone. This may be the reason for inconsistent variation with respect to number of primary particles for the cluster agglomerate. To verify this, the coordinates of primary particles of the agglomerate were generated at random. The average scattering characteristics of the agglomerate were calculated after 600 runs of the program. The H_v to V_h ratio was plotted for different number of primary particles and scattering angle. From Figure 18 it may be seen that the H_v to V_h ratio is no longer a discontinuous function of the number of primary particles. The variation of H_v to V_h ratio lies between 0.8 to 1.2 which is much less than the variation of a cluster agglomerate. The irregular variation of H_v to V_h ratio with respect to number of primary particles may be due to the change of geometry of clusters in an irregular manner. Thus, it is expected that the violation of reciprocity theorem may be due to multiple scattering. The comparison of H_v and V_h intensity in the multiple scattering region of monodisperse polystyrene particle solution may provide guidance as to the applicability of the reciprocity theorem in the multiple scattering region. The experimental system used and the type of experiments undertaken to elucidate this phenomenon are presented in the following sections.

Multiple Scattering

In general scattering problems deal with the effects arising when a given obstacle, or collection of obstacles, is placed in the path of a specified wave. Assuming a source whose field when isolated is known we seek the redistribution of radiation arising from the presence of obstacles. As one physical illustration, an electromagnetic primary wave induces charges and currents in the obstacles, and these give rise to "secondary waves" that constitute the "scattered field". Multiple scattering is the effect which arises from interference of the scattered radiation between the individual wavelets [10, 11].

The interaction of particles with incident radiation and the extent and nature of the scattered field is usually described by considering the following cases (a) Interactive or close proximity scattering: for this case the particles are very close together and as a result the electric fields may interact directly and scatter essentially as an entity (b) In more tenuous systems the particles may act individually but if single scattered wavelet is traced through the system of particles it may be scattered several times before it exits the system of particles. The third case is related to the relative positions of the scatterers. When the particles are located in predictable positions the scattering is referred to as coherent scattering and the scattered intensities at a given point in space is proportional to the sum of the squares of the amplitudes of the individual wavelets. On the other hand, when the particles are located at random positions the scattering intensities may be added directly. This type of scattering is called incoherent scattering. It should be noted that in order to determine the total intensities at a given point in space integration over all possible particle sizes within the particle system is required. This criterion requires that the particles are randomly positioned and that there is no multiple scattering. This condition is almost always valid for particles suspended in fluids and, indeed to molecules themselves. It does not however apply between the particles forming an agglomerate but does between the agglomerates themselves [33]. More details about the criteria and the conditions for multiple scattering is given in the next sections.

Electrical Interaction Between Particles

When the particles are sufficiently close to each other, their polarization fields interact so that in the primary process for a given particle, the polarization fields of the neighboring particles must be taken into account as well as the incident field, the field induced within the particle and the external and scattered field [30]. Churchill et. al. [31] determined the separation distance at which optical interference becomes appreciable and measured the magnitude of the effect. Kerker [32] points out that the mutual interaction between two spheres is negligible for spacings greater than two or three diameters. The limiting δ/r above which optical interference between particles can be neglected is about 1.7 [30]. Here "δ" represents the average distance between the centers of the particles and "r" is the radius of the particle. Hence in the multiple scattering regime if the particles are close enough ($\delta/r < 1.7$) the electrical interaction between the particles should be taken into consideration.

The following approximate relation can be suggested to determine the number of particles per cubic centimeter of solution to avoid electrical interaction or multiple scattering for a given interparticle distance, namely:

$$N = \frac{3.0 \times 10^{12}}{\pi((n+1)d)^3} \qquad (16)$$

where "N" is the maximum allowable number of particles per unit volume, "n" is the number of particle diameter by which the center of particles are separated and "d" is the particle diameter expressed in microns.

Using above approximate equation the maximum number density for no electrical interaction was calculated. On the other hand using Bayvel and Jones' relation [33] the maximum number density for no electrical interaction for particle whose diameter is 0.1 micron is $1.0 \times 10^{13}/cm^3$. According to Table 3 (n=3) for 0.1 micron diameter particle the maximum number density for no electrical interaction is $1.45 \times 10^{13}/cm^3$. Similarly, for 10.0 micron diameter particle the number density from this calculation is $1.492 \times 10^{7}/cm^3$ and for 1.0 micron the number density is $1.4922 \times 10^{10}/cm^3$. Equation 16 was used to calculate the number density required for the existence of multiple scattering, which is calculated in the next section.

Conditions for Multiple Scattering

Kerker and Matijevic [34] measured the intensity of light scattered by four monodispersed polystyrene latexes at scattering angles 45°, 90° and 135° with respect to the forward direction. They compared depolarization ratios and dissymmetries from experiments and from Mie theory. They observed discrepancy between the experimental and theoretical values for the dissymmetry and accounted for it in terms of secondary or multiple scattering. For dilute latex suspensions no depolarization was observed.

Moron and coworkers [35] measured polarization ratio (ρ_u) for series of polystyrene samples by using unpolarized incident light and observed that ρ_u differs appreciably from those predicted by Mie theory. The depolarization ratios ρ_v and ρ_h

were measured as a function of concentration and the measurements extrapolated to zero concentration. The quantities ρ_v and ρ_h were defined as:

$$\rho_v = I_{hv}/I_{vv}$$
$$\rho_h = I_{vh}/I_{hh} \qquad (17)$$

The definition of I_{hv}, I_{vh}, I_{vv} and I_{hh} are given in the previous section. The results were extrapolated to zero concentration to confirm that there is no multiple scattering. For different concentrations studied it was observed that neither ρ_v nor ρ_h is zero. So it was inferred that the discrepancy between the Mie theory and experiment is due to inherent anisotropy of the spherical latex particles. The anisotropy was believed to arise from non-random orientation of polymer chains in the colloidal latex particles. It is to be noted that the observation of Moron and coworkers [35] and of Kerker and Matijevic [34] is different. At dilute solution of latex particles Kerker and Matijevic observed no depolarization whereas Moron and coworkers observed some depolarization. Nappier and Ottewill [18] studied the light scattering properties of four polystyrene latex dispersions and correlated the results with the ratio δ/r. They used the following two phenomena for spherical Mie scatterers to calculate the required value of the ratio δ/r for multiple scattering to occur.

(a) The scattered intensity at a given angle may not be directly proportional to the number of scattering units in the observed volume.

(b) Complete extinction may not result when the polarizer in the incident beam and the analyzer in the scattered beam are crossed.

Comparison of experimental results according to conditions (a) above suggest that multiple scattering is present at δ/r values less than 100. Comparison according to condition (b) above suggest that multiple scattering is present for δ/r less than 200. According to Nappier and Ottewill [36] multiple scattering depends upon the particle size parameter, particle number concentration, the geometry of the scattering cell and the geometry of the receiver. It was concluded that the actual order of δ/r should be checked for each set of instrumental conditions.

Bayvel and Jones [33] stated that multiple scattering is significant when turbidity $(\tau) \geq 0.1$. Here τ is defined as $\int_0^L K_{ext} dx$; K_{ext} is the extinction coefficient and L the path length. The condition for negligible multiple scattering ($\tau << 1$) can be satisfied by making either K_{ext} or L very small. Recently, Konak and coworkers [37] have calculated and experimentally determined the effect of multiple light scattering on transmitted and scattered light. They investigated the effect of multiple light scattering in the transition region between the single and multiple scattering limits both on autocorrelation functions and on measurements of the attenuation of the primary beam. They concluded that the limit of strong multiple light scattering is probably reached at longest path length used in their experiment.

The criteria stated before by Nappier and Ottewill [36], and Jones and Bayvel [33] are used to calculate the maximum number density for single scattering (see Table 4). The details of the experiments that were carried out in this part of the work to further elucidate the effects of multiple scattering are presented in the next section.

Experimental Set Up

The light scattering facility includes a laser source, a focussing system for the incident beam, a sampling volume that contains the scatterers, a light detection system and a detection system. A schematic of the light scattering experimental shown is presented in Figure 19.

The laser beam is focussed on the centerline of the sample holder by lens L_1 of 400mm focal length. The divergence of the Argon ion laser is 0.69mrad and the resulting spot radius is 0.276mm. An iris diaphragm is inserted on the focussing tube to minimize stray light effects due to the continuous expansion of the laser beam. For alignment purposes the tube carrying the focussing elements is mounted on an adjustable platform. The detection optics are mounted on a rotating arm that can be rotated around the central axis of the cell holder at any angle between 0^o and 160^o. Two variable aparture (1-12mm) iris diaphragms define the image seen by the detector. The first iris defines the solid angle of the detection optics and limits the field of view of lens L_2. The second iris in front of the detector defines the spatial resolution on the sampling volume. An analyzer (KLC, model-K1169) of extinction ratio equal to 10^{-6} mounted coaxially with the lens L_2 allows angular intensity measurements in any plane of polarization. An Oriel narrow-band laser line filter (model-52630, band-width 10nm) mounted in front of the detector minimizes the background noise reaching the detector. The scattered light from the sampling volume was detected by the photo-multiplier tube of Thorn EMI Electron tubes Inc. (Model RFI-B2F), which was operated at an input voltage between 1000 to 1500 volts. The output current of the photo-multiplier tube was preamplified by a preamplifier (EG&G, Model-5002) and passed to a lock-in amplifier (PAR, Model-5209) which filter the input signal from noise and provided a digital readout of the signal containing only the reference frequency.

The laser beam transmission directly through the scattering system was detected by a power meter (Spectra-Physics, Model-404) and the output signal similarly passed to a lock-in amplifier (PAR, Model-5207) where the digital output signal was displayed. A special scattering cell and holder (Figure 20) were designed and fabricated for the scattering measurement of polystyrene particle at high concentration. Combinations of different set screws were used to align the scattering cell perpendicular to direction of travel of the laser beam. The scattering cell and holder assembly were painted black inside except a 1cm strip for angular scattering measurement. The top of the scattering cell was provided with three openings. Two of them were used for drawing the vacuum and filling gas and the other was used to monitor the concentration by adding distilled water and polystyrene particle to the cell.

Measurements

The experiment consists of three parts: (a) preparation of the polystyrene solution and scattering cell (b) calibration and background measurements (c) measurements of the particulate media.

The measurements are performed for different ranges of transmission. The supplied polystyrene has concentration of 50% by volume of solids. The concentrated solution is diluted to a low concentration. This low concentrated polystyrene solutions are used so that measurements can be performed from low to high transmission levels. This low concentration polystyrene solution is prepared using an electronic balance of 10^{-4}gm accuracy.

During measurements, the low concentration polystyrene solution was added to the scattering cell using 1cc syringe. The accuracy of the syringe was tested with the help of the electronic balance, model Scientech - 5220.

The water used for the dilution of the concentrated samples was carefully selected to be ultrapure with no contaminants. High performance liquid chromatography grade water supplied by Mallinckrodt Specialty Chemicals Co. was used. The water was also tested by passing the laser beam through it and visually inspecting the scattering. The scattering cell was cleaned using ultra pure water four to five times before the start of each measurement. The scattering cell was held using the cell holder and aligned in such a way that the reflected laser beam will pass through the diaphragm.

Before the start of the calibration runs, vacuum was pulled from the scattering cell and the background signal S_{vv} and reference transmitted intensity I_o was measured. Then propane and methane gas was used and the scattering signal S_{vv} and transmitted intensity I_g was measured. Before taking gas measurement the gas was purged through the scattering cell for at least three times so that there will only be that particular gas in the scattering cell. After the gas measurement, the ultra purity water is added to the scattering cell. Then the background measurements were done for all measured quantities i.e. S_{vv}, S_{hh}, S_{hv} and S_{vh} at all scattering angles. This is because the background signal is a function of polarization of the beam, polarization of the analyzer and of the scattering angle.

Sonifer was used to disperse the polystyrene solution and to break an agglomerate before using it in an experiment. The low concentrated polystyrene solution was added to water using the 1cc syringe. Then the particles were dispersed by bubbling nitrogen through the polystyrene solution. Then all required measurements were carried out. During the measurements a check was conducted after some time interval to verify if the system response remains constant. For example, $S_{vv}(\theta = 90^o)$ measurement is repeated after all measurements of S_{vv}, S_{hh}, S_{hv} and S_{vh}. If same signal is observed then the response of the system is assumed to remain consistent throughout the experiment. The same test was carried out for the polarization rotator and polarizer to verify if the same angular position is achieved in all experimental runs.

Calibration

Calibration of the experiment was carried out using gases whose scattering coefficients are known (methane and propane). The scattering signal from any scattering volume when a detector is located at an angle θ with respect to the incident beam direction is given by [6]

$$Sg_{pp}(\theta) = S_{pp} \cdot \Delta V \cdot \Delta\Omega \cdot I_o \cdot n_{el} \cdot n_{opt} \cdot \tau_\lambda \qquad (18)$$

where ΔV is the scattering volume and $\Delta\Omega$ is the solid angle defined by the detection optics, I_o is the energy flux of the incident beam, whereas n_{el} and n_{opt} are the electronic and optical efficiencies of the system. S_{pp} is the differential scattering coefficient ($cm^{-1}sr^{-1}$) and is defined as the energy scattered per unit time and per unit volume into a unit solid angle about a direction θ. The differential scattering coefficient for a size distribution of particles is given by

$$S_{pp} = N\overline{C_{pp}} \tag{19}$$

where $N(cm^{-3})$ is the particle number density and $\overline{C_{pp}}$ is the mean differential scattering cross section for all spheres in the scattering volume given by

$$\overline{C_{pp}} = \int_{r=0}^{\infty} C_{pp}P(r)dr \tag{20}$$

where C_{pp} is the scattering cross section for a single particle of radius r and P(r) represents the size distribution of particle. The subscript p denotes the polarization state (vertical or horizontal), and the double subscript indicates the states of polarization of the scattered and incident beams. Since the scattering intensity is attenuated as the light travels between the scattering volume and the detector the factor τ_{λ}, was introduced to account for this attenuation. When the scattering cell is filled with a gas and both the polarization rotator and the analyzer are vertically polarized, Eq. (18) yields the scattering signal given by:

$$Sg_{vv}(gas,glass) = I_o \cdot S_{vv}(g) \cdot \Delta V \cdot \Delta\Omega \cdot n_{el} \cdot n_{opt} \cdot \tau_{gl} \cdot \tau_g \tag{21}$$

where τ_{gl} and τ_g are the transmission through the scattering cell and gas respectively. On the other hand when the scattering cell is filled with water and polystyrene solution the scattering signal can be written as

$$Sg_{vv}(glass,\ poly.,\ water) = I_o \cdot S_{vv}(p) \cdot \Delta V \cdot \Delta\Omega \cdot \tau_p \cdot \tau_{gl} \cdot \tau_w \cdot n_{el} \cdot n_{opt} \tag{22}$$

where τ_p and τ_w are the transmission through the polystyrene particle and water respectively. $S_{vv}(p)$ is the scattering coefficient of polystyrene particles in water. Dividing (21) and (22) we obtain the calibration equation as

$$\frac{Sg_{vv}(gas,\ glass)}{Sg_{vv}(glass,\ poly.,\ water} = \frac{S_{vv}(g)\tau_g}{S_{vv}(p)\tau_p\tau_w} . \tag{23}$$

It should be noted that in this experiment reflection losses take place from the surface of the cell therefore the above equation needs to be modified accordingly. Neglecting the multiple reflection within the solution the overall transmission through the glass and medium may be written as [38]

$$T = \tau_1^2(1-\rho)^2(1-\rho_1)^2 \tag{24}$$

where τ_1 is the transmission through the glass and τ_2 is the transmission through the inside medium, ρ is the reflectivity between outside medium and glass and ρ_1 is

the reflectivity between glass and inside medium. It is noted that ρ and ρ_1 can be represented by the following expressions [38].

$$\rho = \left(\frac{n_1 - n_s}{n_1 + n_s}\right)^2 \tag{25}$$

$$\rho_1 = \left(\frac{n_2 - n_1}{n_2 + n_1}\right)^2$$

where n_1 is the refractive index of the glass, n_s is the refractive index of the surrounding medium and n_2 is the refractive index of the inside medium. For calculation n_s and n_1 was assumed to be equal to 1.0 and 1.5 respectively. For case:1 the inside medium was propane with refractive index equal to 1.00111 and for case:2 the inside medium was water with refractive index equal to 1.3625 at 0.488 micron wavelength of incident radiation. Using the above data the ratio of transmission between case:1 and case:2 was calculated to be equal to 1.0794. From three different experimental observations it was found that the above ratio was 1.1, 1.139 and 1.03 respectively, whose average value was 1.0896. These calculations show that τ_{gl} is a function of the inside medium. The transmission through water was more than 1.0 because τ_{gl} for water as inside medium is higher than τ_{gl} for propane as an inside medium. Therefore, Eq. (23) should be modified by substituting the theoretical ratio of transmission between case:1 and case:2 in the original calibration equation.

$$\frac{Sg_{vv}(\text{gas, glass})}{Sg_{vv}(\text{glass, poly., water})} = \frac{Sg_{vv}(g)}{S_{vv}(p)\tau_p \cdot 1.0794} \tag{26}$$

It should be noted that equation (26) can be used even if τ_w is greater than one. Because τ_w takes care of the fact that τ_{gl} in case of water as the inside medium is more than with propane as the inside medium.

A high concentrated polystyrene solution was used to reach the multiple scattering region and as a result the scattering signal was high. On the other hand the scattering signal for gas is much lower compared to polystyrene. It should be noted that with moderate laser powers (typically 500 mw for these measurements) the scattering signal from the polystyrene is expected to overload the measuring instruments. Thus in order to be able to perform the measurements from the calibrating gas a gas with high enough scattering cross section had to be selected. Among all available gases propane was selected as the calibration gas. The scattering signal from methane and propane gas was measured at the start of each experiment. The ratio of the scattering signal of propane and methane was compared with the theoretical value (6.059). This way the experimental system was checked from any possible indiscrepancy for a particular experimental run.

For methane the scattering cross section was used from the calculation of Rudder and Bach [39] which is equal to $4.49*10^{-28} cm^2$. For propane Kent [40] calculated the scattering coefficient to be equal to $3.094*10^{-7} cm^{-1} sr^{-1}$. For double check scattering coefficient of propane from the available data and equations are calculated as described below. From Landolt-Bornstein [41] the refractive index of propane at 0.488 micron wavelength was interpolated and was equal to 1.00111, whereas from Boggard and coworkers [42] the depolarization ratio of propane was found to be equal

to 0.00214. Rudder and Bach [39] suggested an expression for the scattering cross section of an ideal gas as

$$C_{vv} = \frac{12\pi^2(m-1)^2}{N_o^2\lambda^4(3-4\rho_v)} \quad (27)$$

where m is the refractive index of the gas, N_o the number density of scatterers at STP conditions, λ the incident wavelength and ρ_v is the depolarization ratio. Using the above equation and data the scattering cross section of propane was calculated to be $1.31562 * 10^{-26} cm^2$. The scattering coefficient of propane ($N_o \cdot C_{vv}$) was found to be equal to $3.2653 * 10^{-7} cm^{-1} sr^{-1}$. In all subsequent calibrations the scattering coefficient of propane from the present calculation is used.

Results and Discussion

In this section the results of experimental measurements with respect to: (a) The effects of multiple scattering on transmission and scattering from dense particulate media (polystyrene solution) with concentrations in the range 0.1 x 10^9 to 4.0 x 10^9 for a particle diameter of 0.22 micron and (b) The effects of multiple scattering on the depolarized component of scattered intensity are presented.

Number Density Calculation

For many particulate media the transmission and scattering data are used to determine the characteristics of the medium such as number density, and size distribution of the particle dispersions. Information about the standard polystyrene solution used in this study such as diameter, concentration and refractive index of the particle is supplied by the manufacturer. So the actual number density of a particular solution prepared from the concentrated polystyrene can be calculated. The transmission τ_λ is given by

$$\tau_\lambda = I(L)/I_o$$

$$= \exp(-K_{ext}L) \qquad (29)$$

where L is the path length through the medium and K_{ext} is the extinction coefficient which for monodisperse spheres may be written as

$$K_{ext} = NC_{ext} \qquad (30)$$

where C_{ext} is the extinction cross section and N is the number density of the scatterers. Hence N the number density can be calculated from the experimental measurements of τ_λ, L and calculated value of C_{ext} from the Mie theory. The number density calculated using the measured transmission is tabulated in Table 5. Similarly the scattering coefficient of the particulate media can be calculated using the scattering signal and Eqn. (23). On the other hand the scattering cross section can be calculated using the Mie theory. Then for monodisperse solution the following equation can be used to calculate the number density of polystyrene particles.

$$N = S_{vv}(p)/C_{vv}(p) \qquad (31)$$

where N is the number density (cm^{-3}), $S_{vv}(p)$ is the scattering coefficient of the particulate media ($cm^{-1}sr^{-1}$). The number density calculated using the scattering coefficient for a particular experimental run is shown in the Table 6. In Figure 21 and Figure 22 $\ln(\tau)$ and scattering coefficient at 90° respectively are plotted with respect to the number density of the polystyrene particle solution. "Theoretical" indicates the single scattering approximation of the experimental results. From Figure 22 it may be seen that experimental results of scattering coefficients are higher compared to theoretical calculations. The results in Figure 22 indicate that multiple scattering takes place at number density greater than approximately 3.0 x $10^8/cm^3$. It should be noted that the calculated number density according to Jones

and Bayvel's criteria was 1.13 x $10^8/cm^3$ and according to Nappier and Ottewill criteria the number density for 50 interparticle distance was 6.70 x $10^8/cm^3$ and for 200 interparticle distance was 1.1 x $10^7/cm^3$.

The uncertainty in the calculation of number density using scattering coefficient is 10% due to 5% random error in measurement of S_{vv}(glass, poly., water), τ_g, τ_p, τ_w and S_{vv}(gas, glass). From Table 5 it may be seen that the uncertainty in number density calculation decreases with decrease in transmission. Due to multiple scattering the number density calculated at lower transmission or at higher concentration should have higher percentage of error. This is because, in the calculation of number density, a single scattering approximation is made. According to Table 8.1 the above prediction is not observed. This may be attributed to the fact that the uncertainty at low transmission is low compared to that at high transmission. In the previous section it was concluded that the error introduced due to the approximate Equation (6) does not exceed 20% irrespective of type of agglomerate, refractive index, number of primary particles in an agglomerate and size parameter. It is to be noted that the Eqn (6) is based on the fact that the single scattering approximation between the primary particles is valid for the calculation of extinction cross section of an agglomerate. Thus, it appears that the extinction cross section in the multiple scattering region can be approximated to be equal to the extinction cross section in the single scattering region for this particular particle size. With reference to Table 6 and Figure 21 it is observed that the single scattering approximation results are close to the experimental results in the multiple scattering region. Thus it can be argued that the present experimental results validate the approximate relation (Eqn (6)).

With reference to Figure 22 it is seen that the scattering coefficient deviates more from the single scattering approximation with increase in the number density of the particles in a medium. Jones [1] suggested an approximate expression to relate the scattering cross section of an agglomerate to that of its primary particle:

$$C_{vv}(\text{agglomerate}) = N_p^2 C_{vv,s}(d_p, m_p),\ \theta = 90^\circ \qquad (32)$$

where N_p is the number of primary particle in an agglomerate, $C_{vv,s}$ is the scattering cross section of a spherical particle with diameter equal to the diameter of the primary particle (d_p) and refractive index equal to the refractive index of the primary particle (m_p). In the more general case the scattering cross section of an agglomerate may be written as:

$$C_{vv}(\text{agglomerate}) = N_p^{\alpha} C_{vv,s}(d_p, m_p),\ \theta = 90^\circ \qquad (33)$$

Where α is a function of the type of agglomerate and the agglomerate characteristics. Charalampopoulos and Chang [4] used the above expression in conjunction with the measurements from a propane oxygen flame and calculated the exponent α for straight chain and random chain agglomerate. A value of α approximately equal to 2.0 was obtained. It is to be noted that in the single scattering approximation the exponent α will be equal to 1. The higher value of exponent α indicates that in the multiple scattering region the scattering coefficient is higher than that in the single scattering region. In Figure 22 the same trend is observed. Thus the present experimental results for the scattering coefficients possess the same trends as the scattering coefficients for agglomerates (Eq. (33)).

Depolarized Scattered Intensity

The measured depolarized scattered intensities (H_v, V_h) and their ratio are plotted in Figures 23-27 and with respect to transmission and scattering angle. The depolarized intensities are seen to be approximately equal to zero at higher transmission and increase as the transmission is decreased. The H_v to V_h ratio was found to increase from higher transmission to lower transmission and then decreases. At high transmission or at single scattering limit the depolarized component of intensity is zero according to Mie theory for a spherical isotropic scatterer.

The depolarized component of intensities and their ratio are also seen to be functions of scattering angle. For 0.22 micron particle size H_v and V_h intensities decrease with increase in scattering angle whereas the H_v to V_h ratio increases and then decreases with increasing scattering angle for 0.22 micron diameter polystyrene particle. Work is underway in this laboratory to further explore the characteristics and extent of the depolarization in multiple scattering media with variable concentration and particle size.

Error Considerations

The accuracy and precision of the experimental results described in this study may be affected in several ways. The factors that may affect the accuracy are, but not limited to, polarizer leakage, polarizer wobble [43] and reflection in the scattering cell. The precision of the results is influenced by detector noise, where the detector noise depends upon the nature of the detector device and signal to noise ratio and the positioning accuracy of the polarizer.

In this experiment the signal refers to the intensity which leaves the scattering volume and reaches the detector by scattering from the sample. The magnitude of the signal is influenced by the power of the laser. Noise in the signal can be of two types: (i) noise in the light signal (ii) noise in the detector. Noise in the light signal originates from background sources such as room lights. Random fluctuations in the source intensity are also considered noise. Noise in the photomultiplier tube is caused by electrical noise associated with the anode dark current. Thus, whenever the light signal reaching the anode is lower then the signal to noise ratio may be taken into account if reliable measurements are to be obtained.

Polarizers are inserted in the beam path to effect a change in beam polarization, but these elements should not cause any displacement or change in the direction of propagation of the beam. If the plane of the polarizer is not exactly perpendicular to the beam, the beam will be displaced in much the same way that a beam is displaced when travelling through a sheet of plate glass at non-normal incidence. As the polarizer is rotated, the beam displacement will change direction ("wobble") if the rotation axis is not parallel to the normal of the polarizer face. This beam wobble causes a different portion of the light beam to be imaged onto the detector. The amount of beam "wobble" depends upon the optical path length of the polarizer (i.e. sheet thickness) and the amount the polarizer rotation axis may deviate ("wobble") from its ideal position (taken as perfectly normal to the incoming beam). During the alignment of the experimental set up due precaution is taken to minimize the "wobble". The position of the incident beam is determined on a piece of paper without the presence of the polarizer in the direction of the incident beam. Then the polarizer is aligned so that the beam, after passing through the polarizer, will reach the same reference spot marked on the paper.

Conclusions

The results of the work so far may be summarized as follows:

(1) The approximate expression for extinction cross section of an agglomerate is accurate to within 20% irrespective of the type of agglomerate, size range, and number of primary particles.

(2) The trends for scattering cross section and extinction cross section from the present experimental results are consistent with the predictions of the agglomerate model.

(3) H_v to V_h ratio depend strongly on the agglomerate parameters.

(4) This dependence may be used as a diagnostic tool for agglomerate characterization both in flames and colloidal systems.

(5) The reciprocity theorem should be reassessed in multiple scattering environment.

References

1. A.R. Jones. Scattering efficiency factors for agglomerates of small spheres. *J. Phys.D: Appl. Phys.*, 12:1661-1672, 1979.
2. A.R. Jones. Electromagnetic wave scattering by assemblies of particles in the rayleigh approximation. *Proc. R. Soc. London. A.*, 366:111-127, 1979.
3. H. Chang and T. T. Charalampopoulos. Determination of the wavelength dependence of refractive indices of flame soot. *Proc. R. Soc. London*, 430:577-591, 1990.
4. T. T. Charalampopoulos and H. Chang. Agglomerate parameters and fractal dimension of soot using light scattering effects on surface growth. *Combustion and Flame*, 1991.
5. T. T. Charalampopoulos and H. Chang. Effects of soot agglomeration on radiative transfer. *J. Quant. Spectrosc. Radiat. Transfer*, 46 NO. 3:125-134, 1990.
6. T. T. Charalampopoulos. Morphology and dynamics of agglomerated particulates in combustion systems using light scattering techniques. *Prog. Energy combust. Sci.*, 18:13-45, 1992.
7. Jerry C. Ku. Correction for the extinction efficiency factors given by the jones solution for electromagnetic scattering by agglomerates of small spheres. *Journal of Physics. D: Appl. Physics*, 24:71-75, 1991.
8. A. R. Jones and W. Wong. Direct optical evidence for the presence of sooty agglomerates in flames. *Combustion and Flame*, 24:139-140, 1975.
9. G. Prado. Physical aspects of nucleation and growth of soot particles. *Particulate Carbon*, pages 143-175, 1981.
10. S. Levine and G. O. Olaofe. *Journal of Colloid and Interface science*, 27, 1968.
11. A. Lips and S. Levine. Light scattering by two spherical Rayleight particles over all orientations. *Journal of Colloid and Interface Science*, 46 No. 1:139-146, 1974.
12. J. C. Ravey. Light scattering by aggregates of small dielectric or absorbing spheres. *Journal of Colloid and Interface Science*, 1: 139-146, 1974.
13. J. C. Ravey. Computer simulation of morphological and optical properties of aggregates of spheres. *Journal of Colloid and Interface Science*, 50 No. 3:545-558, 1975.
14. D. Felske, Pei-Feng Hsu, and J. C. Ku. The effect of soot particle optical inhomogenity and agglomeration on the analysis of light scattering measurements in flames. *J. Quant. Spectrosc. Radiat. Transfer*, 35, No. 6:447-465, 1986.
15. L. Lamia. An investigation of soot morphologies and volume fractions using classical light scattering. *MS Thesis*, LSU, 1990.
16. G. D. Ulrich and N. S. Subramanian. Particle growth in flames and coalescence as a rate controlling process. *Combustion Science and Technology*, 17:119-127, 1977.
17. J. Lahaye and G. Prado. Morphology and internal structure of soot and carbon blacks. *Combustion Science and Technology*, pages 33-51, 1981.
18. D. M. Roessler, F. R. Faxvog, R. Stevenson, and G.W. Smith. Optical properties and morphology of particulate carbon. *Particulate and Carbon*, pages 57-84, 1981.
19. A. D' Alessio. Laser light scattering and fluorescence diagnostics of rich flames produced by gaseous and liquid fuels. *Particulate Carbon*, pages 207-256, 1981.
20. G. Prado, J. Jagoda, K. Neoh, and J. Lahaye. A study of soot formation in premixed propane/oxygen flames by in-situ optical techniques and sampling probes. *Eighteenth Symposium (international) on combustion*, pages 1127-1136, 1981.

21. C. M. Megaridis and R. A. Dobbins. Comparison of soot growth and oxidation in smoking and nonsmoking ethylene diffusion flames. *Combustion Science and Technology*, 66:1-16, 1989.
22. R. S. Krishnan. Influence of secondary scattering on depolarization measurements. *Proc. Ind. Acad. Sci.*, pages 303-308, 1939.
23. R. S. Krishnan. Scattering of polarized light in colloids. *Proc. Ind. Acad. Sci.*, pages 395-398, 1939.
24. R. S. Krishnan. The reciprocity theorem in colloid optics and its generalisation. *Proc. Ind. Acad. Sci. A*, VII:21-34, 1938.
25. R. S. Krishnan. Studies of light scattering in emulsions. *Proc. Ind. Acad. Sci. A*, pages 98-103, 1938.
26. D. V. Saxon. Tensor scattering matrix for the electromagnetic field. *Physical Review*, 100 No. 6:1771-1775, 1955.
27. D. S. Saxon. Radiation and remote probing of atmosphere. *N A S A CR 140816*, pages 111-127, 1974.
28. F. Perrin. Polarization of light scattered by isotropic opalescent media. *Journal of Chemical Physics*, 10:415-427, 1942.
29. A. R. Jones. Correction to 'electromagnetic wave scattering by assemblies of particles in the Rayleigh approximation'. *Proc. R. Soc. Lond.*, A 375:453-454, 1981.
30. C. Smart, R. Jacobsen, M. Kerker, J. P. Kratohvil, and E. Matijevic. Experimental study of multiple scattering. *Journal of the optical society of America*, Vol-55 NO. 8-947-955, 1965.
31. S. W. Churchill, G. C. Clark, and C. M. Sliepcevich. Light scattering by very dense monodispersions of latex particles. *Discussions of Faraday Soc.*, Vol-30 NO. 192:192-199, 1960.
32. Milton Kerker. The scattering of light and other electromagnetic radiation. *Academic press*, 1969.
33. L. P. Bayvel and Jones A. R. *Electromagnetic scattering and its application*, 1981.
34. M. Kerker and E. Matijevic. Light scattering of monodispersed polystyrene latexes. *Journal of the optical society of America*, Vol-50:722-729, 1960.
35. S. H. Moron, P. E. Pierce, and I. N. Usevitch. Determination of latex particle size by latex particle size by light scattering. *Journal of colloid science*, Vol-18:470-482, 1963.
36. D. H. Napper and R. H. Ottewill. Multiple scattering effects in polystyrene latex dispersions. *Journal of colloid science*, Vol-19:72-80, 1964.
37. C. Konak, J. Jakes, P. Stepanek, F. Petras, M. Karska, J. Krepelka, and J. Perina. Effect of soot agglomeration on radiative transfer. *Applied Optics*, Vol-30 NO. 33:4865-4871, 1991.
38. R. Siegel and J. R. Howell. Thermal radiation heat transfer. *Hemisphere publishing corporation*, 1981.
39. R. R. Rudder and D. R. Bach. Rayleigh scattering of ruby-laser light by neutral gases. *Journal of the optical society of America*, 58, 1968.
40. D. Kent. *Combustion and Flame*, 47:53, 1982.
41. J. Bartels, H. Borchers, and H. Hausen. Zahlenwerte and funktionen aus. *Landolt-Bornstein*, 1962.
42. M. P. Bogard, A. D. Buckingham, R. K. Pierens, and A. H. White. Rayleigh scattering depolarization ratio and molecular polarizability anisotropy for gases. *J. C. S. Faraday*, 74:3008-3015, 1978.
43. B. J. Stagg. Development of a technique to determine the temperature dependence of the refractive index of carbonaceous particulates. *Ph.D. dissertation*, LSU, 1992.

Table 1: Percentage difference in extinction cross section for random chain for diameter of primary particles = 0.01556 micron.

Number of primary particles	% Error with correction m = 2.0 + 1.0i	% Error with correction m = 1.4 + 0.4i
3	-0.334	-0.722
6	-3.641	0.611
9	-0.793	1.141
12	-2.466	0.489
15	-3.451	0.501
18	-3.176	0.489
21	-0.811	0.592
24	-2.180	0.957
27	-1.362	0.900
30	-1.877	-0.138

Table 2: Percentage difference in extinction cross section for random chain for number of primary particles N_p = 18 and m = 2.0 + 1.0i, 1.4 + 0.4i.

Size parameter x_p	% Error* m = 2.0 + 1.0i	% Error* m = 1.4 + 0.4i
0.0050	-2.983	0.354
0.0155	-3.630	0.570
0.0260	-4.708	0.269
0.0366	-2.159	0.326
0.0472	-5.111	0.173
0.0577	-2.147	0.757
0.0683	-3.516	0.564
0.0788	-1.842	1.187
0.0893	-2.021	0.592
0.1000	-0.650	0.645

*The percentage error is defined as $\frac{C_{e,a}[\text{Eq.(6)}] - C_{e,a}[\text{Eq.(7)}]}{C_{e,a}[\text{Eq.(7)}]} \times 100$

Table 3: Agglomerate parameters from the reference [4]

Height above the burner H in mm	Primary particle diameter d_p in micron	Number of primary particles(N_p)	Number of agglomerates $x10^{10}cm^{-3}$	Refractive index (m = n+ik)
6	0.0156	17	1.2	1.6 + 0.53i
10	0.0232	21	0.49	1.73 + 0.64i
12	0.0257	22	0.4	1.73 + 0.64i
16	0.0287	24	0.31	1.73 + 0.64i

Table 4: Maximum number density for no electrical interaction according to the interparticle distance criterion using Eq. (16).

Diameter in Micron	Maxm. number density(n=3) in 1/cc	Maxm. number density(n=2) in 1/cc
0.0155	3.983×10^{15}	0.944×10^{16}
0.0500	1.190×10^{14}	2.825×10^{14}
0.1000	1.490×10^{13}	3.500×10^{13}
0.1100	1.120×10^{13}	2.650×10^{13}
0.2200	1.401×10^{12}	3.321×10^{12}
0.4400	0.175×10^{12}	0.415×10^{12}
0.5000	0.119×10^{12}	0.282×10^{12}
1.0000	1.492×10^{10}	3.535×10^{10}
10.0000	1.492×10^{7}	3.537×10^{7}

Table 5: Number density calculated using transmission measurement of polystyrene solution of diameter 0.22 micron with path length equal to 11.4 cm.

Transmission	Actual number density(cm^{-3}) N_{ac}	Number density from transmission $N_{tr}(cm^{-3})$	$(1.0 - N_{tr}/N_{ac}) * 100$	Percent uncertainty
0.950	0.422×10^{8}	0.578×10^{8}	-37.010	98.480
0.933	0.703×10^{8}	0.785×10^{8}	-11.654	72.546
0.889	0.126×10^{9}	0.134×10^{9}	-6.007	42.496
0.831	0.210×10^{9}	0.211×10^{9}	-0.189	27.008
0.762	0.308×10^{9}	0.308×10^{9}	-0.064	18.395
0.676	0.420×10^{9}	0.446×10^{9}	-6.189	12.769
0.598	0.559×10^{9}	0.585×10^{9}	-4.758	9.730
0.517	0.725×10^{9}	0.751×10^{9}	-3.710	7.579
0.406	0.999×10^{9}	0.102×10^{10}	-2.710	5.546
0.320	0.127×10^{10}	0.129×10^{10}	-1.808	4.397
0.201	0.181×10^{10}	0.182×10^{10}	-0.883	3.119
0.127	0.234×10^{10}	0.234×10^{10}	-0.085	2.431
0.082	0.286×10^{10}	0.284×10^{10}	0.593	2.001
0.043	0.363×10^{10}	0.357×10^{10}	1.541	1.592

Table 6: Number density calculated using scattering measurements at 90° from polystyrene solution of diameter 0.22 micron with path length equal to 11.4cm.

Transmission	Actual number density (cm^{-3}) N_{ac}	Number density from scattering N_{sc} (cm^{-3})	$(1.0 - N_{sc}/N_{ac}) * 100$
0.950	0.422×10^8	0.488×10^8	-15.676
0.933	0.703×10^8	0.855×10^8	-21.588
0.889	0.126×10^9	0.153×10^9	-21.343
0.831	0.210×10^9	0.260×10^9	-26.638
0.762	0.308×10^9	0.398×10^9	-29.108
0.676	0.420×10^9	0.568×10^9	-35.301
0.598	0.559×10^9	0.783×10^9	-40.232
0.517	0.725×10^9	0.106×10^{10}	-46.482
0.406	0.999×10^9	0.156×10^{10}	-56.415
0.320	0.127×10^9	0.211×10^{10}	-66.352
0.201	0.181×10^9	0.346×10^{10}	-91.220
0.127	0.234×10^9	0.513×10^{10}	-119.128
0.082	0.286×10^9	0.722×10^{10}	-152.006
0.043	0.363×10^9	0.115×10^{11}	-218.932

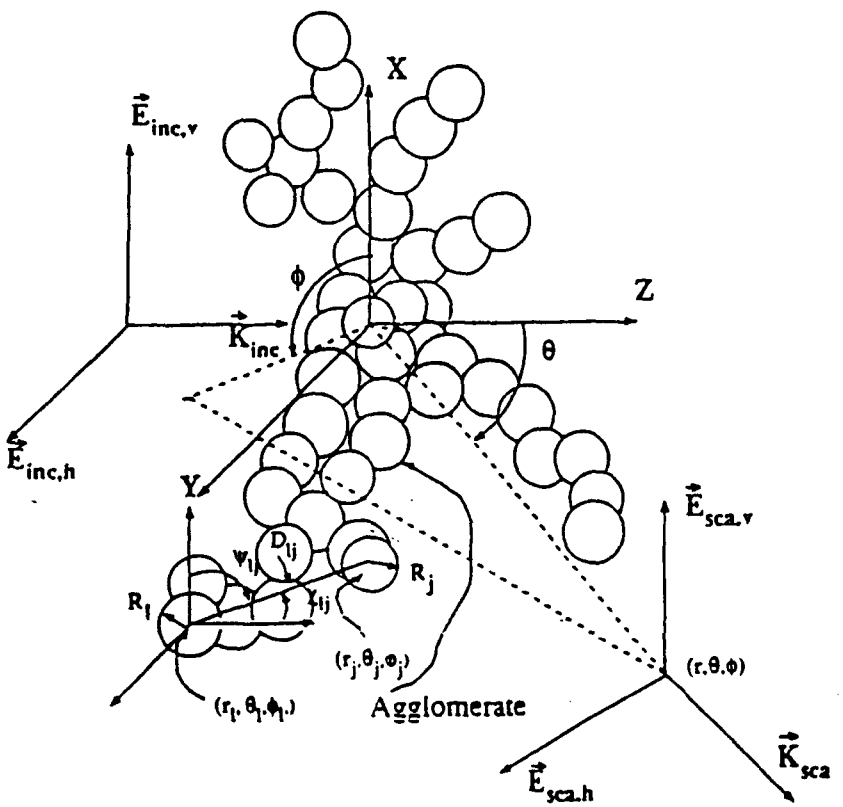

Figure 1: Representation of geometry of agglomerates of small spheres.

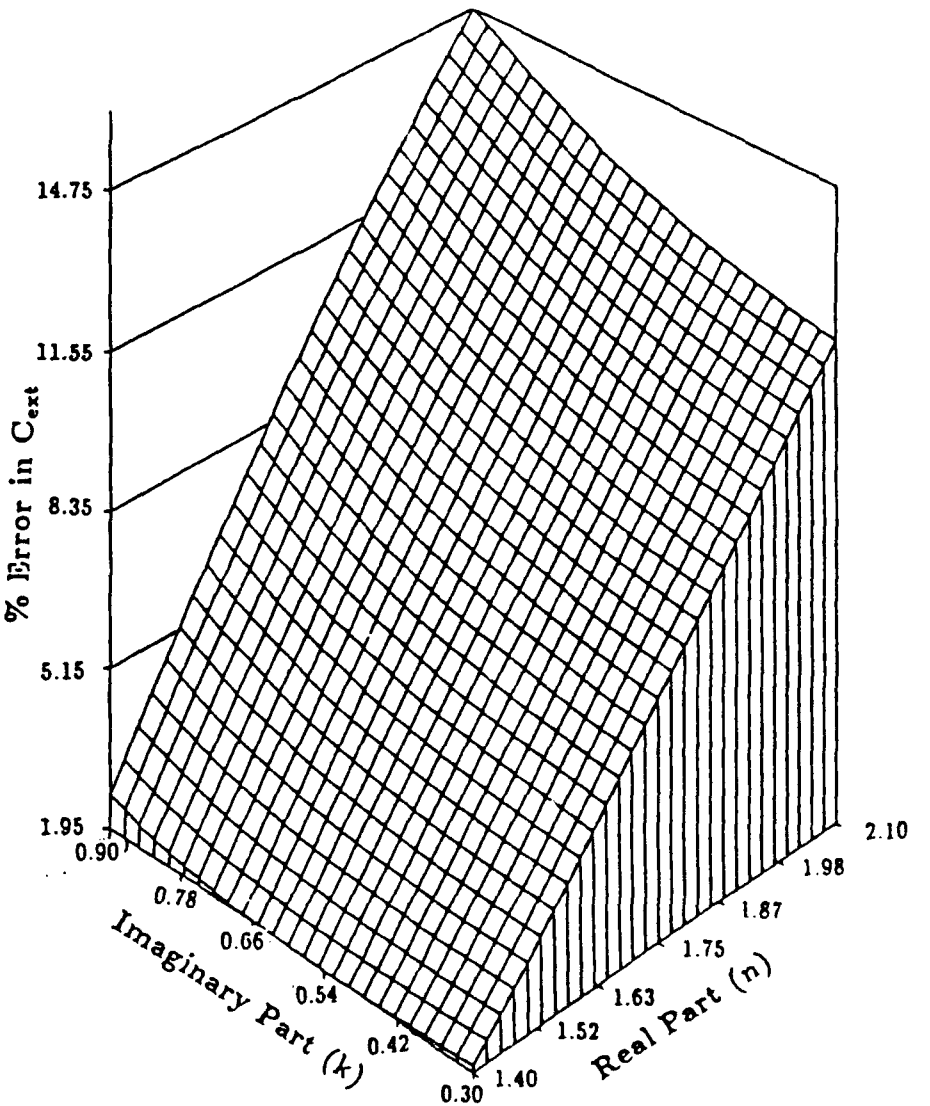

Figure 2: Percentage error in extinction cross section of straight chain (N_p = 10 and size parameter = 0.01).

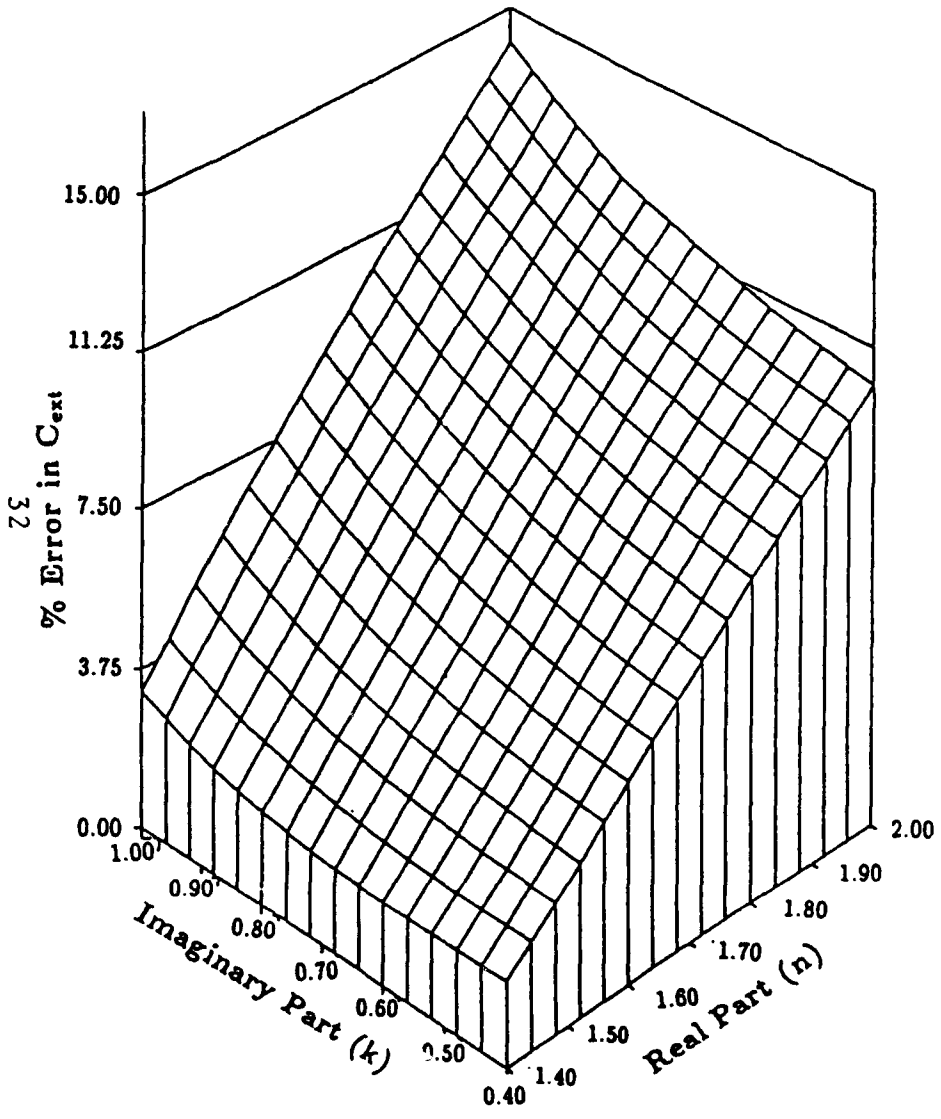

Figure 3: Percentage error in extinction cross section of straight chain (N_p = 10 and size parameter x_p = 0.05).

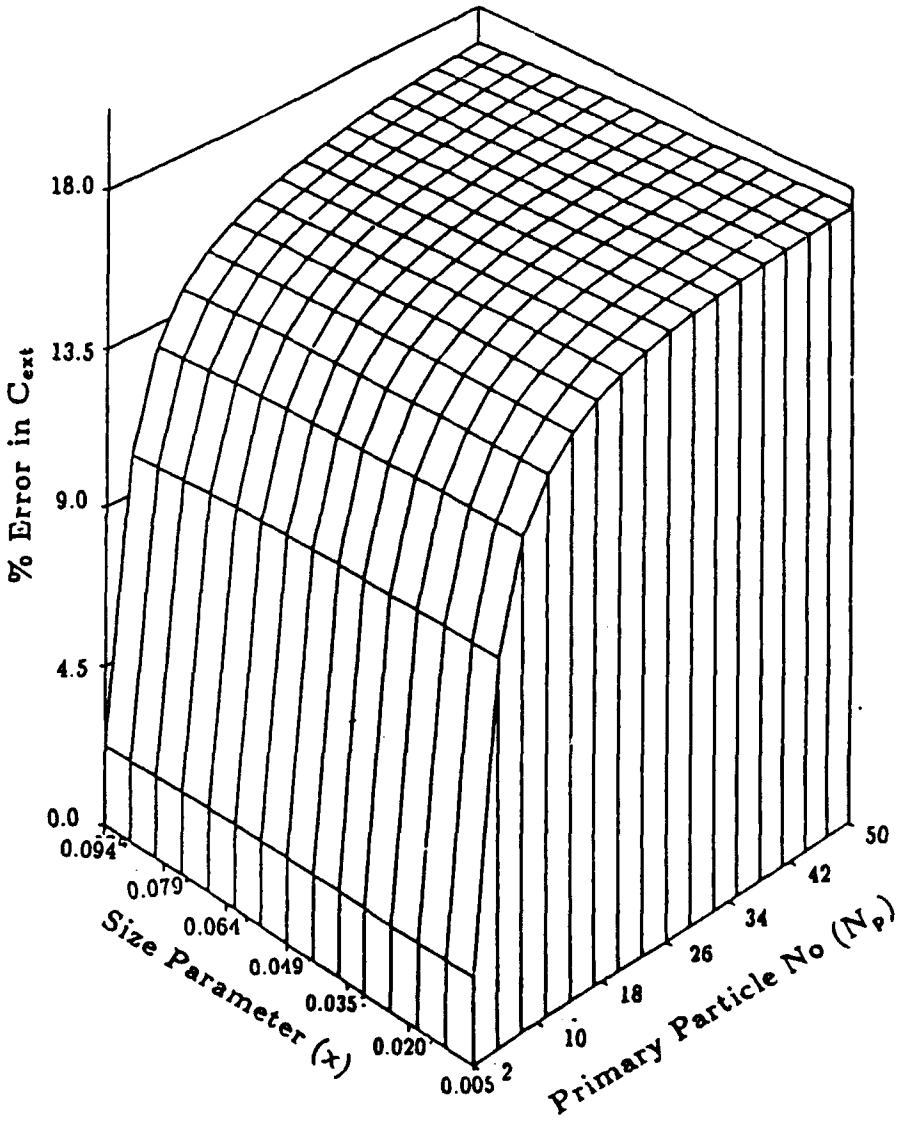

Figure 4: Percentage error in extinction cross section of straight chain (m = 2.0 + 1.0i).

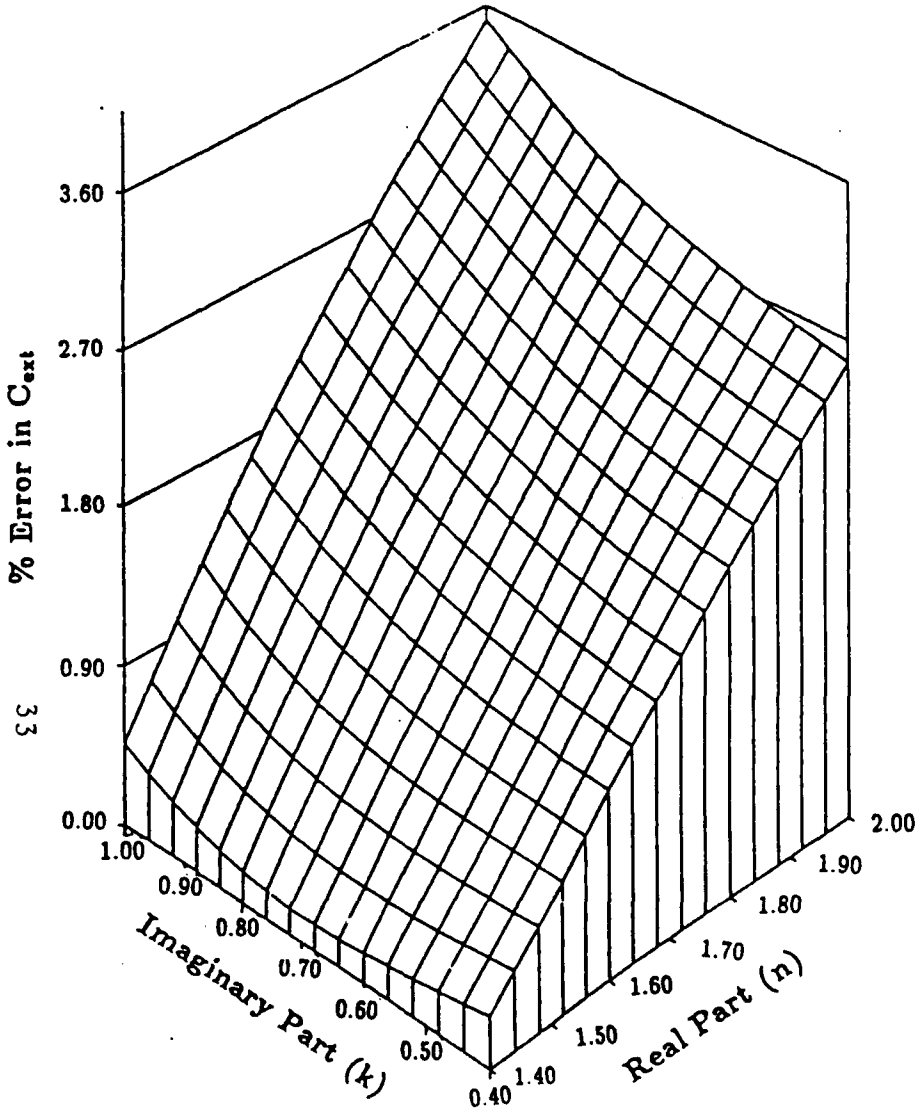

Figure 5: Percentage error in extinction cross section of cluster (N_p = 10 and size parameter x_p = 0.01).

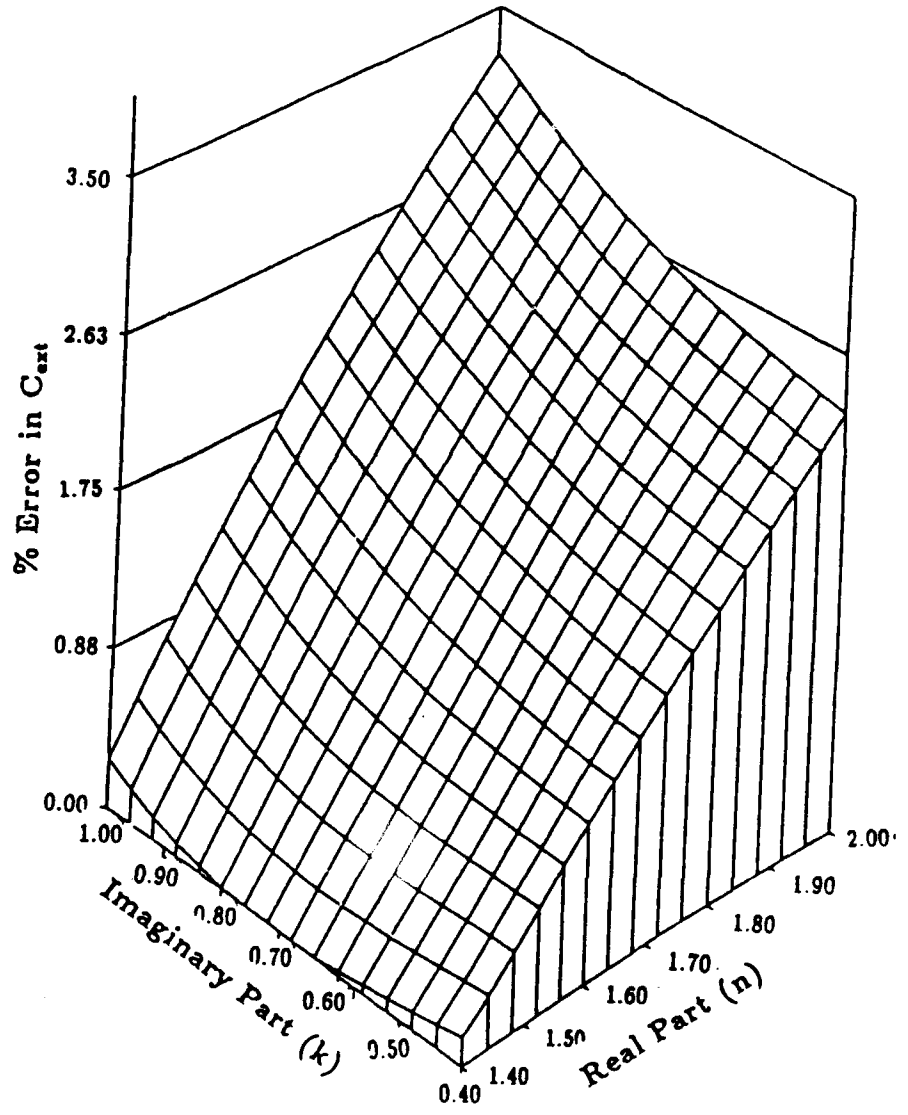

Figure 6: Percentage error in extinction cross section of cluster (N_p = 10 and size parameter x_p = 0.05).

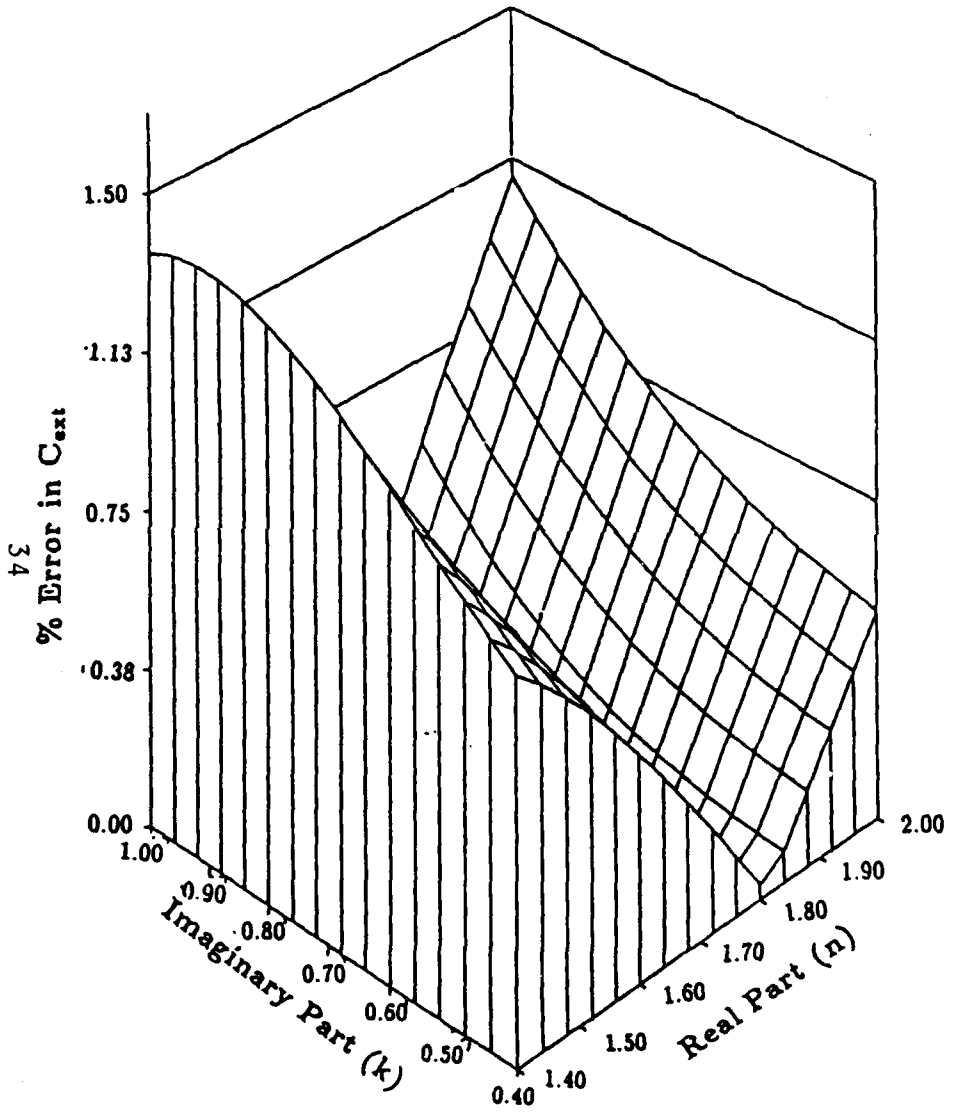

Figure 7: Percentage error in extinction cross section of cluster (N_p = 30 and size parameter x_p = 0.01) with correction.

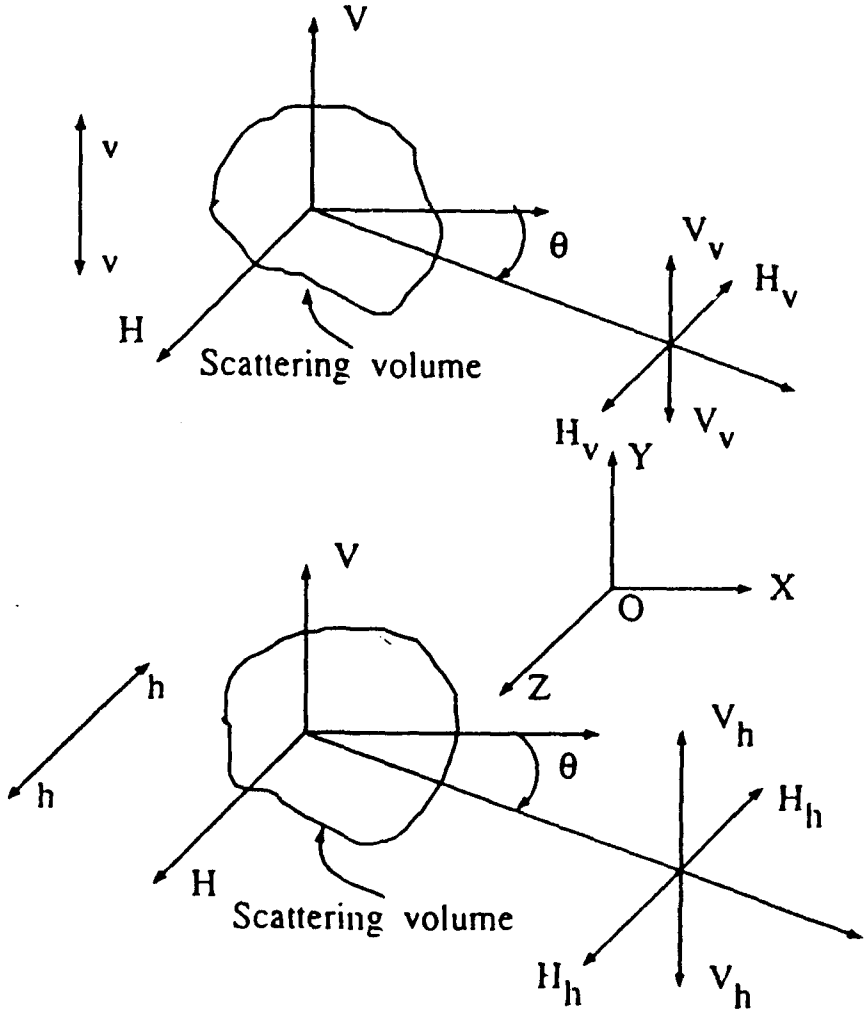

Figure 8: Reciprocity theorem nomenclature.

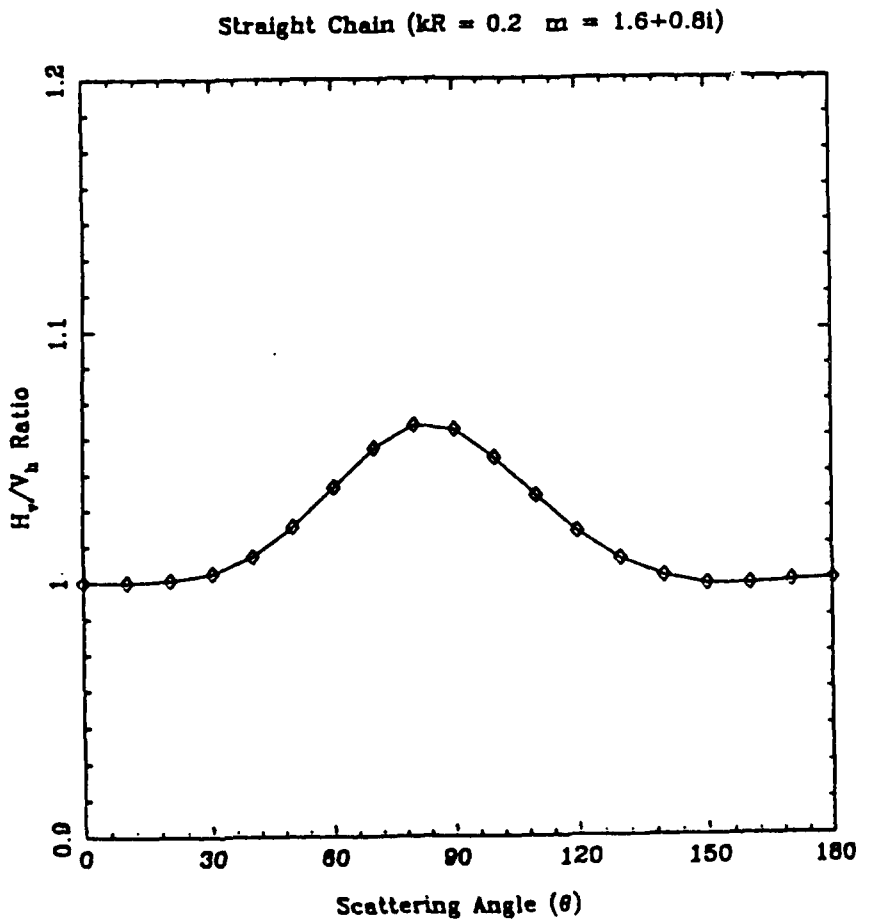

Figure 9: H_v to V_h ratio with respect to scattering angle for straight chain (kr = 0.2, m = 1.6 + 0.8i, N_p = 10).

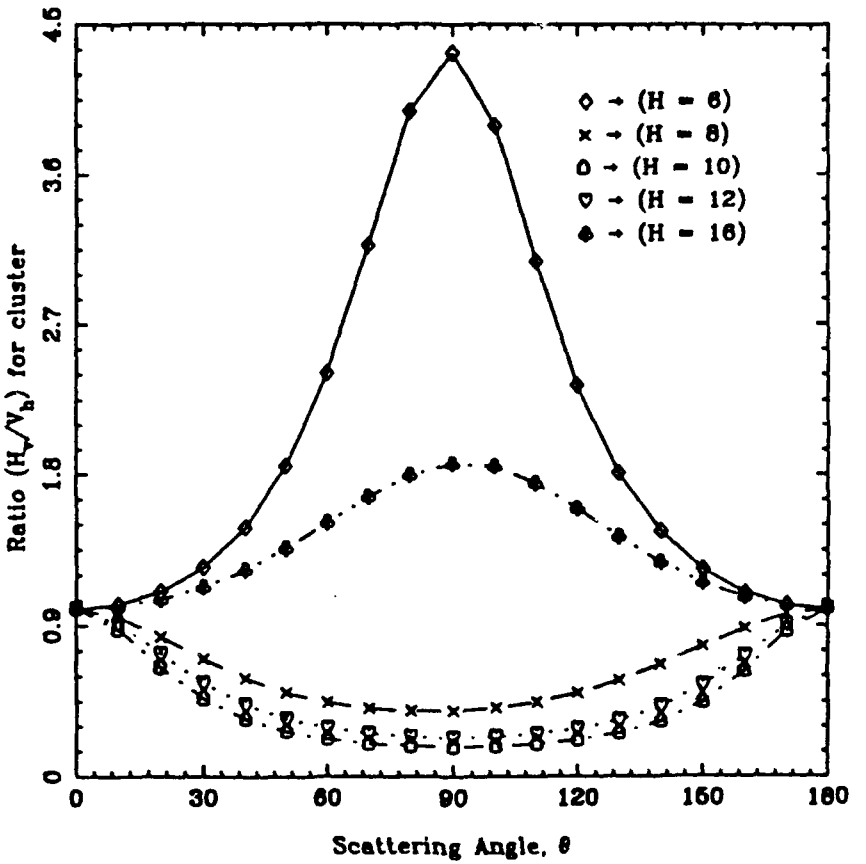

Figure 10: H_v to V_h ratio with respect to scattering angle for cluster at different flame heights (H).

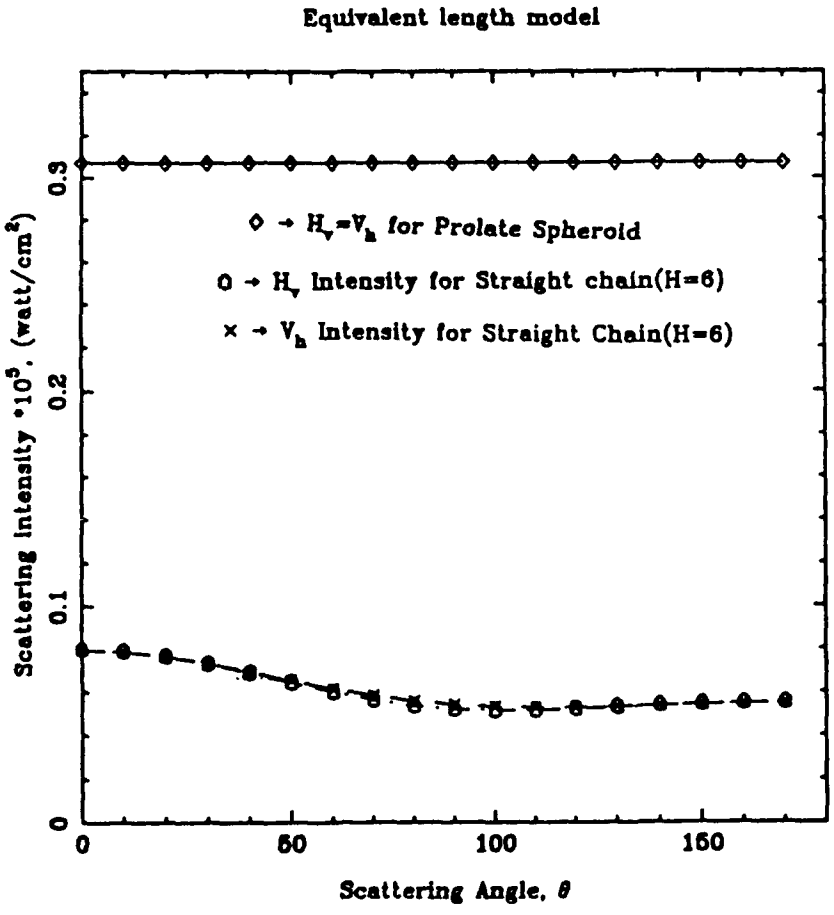

Figure 12: Equivalent length prolate spheroid model for straight chain at 6mm flame height for depolarized component of scattered intensity.

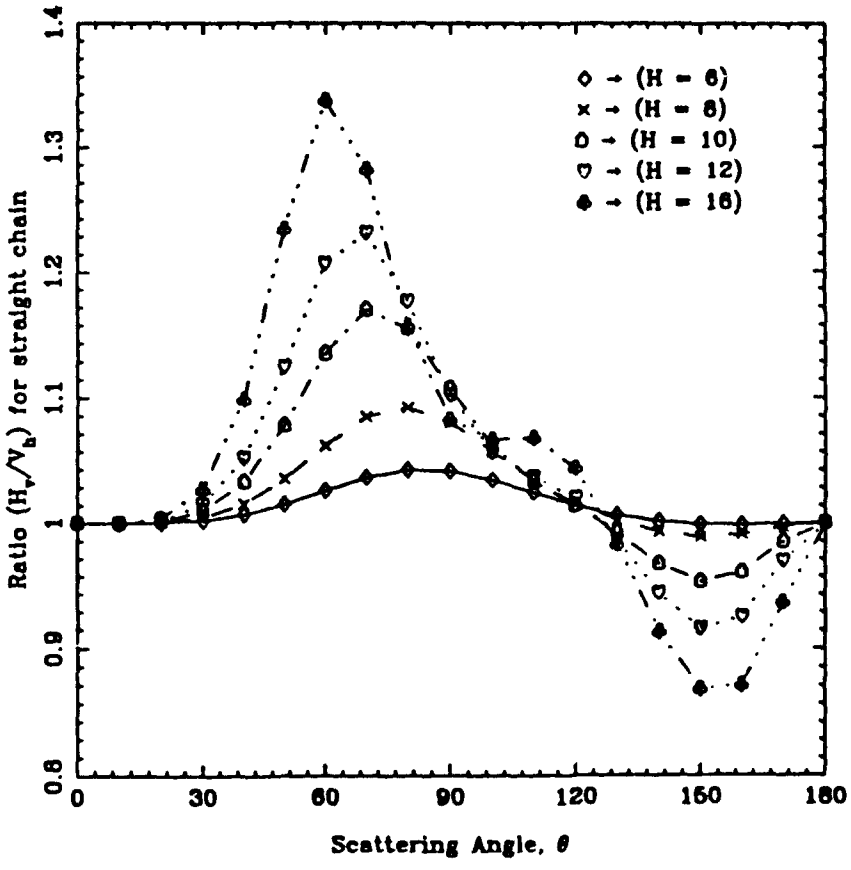

Figure 11: H_v to V_h ratio with respect to scattering angle for straight chain at different flame heights (H).

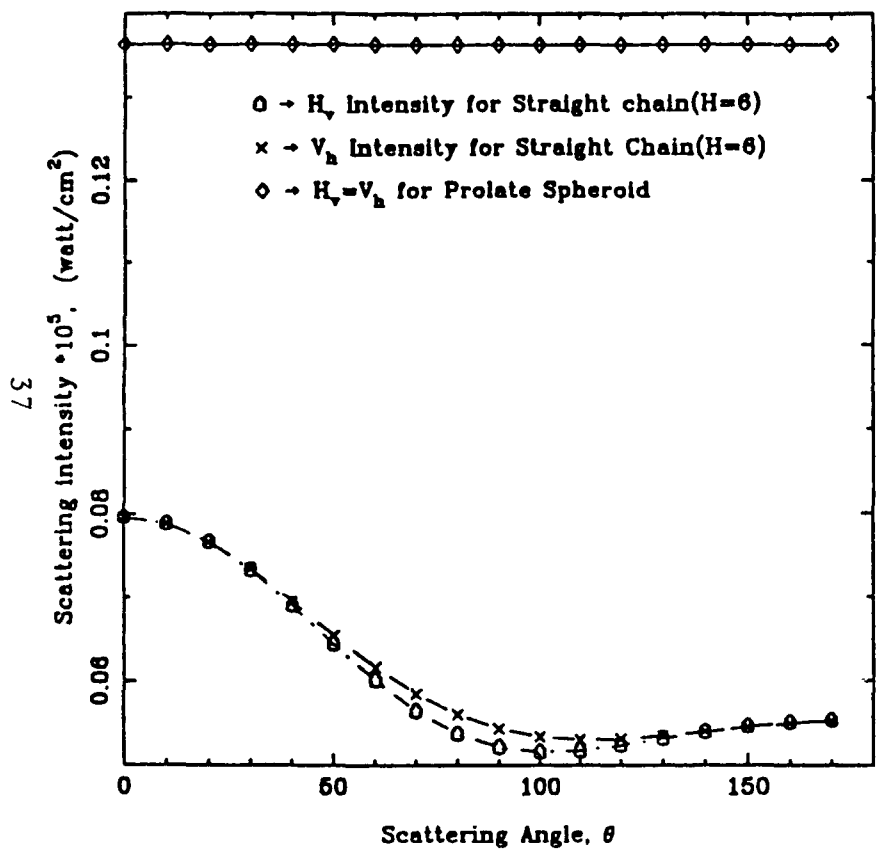

Figure 13: Equivalent volume prolate spheroid model for straight chain at 6mm flame height for depolarized component of scattered intensity.

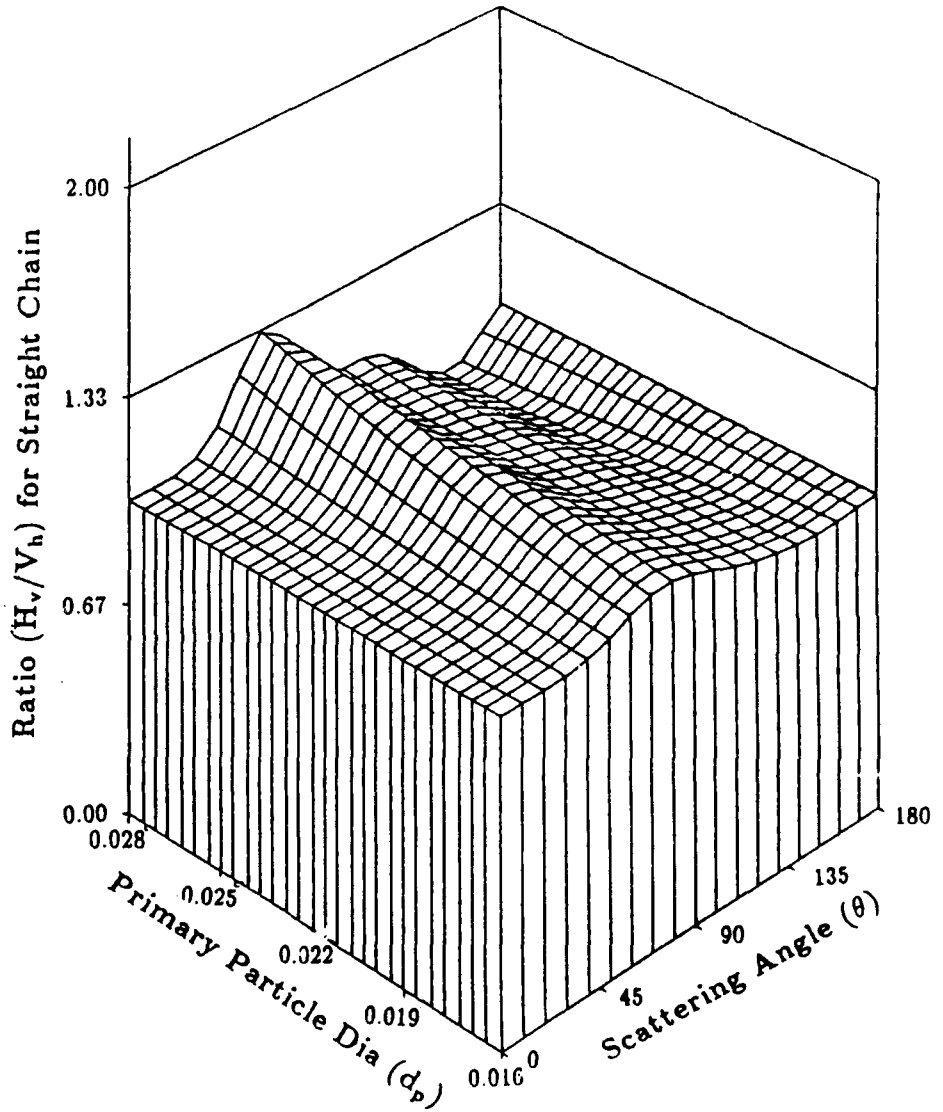

Figure 14: H_v to V_h ratio with respect to scattering angle and diameter for straight chain (N_p = 24, m = 1.73 + 0.64i).

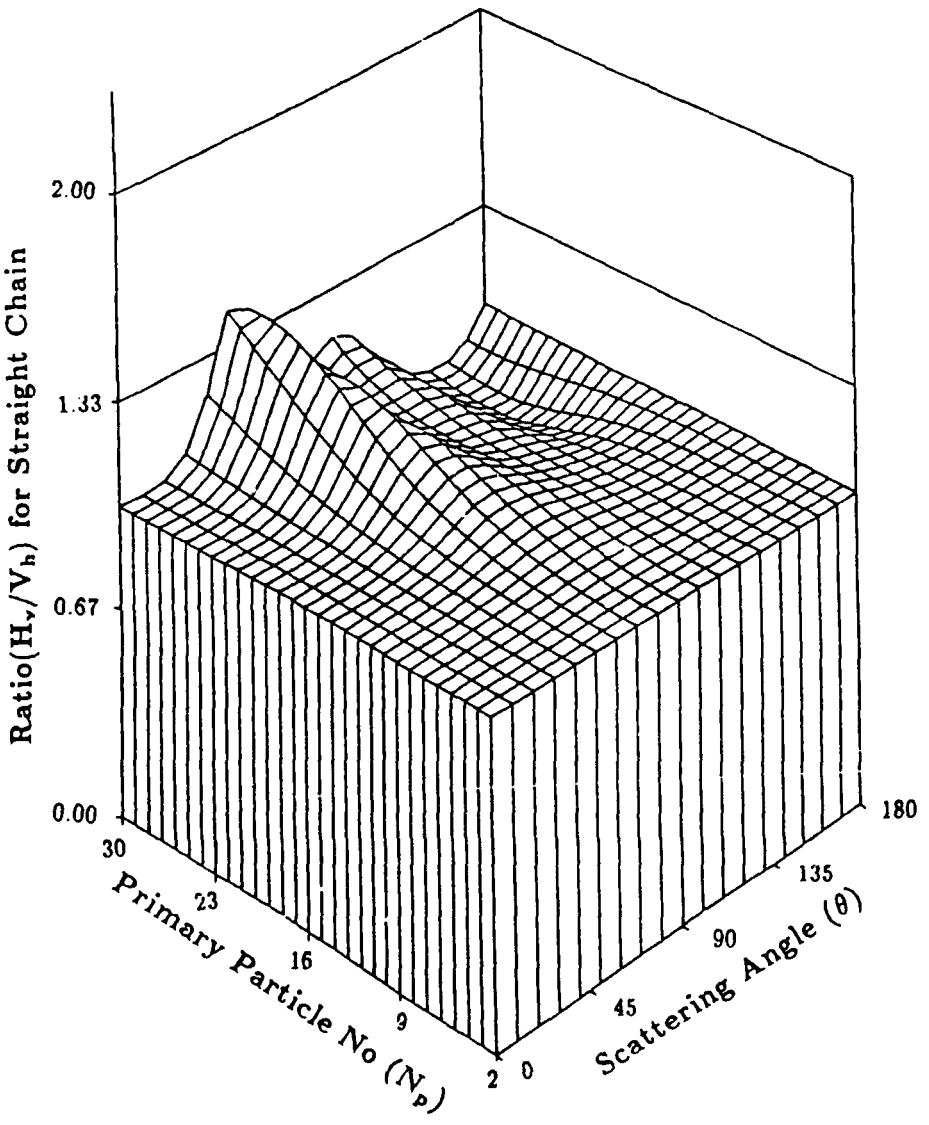

Figure 15: H_v to V_h ratio with respect to scattering angle and number of primary particles for straight chain (dia = 0.0287 μm, m = 1.73 + 0.64i).

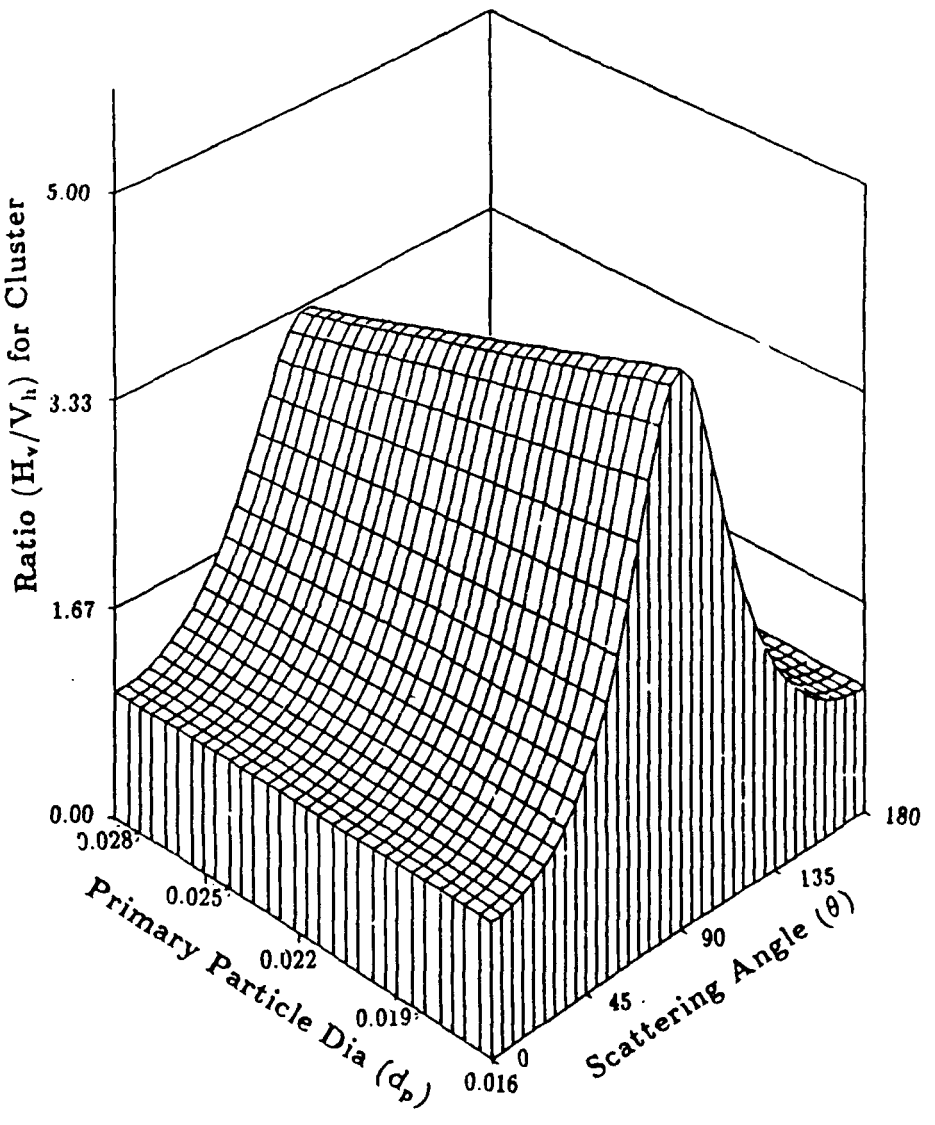

Figure 16: H_v to V_h ratio with respect to scattering angle and diameter for cluster (N_p = 17, m = 1.6 + 0.53i).

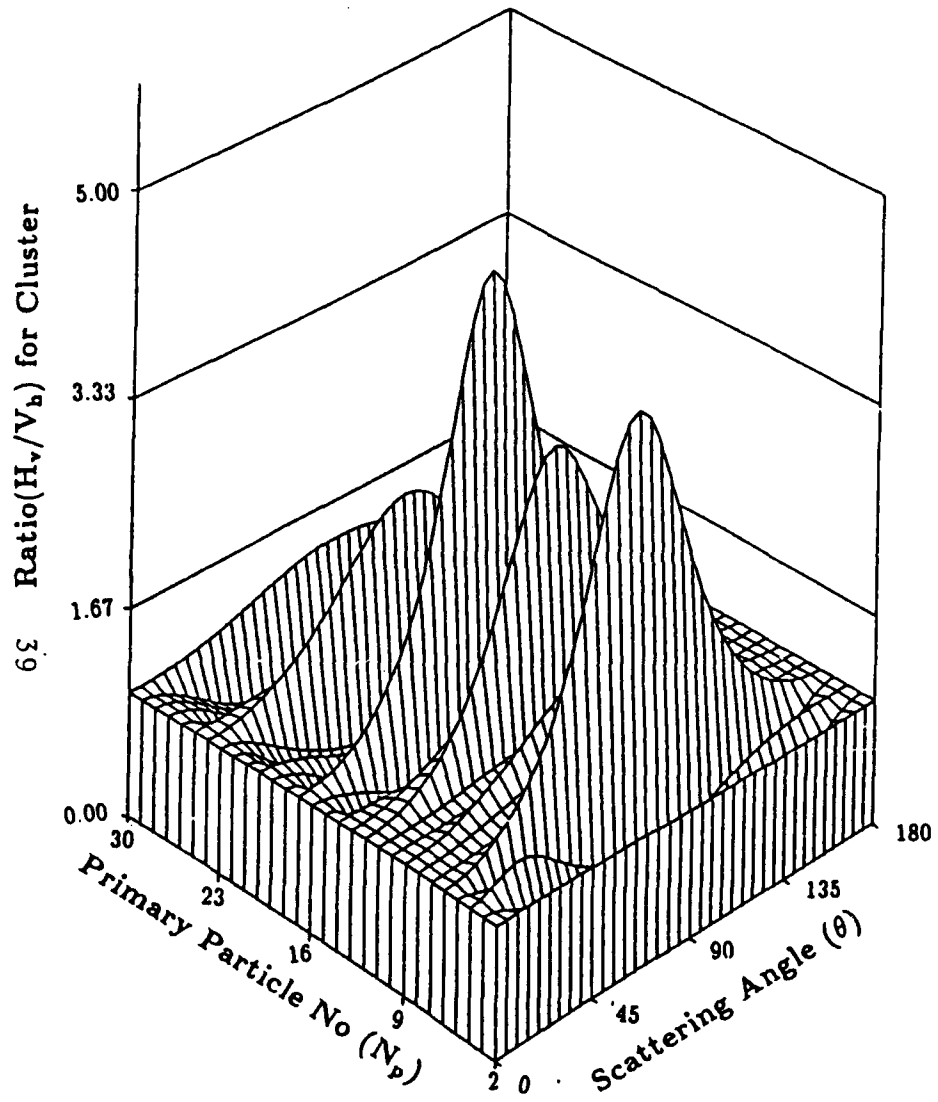

Figure 17: H_v to V_h ratio with respect to scattering angle and number of primary particles for cluster (dia = 0.0156 μm, m = 1.6 + 0.53i).

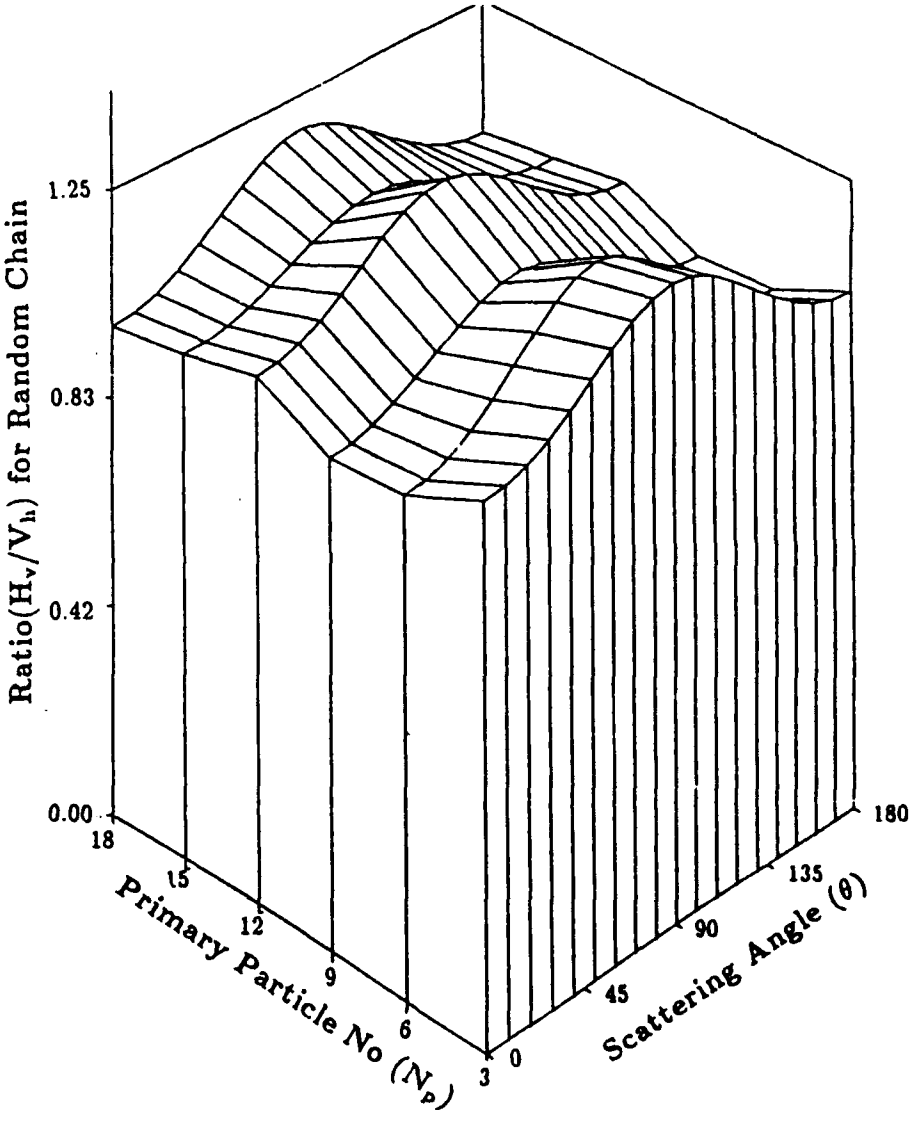

Figure 18: H_v to V_h ratio with respect to scattering angle and number of primary particles for random chain (dia = 0.0156 μm, m = 1.6 + 0.53i).

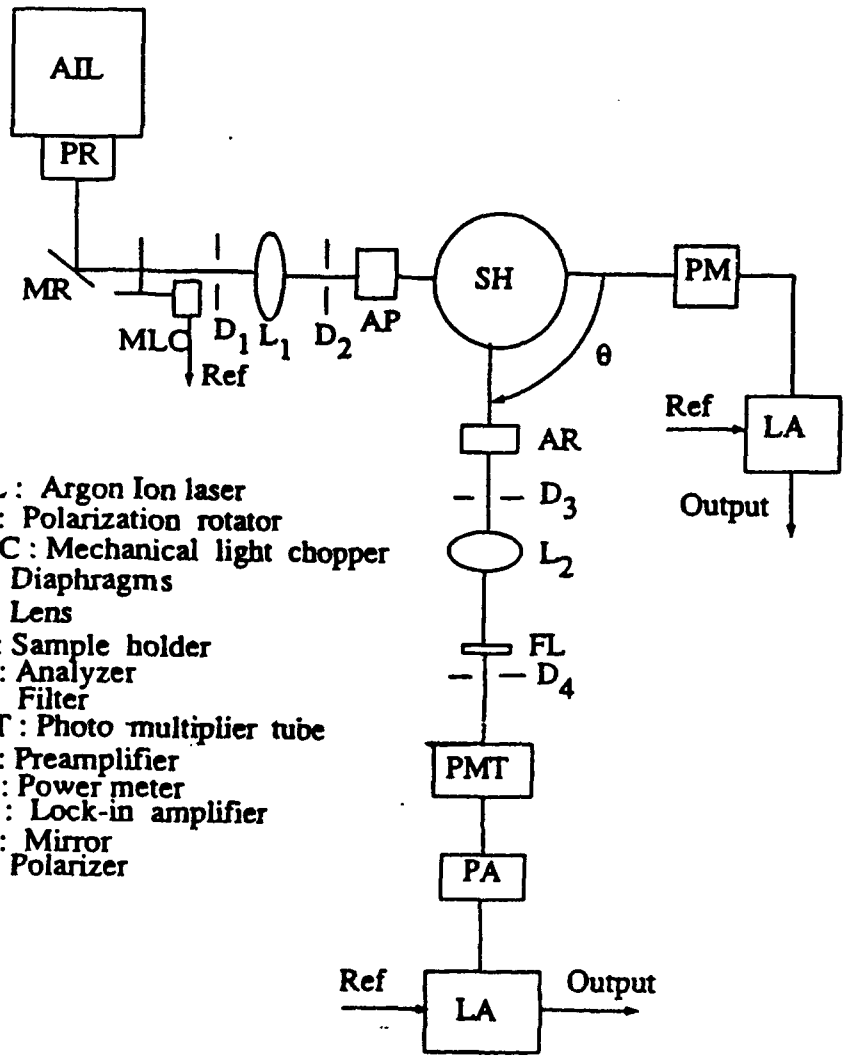

Figure 19: Schematic of the light scattering system

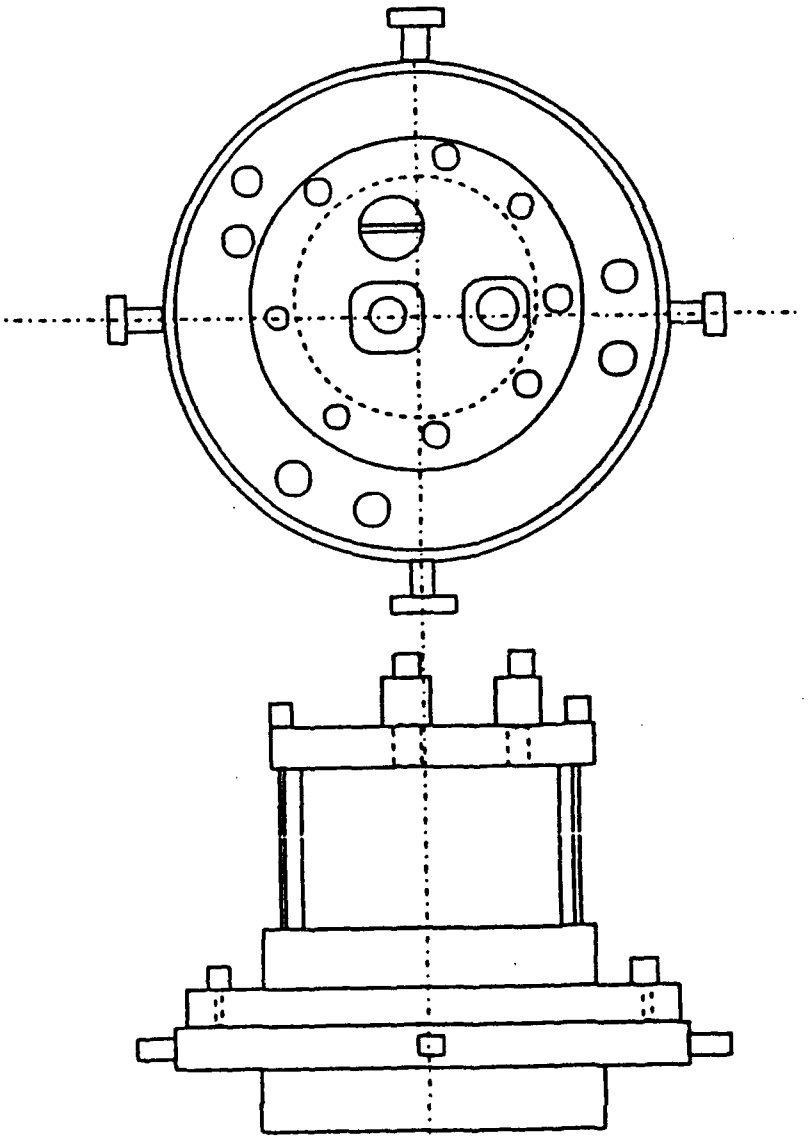

Figure 20: Front and top view of the scattering cell and its holder assembly.

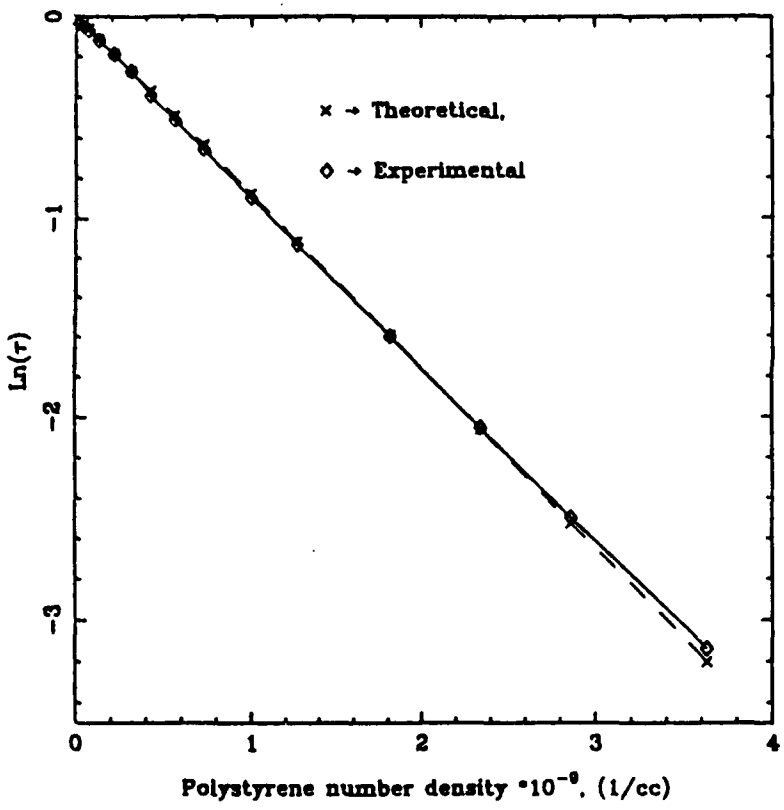

Figure 21: Ln(τ) versus number density (cm^{-3}) plot of experimental results and single scattering theoretical results.

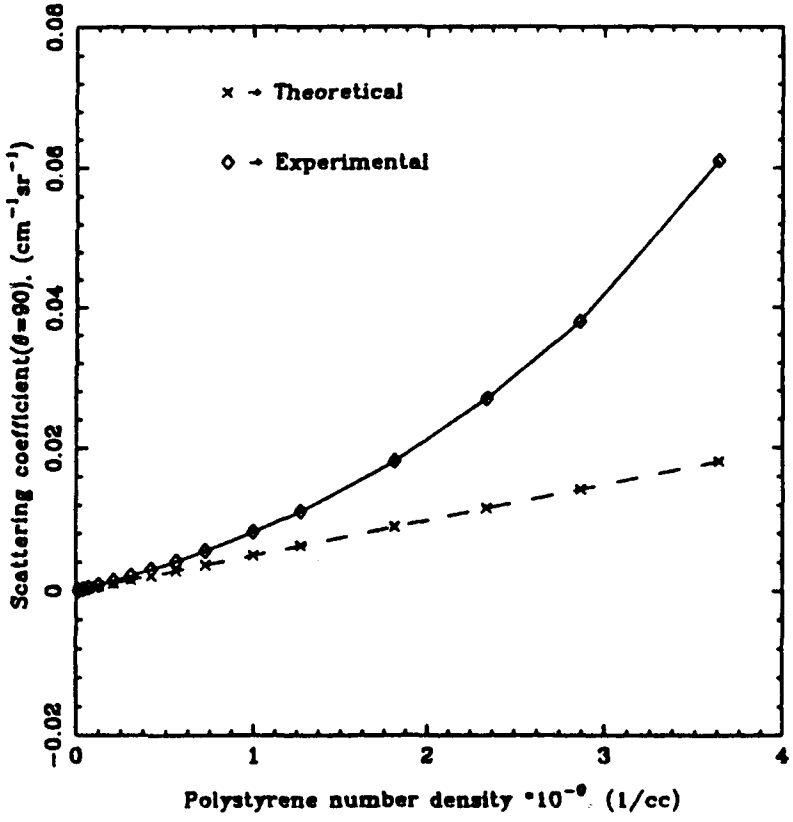

Figure 22: Scattering coefficient (θ=90) versus number density (cm^{-3}) plot of experimental results and single scattering theoretical results.

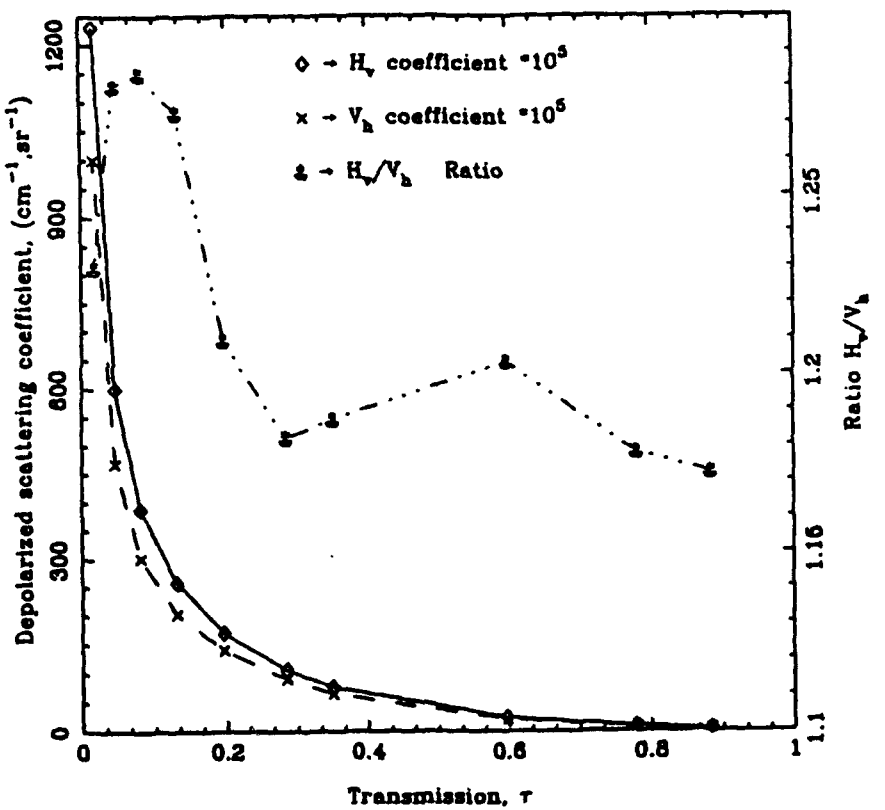

Figure 23: Depolarized scattering coefficient and their ratio versus transmission of 0.22 micron spheres at 50° scattering angle.

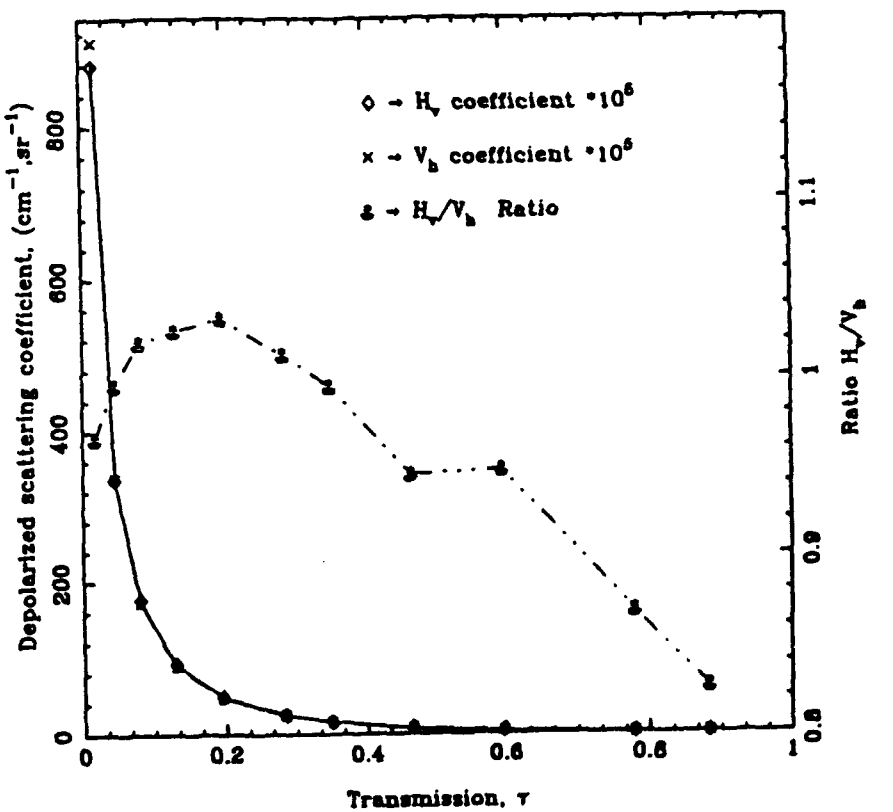

Figure 24: Depolarized scattering coefficient and their ratio versus transmission of 0.22 micron spheres at 90° scattering angle.

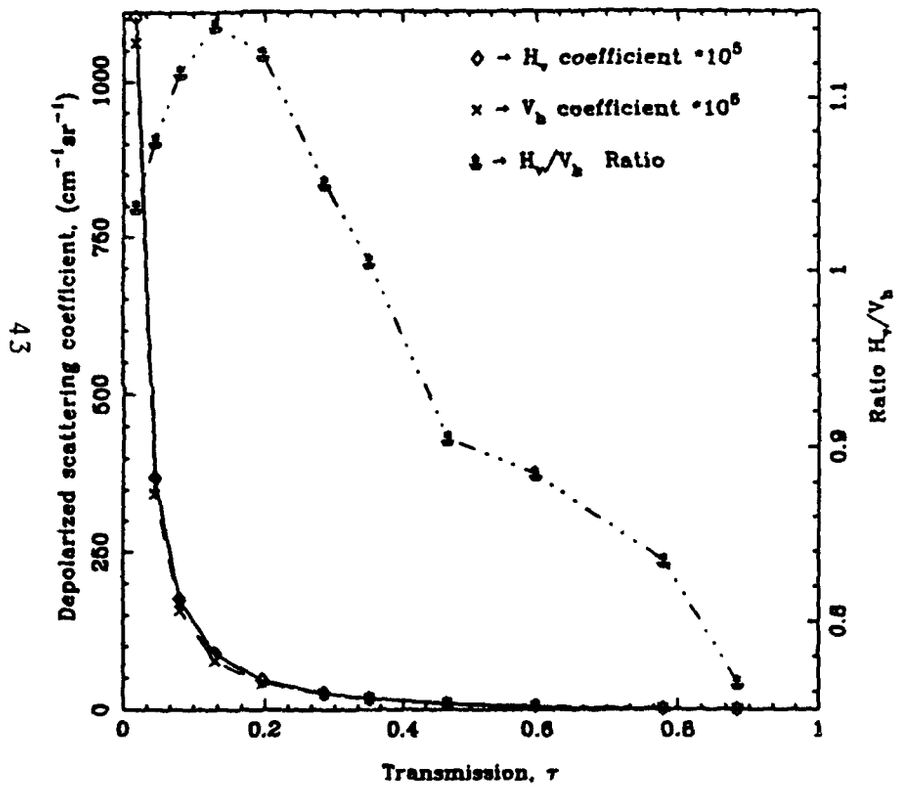

Figure 25: Depolarized scattering coefficient and their ratio versus transmission of 0.22 micron spheres at 110° scattering angle.

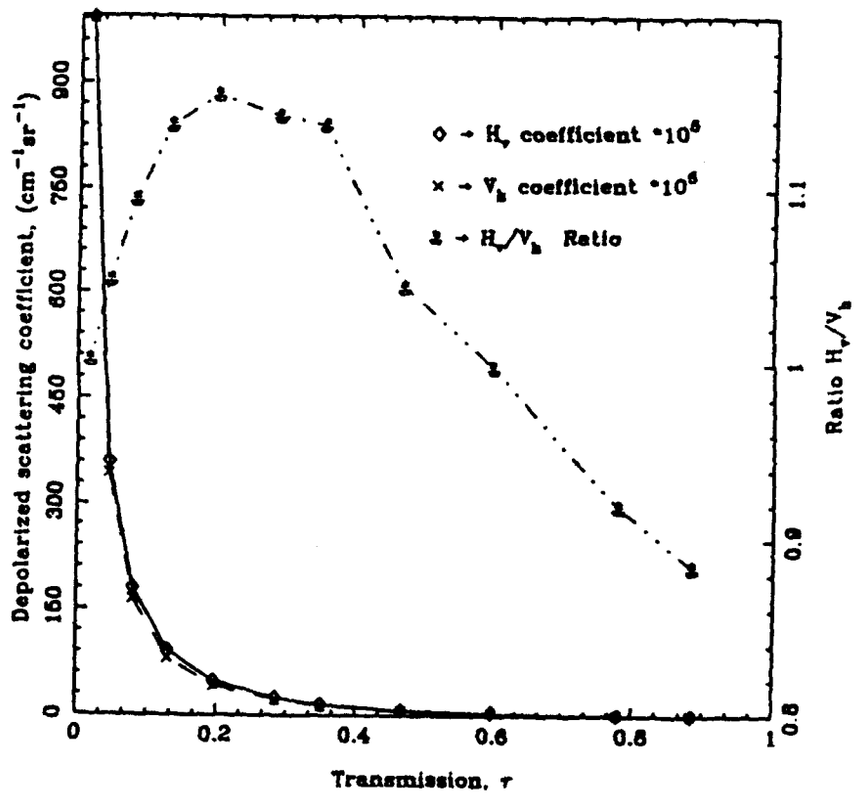

Figure 26: Depolarized scattering coefficient and their ratio versus transmission of 0.22 micron spheres at 130° scattering angle.

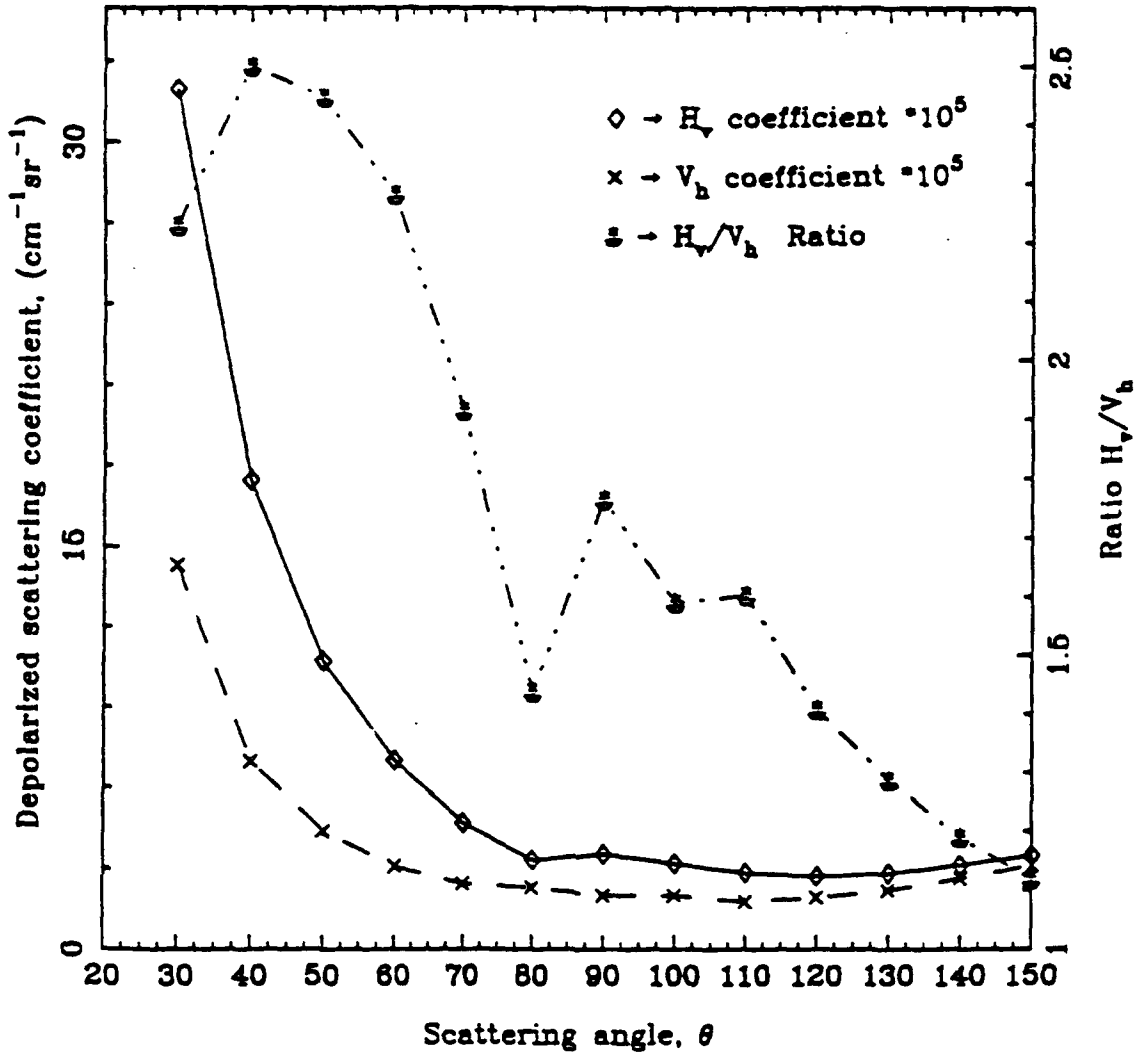

Figure 27: Depolarized scattering coefficient and their ratio versus scattering angle plot of 0.22 micron spheres at 0.571 transmission.

III. PERSONNEL

During the first year of study the Principal investigator was assisted in the project by Dr. David Hahn a graduate of LSU Mechanical Engineering Department and one of PI's ex-graduate students. Dr. Hahn worked in the project for the Fall '92 semester. Glenn Waguespack and Demetris Venizelos both Ph.D. candidates were also assisted in the project. Both students have completed their Ph.D. Qualifying examinations and they are expected to complete their degree requirements in two years time. Undergraduate student workers also assisted in the project. Mark Morris and Robert Woodward both seniors in Mechanical Engineering and Angel Borrel a freshman in Chemical Engineering also assisted in the set up of facilities and experimentation.

IV. PUBLICATIONS/PRESENTATIONS

During the first year of study two archival journal papers directly related to the proposed work were accepted for publication.

1. "Depolarization Characteristics of Agglomerated Particulates - Reciprocity Relations" Accepted for Publication in the Journal of Physics D: Applied Physics, Paper No. D/48055/PAP (see Appendix A).

2. "On the Optical Properties of Submicron-Inhomogeneous Flame Particulates" Accepted for Publication in the Journal of Physics D: Applied Physics, Paper No. D/47374/PAP (see Appendix B).

In addition the following papers were accepted for publication, presented in conferences or submitted for publication in the first year of study.

1. "Method to Account for Window Birefrigence Effects in Ellipsometry Analysis"

Accepted for publication in the Journal of Physics D: Applied Physics, Paper No. D/45462/PAP.

2. Refractive Indices of Pyrolytic Graphite, Amorphous Carbon and Flame Soot in the Temperature Range 25 degrees to 600 degrees C. Combustion and Flame, Vol. 94:381-396 (1993).

3. "A High Temperature Ellipsometer System to Determine the Optical Properties of Materials-Faraday Effects" Accepted for publication in the Journal of Applied Optics, Paper # AO 6621.

4. "Source Optics Polarization Effects on Ellipsometry Analysis", Paper No. 7181 Journal of Applied Optics (In Review).

5. Papers presented in the Joint Technical Meeting of the Central and Eastern States Section of the Combustion Institute March 15-17, 1993 New Orleans, LA.

a. Refractive Indices of Carbonaceous Materials in the Temperature Range 25°C to 600°C (see Appendix C)

b. Optical Properties of Two-Component Flame Particulates" (see Appendix D) and

c. Extinction and Depolarization Characteristics of Agglomerated Particulates (see Appendices).

V. INTERACTIONS RELATED TO RESEARCH

The Principal Investigator ensures that the results of the ongoing research are made available to the industrial and university community. In addition an effort is underway to work closely with the industrial sector especially with Columbian Chemicals Company to implement some of the techniques that we have been developing in our laboratory for product quality control. Furthermore, the light scattering codes for data inversion are made available to other researchers upon request.

INSTITUTE OF PHYSICS PUBLISHING

APPENDIX A

Techno House Redcliffe Way
Bristol BS1 6NX England

Telephone 0272 297481
Telex 449149 INSTP G
Facsimile 0272 294318

Ref: D/48055/PAP

17 August 1993

Dr T Charalampopoulos
Mechanical Engineering Department
Louisiana State University
Baton Rouge
LA 70803-6413
USA

Email:prod1@ioppublishing.co.uk
x400 :/s=prod1/o=ioppl/prmd=iopp/admd=0/c=gb

Dear Dr Charalampopoulos

TITLE: Depolarization characteristics of flame soot
AUTHORS: T Charalampopoulos et al

We have pleasure in informing you that this Paper has been accepted for publication in Journal of Physics D: Applied Physics. It has now been passed to Tessa Edmonds of our Production Department to whom all further correspondence should be addressed.

The typescript will be prepared for the printer and you will receive proofs in due course. These should be checked and returned without delay.

Yours sincerely

Stephen Byford
Assistant Managing Editor
Journal of Physics D: Applied Physics

APPENDIX A

Journal of Physics
Applied Physics
Ref. D/48055/PAP
In Print

Depolarization Characteristics of Agglomerated Particulates - Reciprocity Relations

by

T.T. Charalampopoulos* and
P. Panigrahi

Mechanical Engineering Department
Louisiana State University
Baton Rouge, LA 70803
U.S.A.

Submitted: June 26, 1993
Classification No: 7890

*To whom correspondence should be addressed.

Abstract

Knowledge of the morphological characteristics of agglomerated structures in combustion systems is important for accurate prediction of radiative transfer in absorbing and scattering media, surface growth of particulates, as well as in the quality control of material synthesis through the aerosol route. Especially nowadays when stringent governmental regulations are issued regarding the permissible amounts of emitted particulate matter accurate knowledge of size and morphology of the particulates becomes increasingly important. This study focuses on the depolarization properties of agglomerated particulates such as flame soot and other highly absorbing or dielectric particulates. Calculations of the depolarization ratios for randomly oriented straight chains, randomly branched chains and clusters, composed of primary particles in the Rayleigh regime, show that the reciprocity relations are not satisfied for the agglomerated structures considered in this study. To the contrary these ratios were found to be strongly dependent on the agglomerate parameters and the type of agglomerate considered.

Introduction

Agglomerated particulate structures of variable degree of complexity occur in many environments such as combustion systems, and atmospheric and colloidal dispersions to mention a few. The study of particulate size and morphology is of critical importance in many areas of research and practical applications. Questions related to knowledge of interstellar dust, fog and rain predictions, control of toxics in air and water and radiation from luminous flames rely on an understanding of the physical, chemical and optical properties of suspended particles. In particular, combustion generated soot particulates have wide ramifications in radiative transfer, pollution studies and climate control. Some applications seek to enhance soot production since its high emissivity contributes to the augmentation of the rate of heat transfer and thus temperature reduction of the flame system in hand. Other applications seek to reduce soot output; for example, soot emissions from mobile and stationary combustion units can lead to air pollution and can block exit ports of jet engines.

There are two methods for the study of the characteristics of flame particulates: ex-situ and in-situ. In the first method the particles are collected from the flame using sampling probes. Size and shape information can subsequently be obtained using electron microscopy. In the in-situ method a light beam is incident on the particles and the amount of light energy scattered as function of the scattering angle and/or polarization state in conjunction with the energy absorbed by the particles is monitored by light detectors. The ex-situ method, although simple to use, possesses disadvantages because the sampling process perturbs the flow field and as a result both the actual size and shape of the particles may be altered. In addition the sampling probes may not sustain the adverse temperatures and/or reactive conditions of the system. The in-situ technique though more complex, can yield

valuable information about the size and shape of the particles. Electron micrographs of soot samples collected from flames demonstrate clearly the existence of agglomerated structures that depend on the flame conditions. Jones and Wong [1] determined the presence of soot agglomerates in flames from direct optical evidence. Several particle shapes are possible due to agglomeration such as clusters, straight chains or randomly branched chains. The absorption and scattering efficiencies of agglomerated structures consisting of Rayleigh size primary particles can be predicted using the models developed by Jones [2-3]. In a recent study [4] the primary particle diameter, number of primary particles, the number density of agglomerated soot particles and the fractal dimension was determined from in-situ scattering/absorption and dissymmetry measurements in a premixed propane/oxygen flame. The data were analyzed using the refractive index of the particles obtained from the spectral extinction data from the same flame using the Kramer-Kronig method of analysis [5]. However, since in most cases the refractive index of the particles is not known additional measurements coupled with independent relations for the scattering properties of agglomerates are needed in order to unambiguously determine the agglomerate parameters. In this respect it should be noted that as has been pointed out by Krishnan [6] the depolarization ratios for incident unpolarized light and light polarized in the vertical and horizontal polarization orientations are related to the size, shape and structures of the particles. Similar observations were made more recently [7]. In this study the depolarization characteristics of agglomerated particulates with variable shape, number of primary particles and refractive indices covering the range of properties from dielectric to heavily absorbing particles are explored.

Theory

a. Scattering from assemblies of Rayleigh spheres

Jones [2] used Saxon's integral equation [8] to determine the scattered electric field at any point in space taking multiple scattering into consideration. Referring to figure 1 the scattered electric field at any point (r, θ, ϕ) from the origin is given by

$$E_{scat}(r) = E_{inc}(r) + k^2 \sum_{j=1}^{N_p} \int_{v_j} E(r_j)(m^2 - 1)G(r,r_j)dV_j$$

$$+\sum_{j=1}^{N_p} \int_{v_j} [\nabla_j(\nabla_j \cdot E(r_j)(m^2 - 1))]G(r,r_j)dV_j \,, \qquad (1)$$

where E_{inc} is the incident electric field, k the wavenumber $2\pi/\lambda$, N_p the number of particles in the agglomerate, m the refractive index n + ik and $G(r, r_j)$ is the spherical Green's function. The internal field of any sphere is obtained by assuming uniform internal field in each sphere and integrating the Green's function. The result is a system of $3N_p$, linear simultaneous equations:

$$E(r_\iota) = \frac{3}{m^2 + 2} E_{inc}(r_\iota) + \frac{i}{3}\left(\frac{m^2 - 1}{m^2 + 2}\right) \sum_{\substack{j=1 \\ j \neq \iota}}^{N_p} (kR_j)^3 T_{j\iota} E(r_j), \; \iota = 1, \ldots, N_p \qquad (2)$$

where T_{j1} is a 3 x 3 matrix in terms of spherical Bessel functions and the Legendre functions $\left(h_m^{(n)} \text{ and } P_m^{(n)}\right)$. The first term on the right hand side of eq. 2 represents the phase effect, whereas the second term represents the effect of field interaction or multiple scattering between the primary particles that constitute the agglomerate. The scattering cross section of the agglomerate is given by

$$C_{s,A} = \frac{|m^2 - 1|^2}{9r^2} k^2 R^6 \sum_{j=1}^{N_p} \sum_{j'=1}^{N_p} \exp[ik(r_j \cos\beta_j - r_j \cos\beta_{j'})](\Theta_j \Theta_{j'}^* + \Phi_j \Phi_{j'}^*) \quad . \qquad (3)$$

The asterisk dcnotes the complex conjugate of Θ_j and Φ_j which are defined as

$$\begin{aligned} \Theta_j &= \cos\theta \cos\phi E_x(r_j) + \cos\theta \sin\phi E_y(r_j) - \sin\theta E_z(r_j) \quad , \\ \Phi_j &= \sin\phi E_x(r_j) - \cos\phi E_y(r_j) \quad , \\ \cos\beta_j &= \cos\theta_j \cos\theta + \sin\theta_j \sin\theta \cos(\phi_j - \phi) \quad . \end{aligned} \qquad (4)$$

Here, θ and ϕ are, respectively unit vectors in the θ and ϕ directions and E_x, E_y, E_z are the respective component of the electric field vector.

With reference to figure 2 the scattered intensity is described in the following manner. H stands for horizontal and V stands for vertical polarization orientation. Specifically, H_v is the component of the scattered intensity corresponding to the following setting: The polarizer is placed in front of the detector with its axis coinciding with the scattering (measurement) plane whereas the incident electric field vector oscillates perpendicular to the scattering plane. Similarly V_h is the component of the scattered intensity detected with the polarizer axis oriented perpendicularly on the scattering plane and the incident electric field vector oscillating in the scattering plane.

b. Reciprocity relations

Krishnan [9] stated that reciprocity theorem ($H_v = V_h$) is valid not only for a single nonspherical particle, but for a solution containing a large number of particles which have no preferred orientation in the plane of observation. H_v and V_h intensity for an individual particle of arbitrary size and shape oriented in a specific way are not equal to each other. But if an averaging is carried out over all orientations of the particle in the horizontal plane which are similarly situated with respect to a vertical axis the H_v and V_h intensities are equal [9]. Krishnan undertook an experimental investigation to verify the reciprocity theorem. Using double image prism he took photographs of H_v, V_h, V_v and H_h intensity of graphite solution, sulphur suspensions, red gold solutions, bredig's silver solution, stearic acid solutions, dilute milk, dilute toluene emulsions and concentrated toluene emulsions. In all these measurements it was observed that H_v and V_h are exactly identical in intensity and colour establishing the validity of reciprocity theorem. However measurements of H_v and V_h intensity of spherical particle by increasing concentration in the multiple scattering region were not considered.

On the other hand Perrin [10] has stated the law of reciprocity more explicitly. According to Perrin if two incident polarized beams have equal intensities, the inverse emerging beams of the same polarization, which are associated with them, also have equal intensities. With reference to figure 3 let us consider a monochromatic beam emerging from a Polarizer P_1, having an intensity I_1, is incident in a particular direction upon a system in which light can be scattered and absorbed. Let us also assume that the scattered beam after passing through polarizer P_2 has an intensity I_1'. There are two inverse beams which coincide with these but travel in the reverse direction. The first of these emerges from P_2 with intensity I_2;

the second emerges from P_1 with intensity I_2'. Then according to reciprocity theorem I_1' is equal to I_2'.

Saxon [11] described the scattering of an incoming electromagnetic wave by an unrestricted scattering object in terms of a tensor scattering matrix. Unrestricted scatterer means no restriction on the scatterer. This implies that the reciprocity theorem should also apply to the assembly of soot aggregates that are dissipative in nature from optical standpoint as well as to aggregates composed of non-absorbing primary particles. According to Saxon, the reciprocity relation may be written as:

$$q.A_q(n,n_o) = q.A_q(-n_o,-n) \tag{5}$$

where n_o is a unit vector in the direction of the incident plane wave, q is a unit vector in the direction of polarization and $A_q(n,n_o)$ is the amplitude of the wave scattered in the direction n. This relation implies that if we interchange the direction of the incident wave and the direction of observation, the component of the scattered wave in the direction of polarization remains unchanged. Bayvel and Jones [12] expressed the relationship between incident and scattered waves using a scattering matrix, namely:

$$\begin{pmatrix} E_{h,scat} \\ E_{v,scat} \end{pmatrix} = \begin{pmatrix} S_2 & S_3 \\ S_4 & S_1 \end{pmatrix} \begin{pmatrix} E_{h,inc} \\ E_{v,inc} \end{pmatrix} \frac{\exp(ik_o r)}{k_o r} . \tag{6}$$

where $k_o = \frac{2\pi}{\lambda_o}$ is the wave number, λ_o the wavelength in vacuum and $S_i (i = 1,2,3,4)$ are the components of the scattering matrix. If the direction of incidence and scattering are interchanged then a relationship exists between the original scattering matrix and that for the reversed situation and in that case

$$S = \begin{pmatrix} S_2 & -S_4 \\ -S_3 & S_1 \end{pmatrix} . \qquad (7)$$

This relationship is referred to as the reciprocity theorem. The theorem was verified by Lips and Levine [13] for two spherical particles over all orientations. Ravey [14] in the formulation of scattering of electromagnetic waves by an ellipsoid of arbitrary size and optical properties demonstrated that reciprocity relation holds for his analysis. Jones in the original work [2] calculated the H_v/V_h ratio as function of the angle for straight chain of random orientation and concluded that the reciprocity theorem was not satisfied. Bayvel and Jones [12] on the other hand remarked, that the violation of the reciprocity theorem might be due to an error which was undiscovered or genuine. Subsequently, Jones [15] noted that the observed anomaly in the original work [2] was due to a computational error. Results were presented only for straight chains with size parameter 0.2, refractive index $\overline{m}$ = 1.6 + 0.8i and primary particle number density Np = 10 and was reported that the H_v/V_h ratio was unity to within less than 6%. This deviation was attributed to rounding error and was inferred that the reciprocity theorem was satisfied. In this study in order to test further the validity of the reciprocity relations for all types of agglomerate parameters and refractive indices of the primary particles extensive calculations for the H_v/V_h ratio were carried out. The parameters used cover the range of properties for both absorbing and dielectric particles.

Numerical Calculations

Referring to figure 3, let us assume that P_1 is oriented vertically and P_2 is oriented horizontally. Then for the forward direction $q.A_q(n,n_o)$ is the H_v intensity and for the reversed direction $q.A_q(-n_o,-n)$ is the V_h intensity. By using equation (8) for the forward direction we obtain the following relations for the H_v and V_h components

$$H_v = E_{h,scat} = \frac{\exp(ik_o r)}{k_o r} S_3 \cdot E_{v,inc} \qquad (8)$$

and

$$V_h = E_{v,scat} = \frac{-\exp(ik_o r)}{k_o r} S_3 \cdot E_{h,inc} \qquad (9)$$

According to Saxon the reciprocity relation is independent of the nature of scatterer. So any agglomerate can be considered as a single scatterer and reciprocity theorem should be valid for agglomerates also. It should be noted for a single isotropic spherical scatterer the reciprocity relation yields $H_v = V_h = 0.0$ [16].

As a first step towards elucidation of the applicability of the reciprocity theorem for agglomerates calculations were carried out similar to those by Jones [44]. Figure 4 shows the H_v to V_h ratio with respect to scattering angle for straight chain with size parameter ($kr = 0.2$), refractive index($m = 1.6 + 0.8i$) and number of primary particles ($N_p = 10$). The agreement between the present results and those reported by Jones [15] is very good. In order to investigate the applicability of the reciprocity theorem to the agglomerated structures occurring in flame systems such as soot numerical calculations were carried out using the soot agglomerate parameters obtained from in-situ light scattering/extinction and dissymmetry measurements [4]. The measured scattering/extinction coefficients and the dissymmetry ratios in the vertical-vertical

polarization orientation are shown in Table 1. The inferred agglomerate parameters primary particle diameter d_p, number of primary particles per agglomerate and the number density of agglomerates is shown in Table 2 along with the refractive indices [5] used for the data inversion. The corresponding calculated H_v and V_h scattering cross sections for different type of agglomerates at various positions above the burner surface is shown in Table 3. On the other hand the ratio H_v/V_h for cluster as function of the scattering angle at different axial locations above the burner surface is shown in Figure 5. As may be seen the ratio H_v/V_h differs from the expected value of 1.0 by a factor of 0.1 to 4.3. For the case of random straight chain configuration (see Figure 6) the H_v/V_h ratio also differs from the value of 1.0 by a factor of 1.3 or more. To demonstrate the variation of the H_v/V_h ratio for soot agglomerates with respect to the individual properties like diameter and number of primary particles further calculations were carried out. As may be seen from figures 7-11 the H_v/V_h ratio varies with the type of agglomerate, primary particle diameter, number density and scattering angle. It should be noted that the smallest departure from the expected H_v/V_h ratio of 1.0 for all the configurations examined was exhibited by the randomiy oriented branched chain (Figure 11).

Discussion

It should be noted that several points need to be addressed. With reference to figures 7 and 8 for straight chain there is a systematic increase of H_v to V_h ratio with respect to either diameter or number of primary particles. The variation of H_v/V_h with respect to the primary particle diameter appears to follow the same trends of its variation with respect to the number of primary particles for straight chain. However as may be seen from figures 9 and 10 for the cluster agglomerate the variation of H_v to V_h ratio curve with respect to the number of primary particles is discontinuous and with respect to diameter is continuous. In the computer program used for the present calculations the coordinates of the primary particles for clusters are fixed. Since the H_v and V_h intensities are functions of the geometry of the agglomerate by increasing the number of primary particles the geometry of the cluster changes in a fixed manner. Thus, the ratio of H_v to V_h is not a function of the number of primary particles alone. To verify this, the coordinates of primary particles of the agglomerate were generated at random. The average scattering characteristics of the agglomerate were calculated after 600 different combinations of the coordinates of the primary particle within the agglomerate. The H_v to V_h ratio was plotted for different number of primary particles and scattering angle. From figure 11 it may be seen that the H_v to V_h ratio no longer varies abruptly with the number of primary particles. The variation of H_v to V_h ratio lies between 0.8 to 1.2 which is much less than the variation of a cluster agglomerate. Therefore, the explanation for the departure of the H_v/V_h ratio from the value of 1.0 may be due to the geometric anisotropy of the structure itself and is not a consequence of the computational scheme. In this respect it should be mentioned that the three different computer programs that were utilized for the calculations of the depolarization ratios of the three different types of agglomerates, as it would have

been expected, yield identical results for one and/or two primary particles. Therefore the differences associated with larger number of primary particles may be attributed to different levels of geometrical anisotropy. Note that calculations of the H_v and V_h ratio for agglomerates with refractive indices characteristic of the dielectric material, although not presented here, do show that the H_v/V_h ratio departs significantly from the expected value of one. The same trends were noted for strongly absorbing materials such as metals. It should be emphasized that the model used for the calculations presupposes that the individual primary particles are sufficiently small and that their internal fields are constant and uniform. For the soot agglomerates, especially during the initial phases of agglomeration in typical premixed and diffusion hydrocarbon flames, the primary particles may be in the Rayleigh regime and thus the first criterion for the applicability of the model is satisfied. However the assumption of the uniformity of the internal field within the primary soot particles may not be absolutely valid. Measurements of the depolarized intensities from submicron concentrated polystyrene particle dispersions in distilled water (in the author's laboratory) indicate that multiple scattering within the agglomerate may be the cause for the observed anomaly. Nevertheless a more rigorous explanation supported by independent corroboration is not plausible at this time. Finally, in the context of laser diagnostics the present results indicate that the measurement of the H_v and V_h from a cloud of agglomerates may be used to yield additional information for the determination of the agglomerate morphology.

Summary

The results of the present study may be summarized as follows:

a. The depolarization characteristics of agglomerated particulates were examined in the content of reciprocity theorem.

b. It was found that the depolarized intensity for straight chains, randomly branched chains and clusters are strong functions of primary particle diameter, scattering angle and number of primary particle in the agglomerate.

c. For all types of agglomerates investigated in this study and the range of parameters considered it was found that the reciprocity theorem is not satisfied.

d. The observed discrepancy may be attributed to multiple scattering within the agglomerate.

Acknowledgments: This research was supported by the AIR FORCE OFFICE OF SCIENTIFIC RESEARCH/USA, Grant F49620-92-J-0447 under the technical monitoring of Dr. J.M. Tishkoff.

References

1. Jones A R and Wong W 1975 *Comb. Flame* **24** 139-140
2. Jones A R 1979 *Proc. R. Soc. London* **A336** 111-127
3. Jones A R 1979 *J. Phys. D: Appl. Phys.* **12** 1661-1672
4. Charalampopoulos T T and Chang H 1991 *Comb. Flame* **87** 89-99
5. Chang H and Charalampopoulos T T 1990 *Proc. R. Soc. London* **430A** 577-591
6. Krishnan R S 1939 *Proc. Ind. Acad. Sci.* 303-308
7. Charalampopoulos T T 1992 *Prog. Energy Comb. Sci.* **18** 13-45
8. Saxon D S 1974 *NASA Report CR140816* 111-127
9. Krishman R S 1938 *Proc. Ind. Acad. Sci. A VII* 21-34
10. Perrin F 1942 *J. Chem. Phys.* **10** 415-427
11. Saxon D S 1955 *Phys. Review* **100** No. 6 1771-1775
12. Bayvel L P and Jones A R 1981 Applied Sciences Publishers
13. Lips A and Levine S 1974 *J. Coll. Interf. Sci.* **46** No. 1 139-146
14. Ravey J C 1976 *J. Coll. Interf. Sci.* **56** No. 3 540-556
15. Jones A R 1981 *Proc. R. Soc. Lond.* **A375** 453-454
16. Kerker M 1969 Academic Press, New York

Table 1. Scattering coefficients (σ_{vv}, 90°), extinction coefficient (K_e), and vertical-vertical dissymmetry ratios R_{vv} (45°) as a function of position (H) above the burner surface for a premixed-propane-oxygen flame with a fuel equivalence ratio of ϕ_o = 1.8.

H (mm)	σ_{vv} (cm^{-1} str^{-1})	K_e (cm^{-1})	R_{vv} (45°)
6	$4.4 \times 10^{-6} \pm 12\%$	$0.038 \pm 1\%$	$1.24 \pm 5\%$
8	$1.6 \times 10^{-5} \pm 13\%$	$0.056 \pm 1\%$	$1.42 \pm 4\%$
10	$3.4 \times 10^{-4} \pm 12\%$	$0.067 \pm 1\%$	$1.75 \pm 3\%$
12	$5.4 \times 10^{-4} \pm 15\%$	$0.077 \pm 1\%$	$2.01 \pm 3\%$
14	$7.0 \times 10^{-4} \pm 14\%$	$0.081 \pm 1\%$	$2.25 \pm 3\%$
16	$8.8 \times 10^{-4} \pm 15\%$	$0.087 \pm 1\%$	$2.53 \pm 3\%$

Table 2: Agglomerate parameters of flame soot inferred from the analysis of the data of Table 1.

Height above the burner H in mm	Primary particle diameter d_p in microns	Number of primary particles (N_p)	Number of agglomerates $x10^{10}cm^{-3}$	Refractive index (m = n + ik)
6	0.0156	17	1.2	1.6 + 0.53i
10	0.0232	21	0.49	1.73 + 0.64i
12	0.0257	22	0.4	1.73 + 0.64i
16	0.0287	24	0.31	1.73 + 0.64i

Table 3: H_v and V_h scattering cross sections (cm^2) at 120° scattering angle for different agglomerates at different flame heights with number of primary particles and refractive index from Table 2.

H/mm	Straight chain		Cluster		Random chain	
	H_v $x10^{-16}$	V_h $x10^{-16}$	H_v $x10^{-17}$	V_h $x10^{-17}$	H_v $x10^{-17}$	V_h $x10^{-17}$
6	0.3197	0.3136	0.2955	0.5971	0.4825	0.4524
10	6.7198	6.6052	0.8867	4.0958	12.788	12.1729
12	12.2694	12.0282	2.9316	10.2607	24.0021	24.6837
16	24.9140	23.8630	20.0811	12.5952	53.0470	52.7570

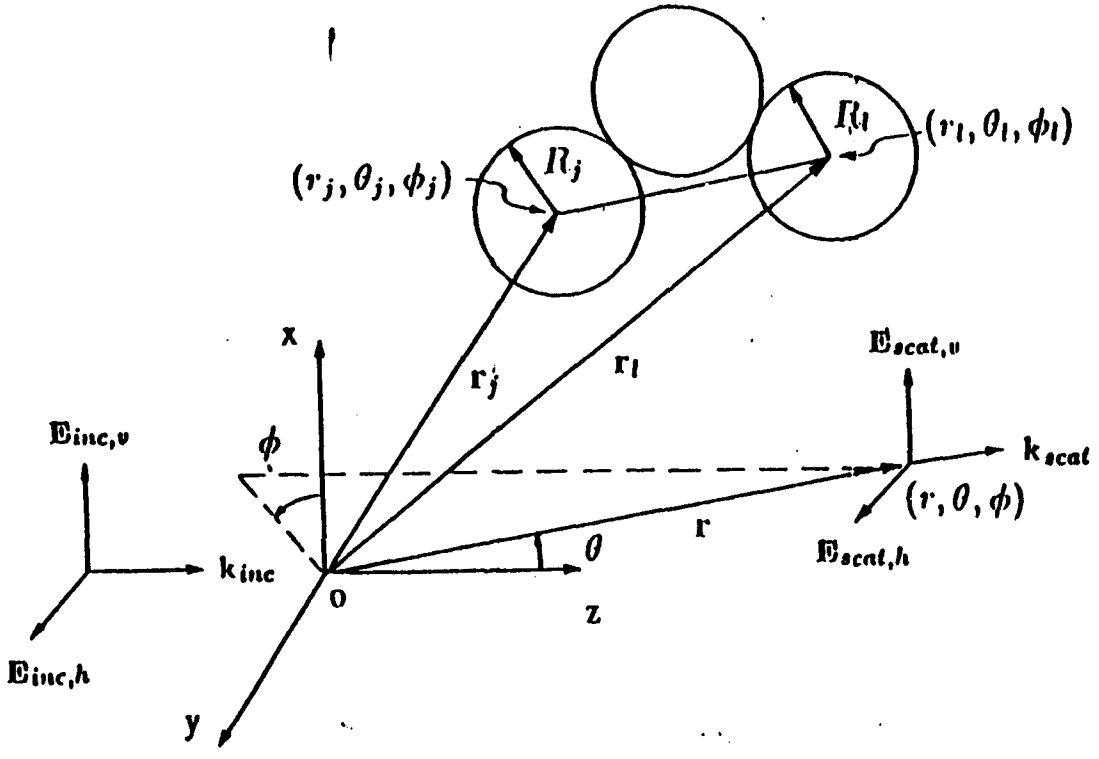

Figure 1. Coordinate system for the scattering from assemblies of Rayleigh spheres.

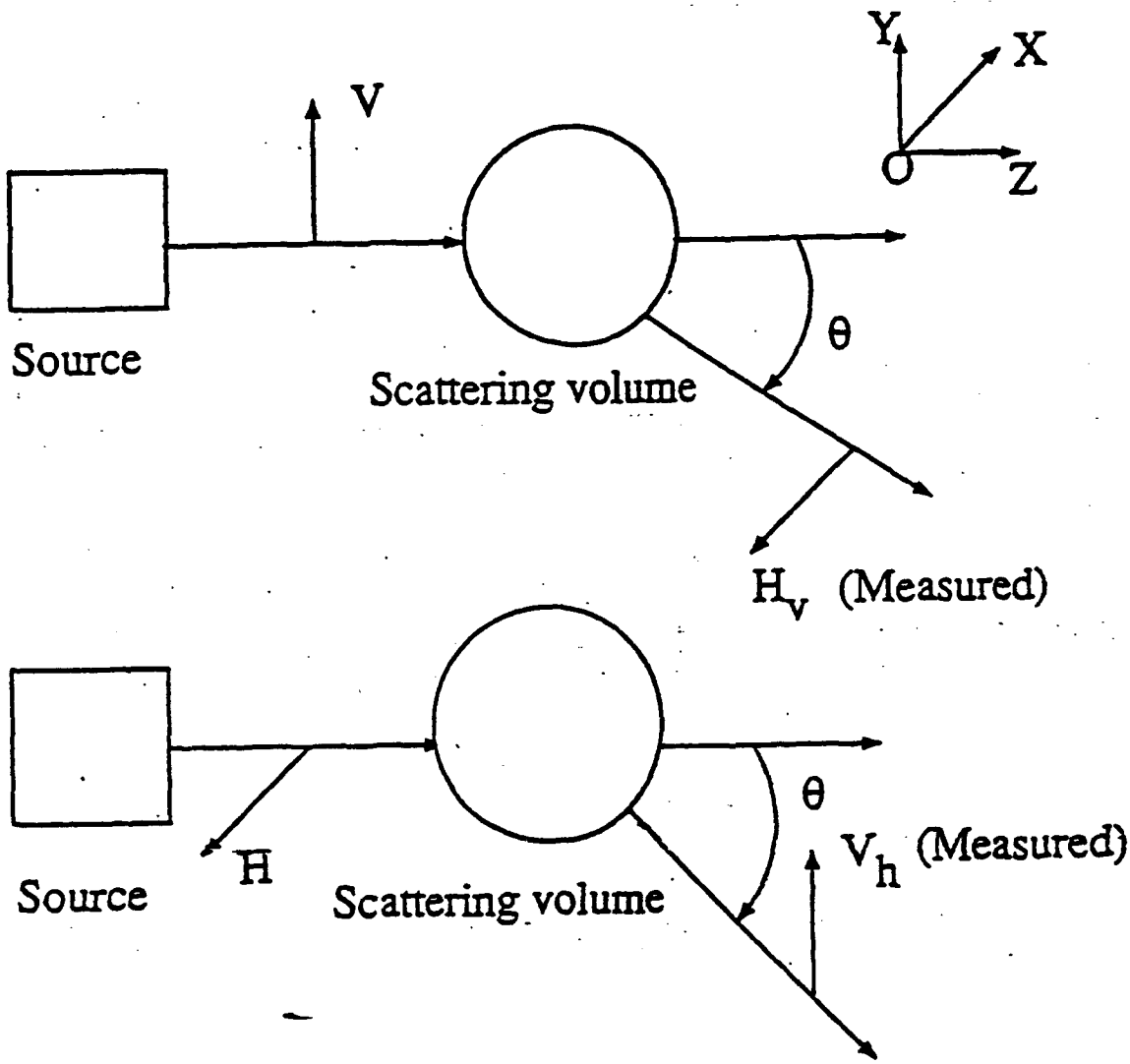

Figure 2. Coordinate system illustrating the implications of Reciprocity Theorem.

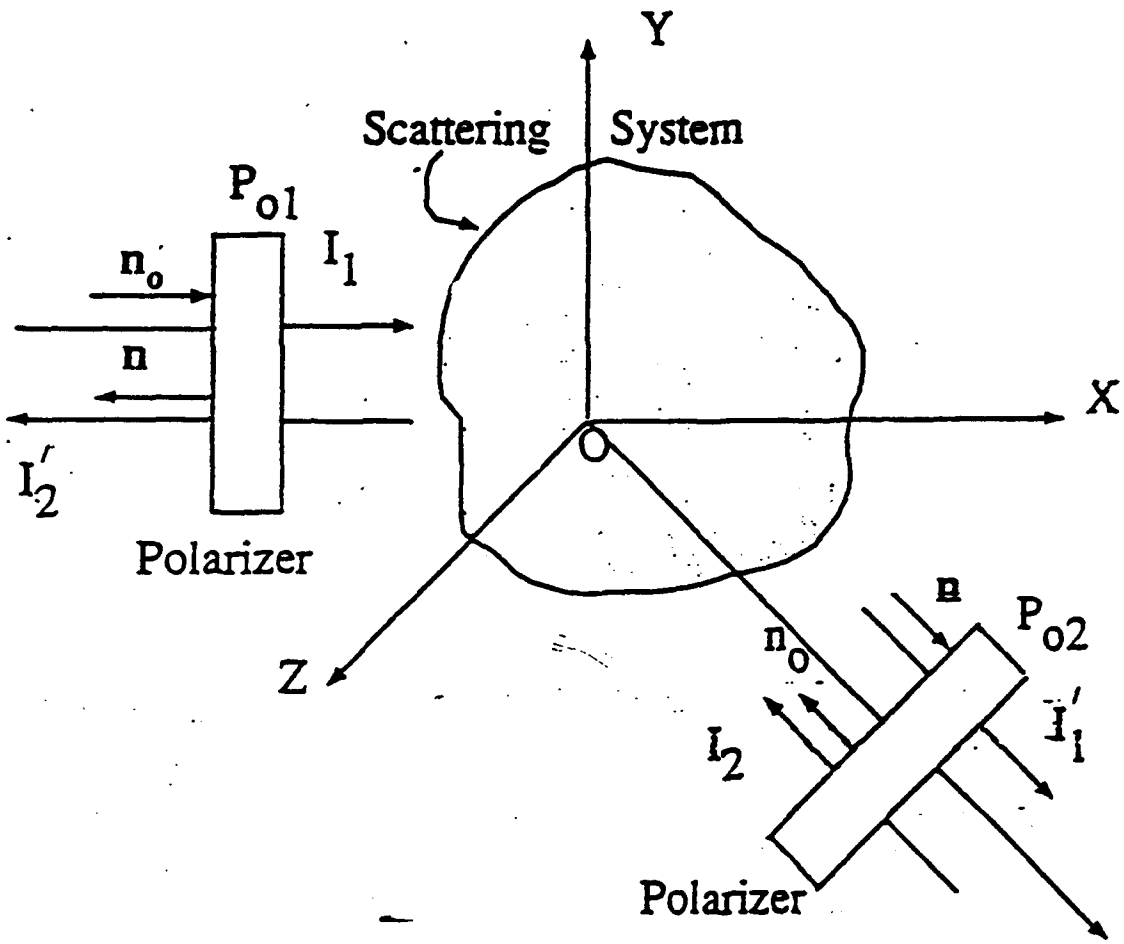

Figure 3. Schematic illustrating the depolarization of a light beam due to a scattering system.

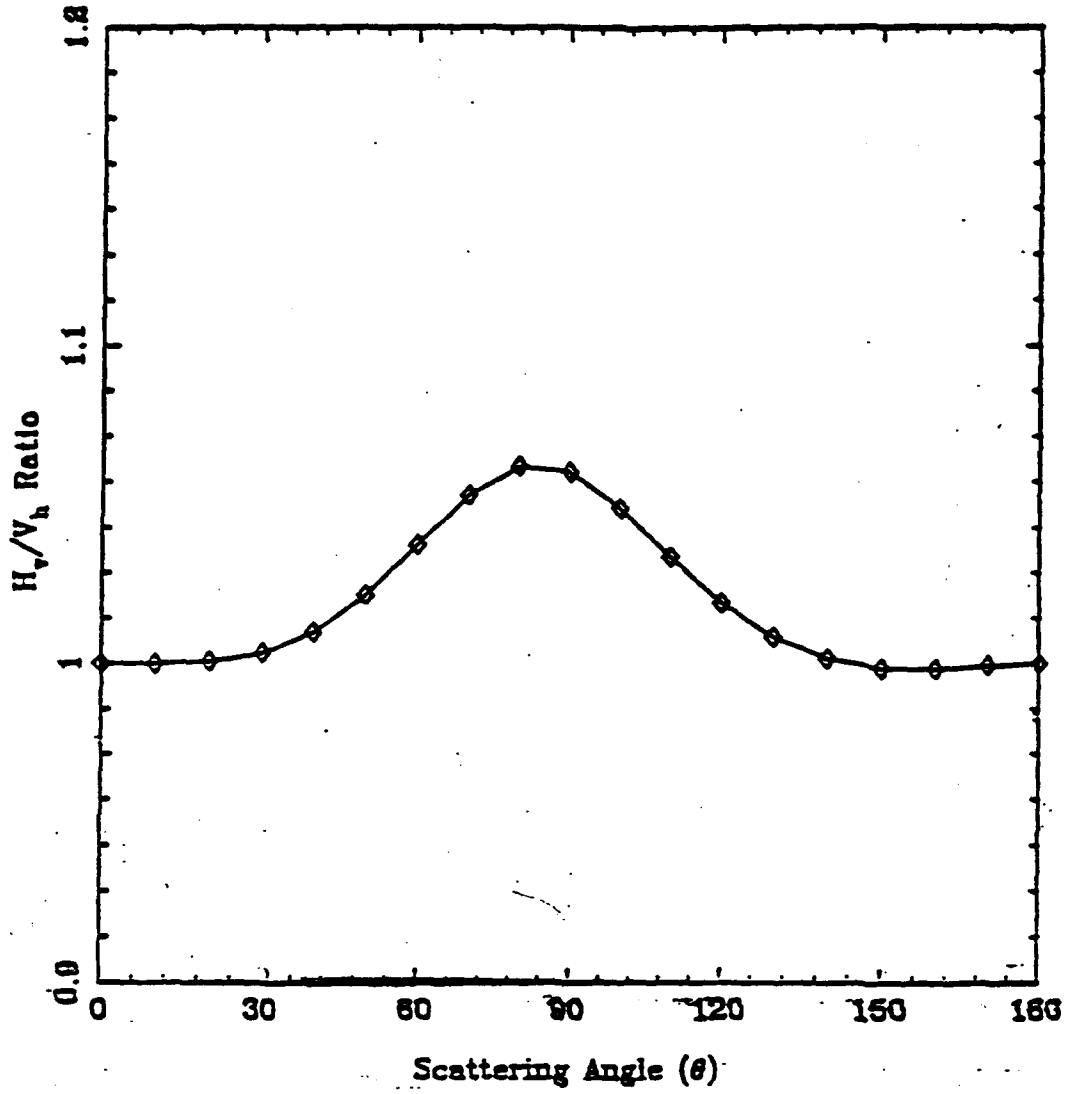

Figure 4. H_v to V_h ratio as function of scattering angle from straight chain with size parameter (Kr = 0.2), refractive index $\overline{m}$ = 1.6 - 0.8i and number of primary particles N_p = 10.

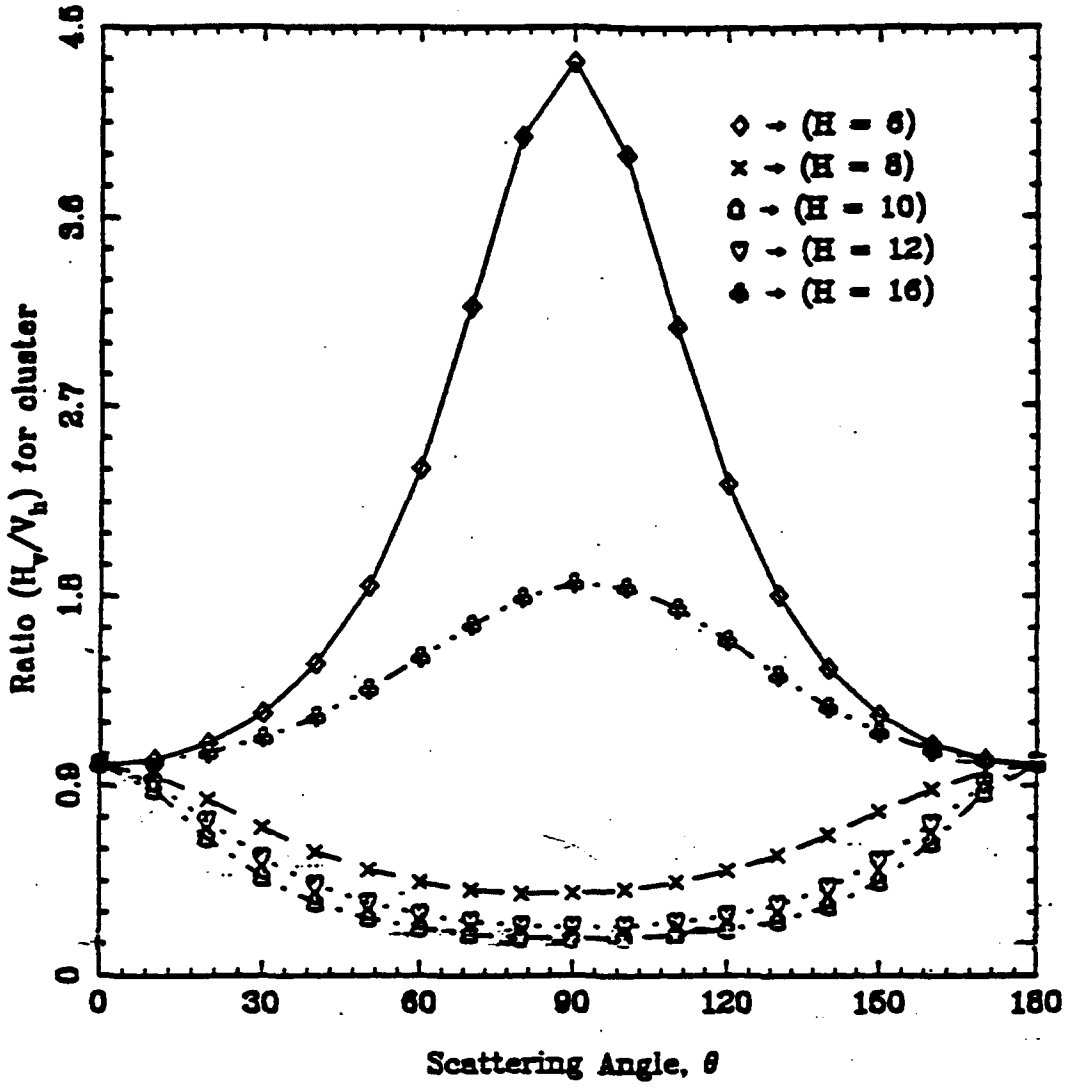

Figure 5. H_v/V_h ratio for clusters as function of scattering angle θ for various positions (H) above the burner surface. The number of primary particles and refractive indices used are given in Table 2.

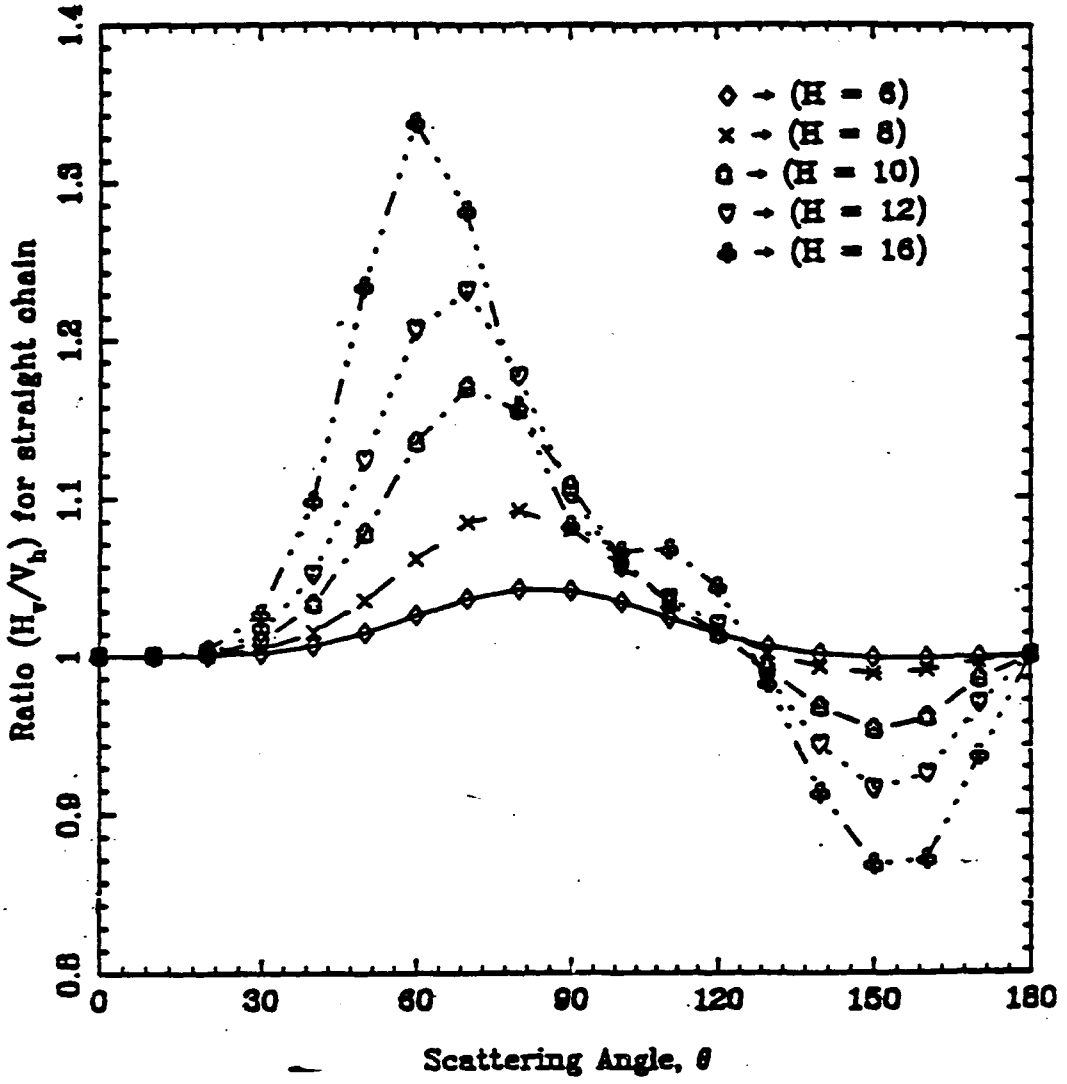

Figure 6. H_v/V_h ratio for straight chain as function of scattering angle for various positions (H) above the burner surface. The number of primary particles and refractive indices used are given in Table 2.

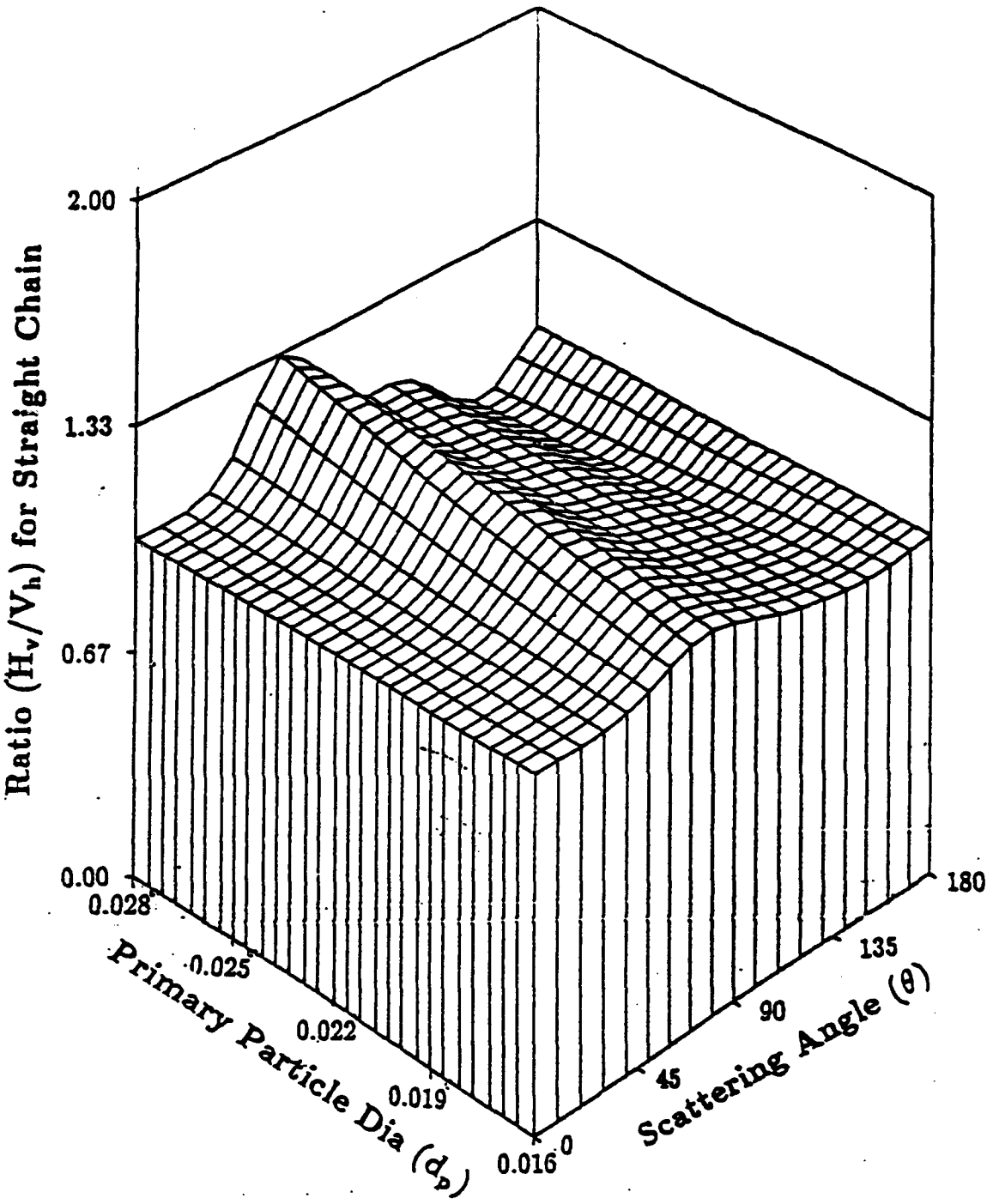

Figure 7. H_v/V_h ratio as function of scattering angle and primary particle diameter. The number of primary particles was 24 and the refractive index m = 1.73 + 0.64i.

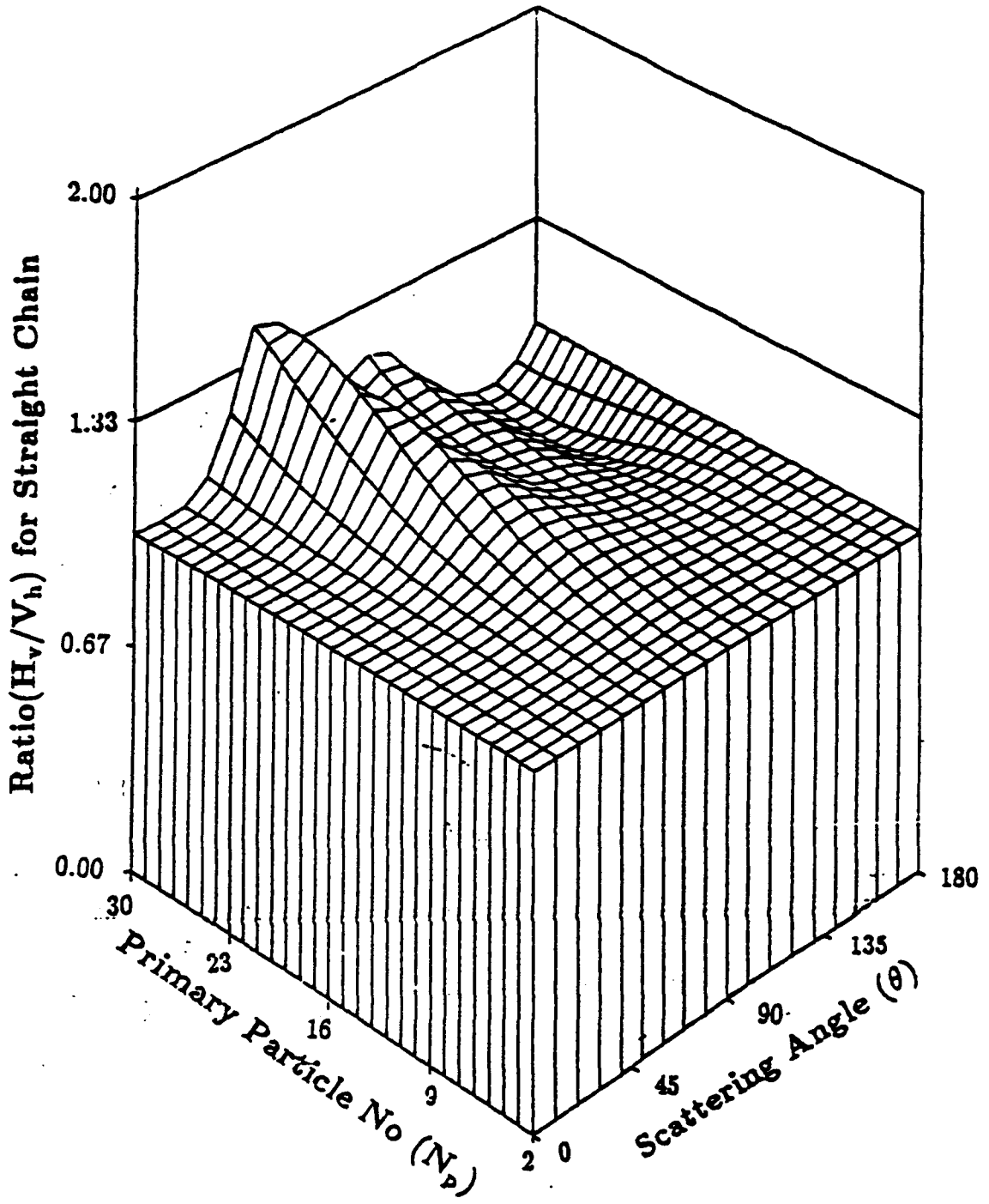

Figure 8. H_v/V_h ratio as function of primary particle number and scattering angle (θ) for straight chain. The primary particle diameter d_p was 0.0287 μm and the refractive index m = 1.73 + 0.64i.

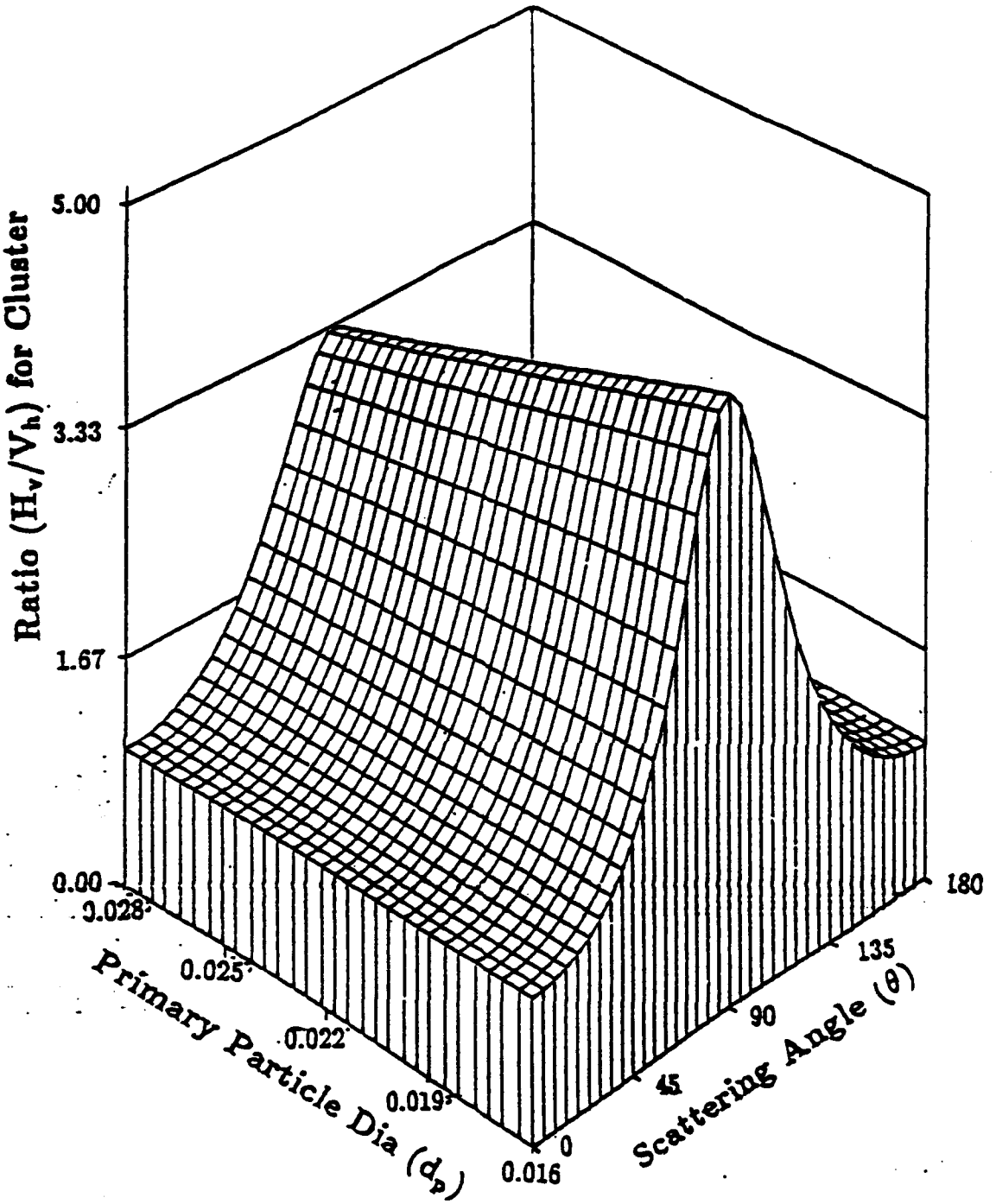

Figure 9. H_v/V_h ratio as function of scattering angle and diameter for cluster. The number of primary particles was 17 and the refractive index m = 1.6 + 0.53i.

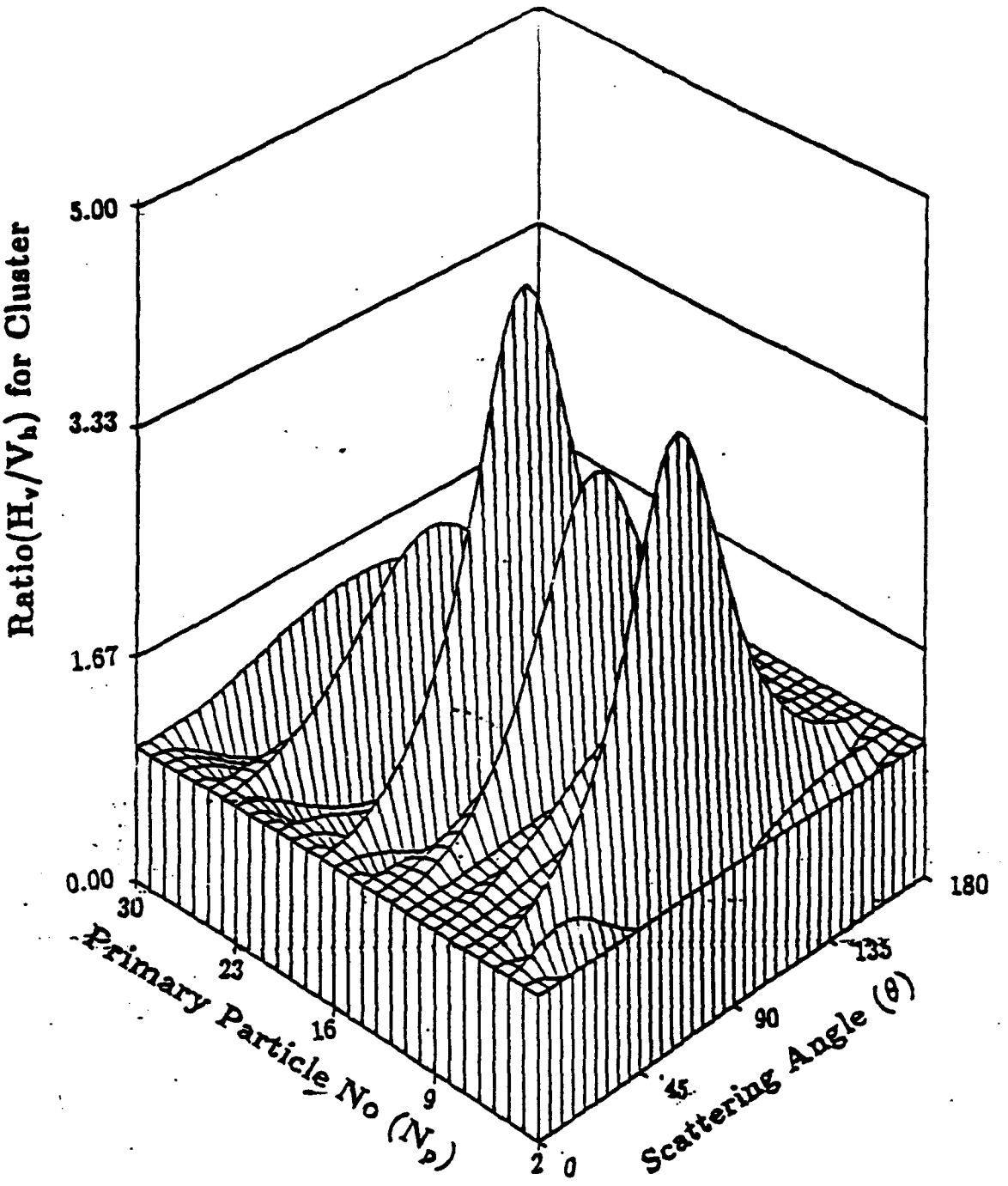

Figure 10. H_v/V_h ratio as function of scattering angle and number of primary particles for cluster. The primary particle diameter used was 0.0156 μm and the refractive index m = 1.6 + 0.53i.

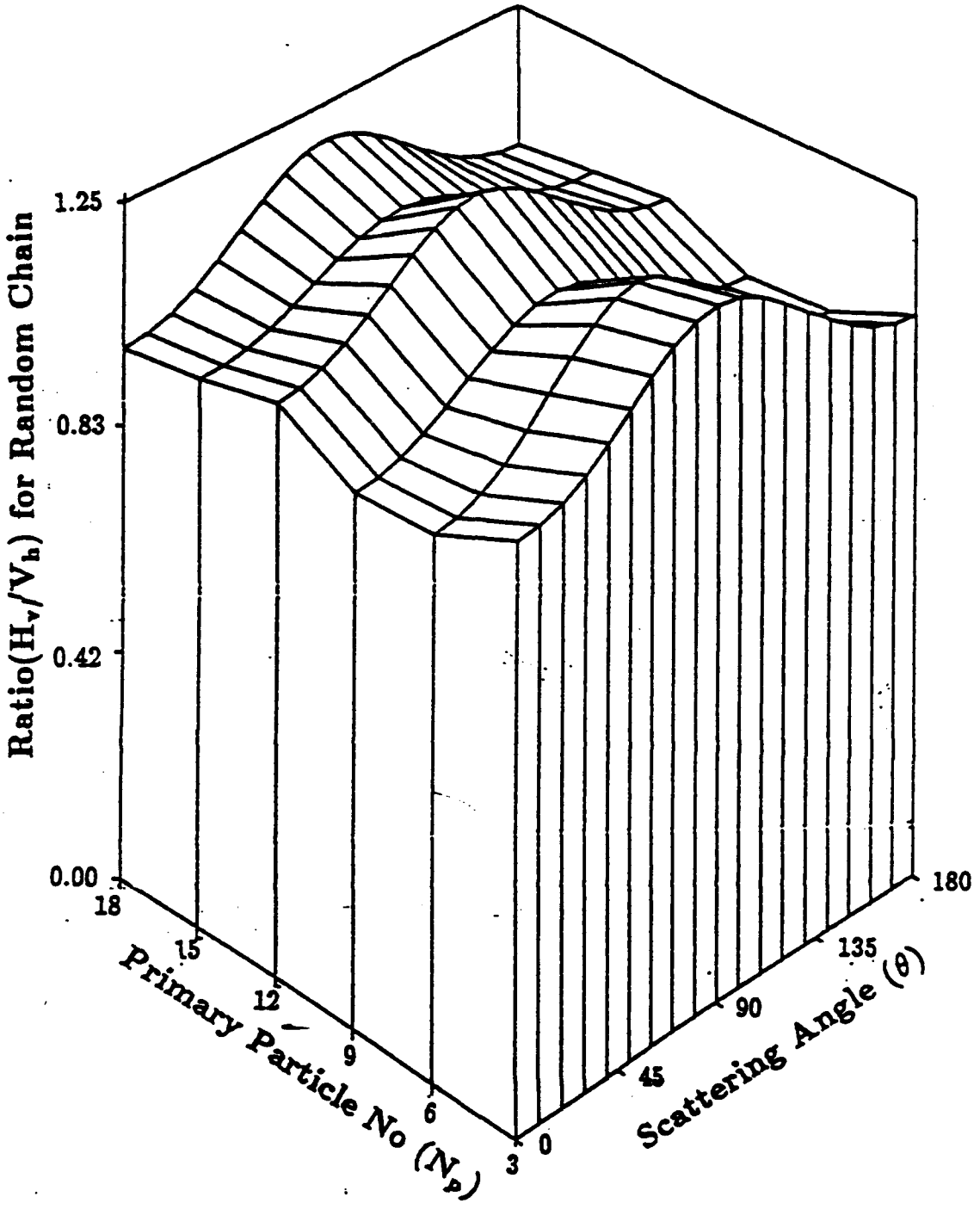

Figure 11 H_v/V_h ratio as function of scattering angle and number of primary particles for randomly branched chain. The primary particle diameter used was 0.0156 μm and the refractive index m = 1.6 + 0.53i.

INSTITUTE OF PHYSICS PUBLISHING

APPENDIX B

Techno House Redcliffe Way
Bristol BS1 6NX England

Telephone 0272 297481
Telex 449149 INSTP G
Facsimile 0272 294318

Ref: D/47374/PAP

3 August 1993

Dr T Charalampopoulos
Mechanical Engineering Department
Louisiana State University
Baton Rouge
LA 70803-6413
USA

Janet:prod1@ioppublishing.co.uk
x400 :/s=prod1/o=iopp1/prmd=iopp/admd=0/c=gb

Dear Dr Charalampopoulos

TITLE: On the optical properties of ...
AUTHORS: D W Hahn et al

We have pleasure in informing you that this Paper has been accepted for publication in Journal of Physics D: Applied Physics. It has now been passed to Tessa Edmonds of our Production Department to whom all further correspondence should be addressed.

The typescript will be prepared for the printer and you will receive proofs in due course. These should be checked and returned without delay.

Yours sincerely

Stephen Byford
Assistant Managing Editor
Journal of Physics D: Applied Physics

APPENDIX B

Journal of Physics D:
Applied Physics
Ref. D/47374/PAP
In print

ON THE OPTICAL PROPERTIES OF SUBMICRON-INHOMOGENEOUS FLAME PARTICULATES

D.W. Hahn* and T.T. Charalampopoulos**

Mechanical Engineering Department

Louisiana State University

Baton Rouge, LA 70803

(Submitted: May 1993)

****To whom correspondence should be addressed.**

***Present address**
Center of Devices and Radiological Health
Food and Drug Administration
HFZ-134
1901 Chapman Avenue
Rockville, Maryland 20857

ABSTRACT

The application of Maxwell Garnett effective medium model and of the coated sphere model is examined in the context of analysis of light scattering/absorption data from inhomogeneous particulates. It is shown that the particle optical inhomogeneity may not be in general neglected when light scattering/absorption data are to be analyzed for volume fractions of particulates. Furthermore, the present results demonstrate that in the visible wavelengths for particles less than 100 nm in diameter the Maxwell Garnett effective medium model and coated sphere model may yield equivalent results for extinction efficiencies and particle volume fractions.

1. Introduction

Inhomogeneous particulates may be encountered in a variety of research and practical applications. For example, carbon blacks, fumed silica, titanium dioxide, uranium dioxide and superconducting ceramic powders are made in a variety of aerosol reactors that include flames, furnaces, plasmas as well as shock tubes[1]. The short residence times and large outputs that can be accomplished in flame reactors have motivated research towards the synthesis of pure oxide powders such as ZnO and MgO and in the manufacturing of structural ceramics by aerosol made nitride, boride and carbide powders. Furthermore, in combustion systems such as incinerators and boilers the particles may contain calcium, zinc, arsenic, mercury, iron and iron oxides and thus are optically inhomogeneous.

With respect to the scattering behavior of inhomogeneous particulates two main problems exist (i) Lack of the appropriate theory to predict accurately the effects of the particle optical inhomogeneity on the scattering and absorption cross sections and (ii) Lack of knowledge of the actual morphology of the agglomerates that are commonly encountered in reacting systems[2-3]. For inhomogeneous particles the effective refractive index is usually unknown and thus the inference of particle size from scattering and absorption measurements may possess significant uncertainties[4]. Such uncertainties may lead to biased interpretation of light scattering measurements especially when the effectiveness of a particular metal additive in the suppression of soot emissions from combustion systems[5-6] is to be determined.

The light scattering and absorption characteristics of optically isotropic particles are fairly well understood[7-9]. However, the accurate prediction of the effects of: (a) Non-spherical shape, (2) Non-homogeneity, (3) Orientation, (4) Optical anisotropy and associated distributions, in the analysis of light scattering/absorption data have

yet to be established. The purpose of this study is to examine the models which are available for the prediction of the optical properties of two component particulates, namely the Maxwell Garnett effective medium model and the coated sphere model. To this end, light scattering and extinction efficiency calculations are presented as functions of the relative component concentration for particle diameters less than 100 nm and the wavelength 488 nm where scattering/extinction measurments are commonly performed. In addition, light scattering/absorption data collected from a premixed propane/oxygen flame seeded with iron pentacarbonyl are analyzed for volume fractions using both the effective medium and coated sphere models. The results are discussed and the similarities and limitations of the two models are assessed.

2. Scattering and Absorption by Homogeneous and Inhomogeneous Particulates

As noted earlier the accurate prediction of the scattering and absorption behavior of inhomogeneous particles is still an unresolved problem. Since in this study scattering and extinction efficiency calculations are carried out and flame data are analyzed for volume fractions using both homogeneous and inhomogeneous analysis the corresponding theoretical models are briefly discussed in the following sections.

a. Homogeneous Particulates

For a cloud of optically homogeneous spherical particles with a size distribution function P(r) the mean scattering coefficient is given by

$$K_{pp} = N\bar{C}_{pp} \tag{1}$$

The subscript p denotes the polarization state (vertical or horizontal), and the double subscript indicates the state of polarization of the incident and scattered beams, N (cm^{-3}) is the particle number density and $\bar{C}_{pp}$($cm^2\ sr^{-1}$) is the mean differential scattering cross-section for all spheres in the scattering volume given by

$$\bar{C}_{pp} = \int_{r=0}^{\infty} C_{pp} P(r) dr. \tag{2}$$

The differential scattering cross-section for a homogeneous spherical particle of radius r is given by the expression

$$C_{pp} = \frac{\lambda^2}{4\pi^2} i_{pp}\,. \tag{3}$$

where λ is the wavelength of the incident radiation and i_{pp} are the Mie scattering amplitude functions[7-9].

$$i_{vv} = \left| \sum_{v=1}^{\infty} \frac{2v+1}{v(v+1)} (a_v \pi_v + b_v \tau_v) \right|^2 . \tag{4}$$

$$i_{sm} = \left| \sum_{v=1}^{\infty} \frac{2v+1}{v(v+1)} (a_v \tau_v + b_v \pi_v) \right|^2 . \qquad (5)$$

The functions a_v and b_v are the electric and magnetic multiple coefficients of the scattered light expressed in terms of the size parameter $x = 2\pi r/\lambda$ and complex refractive index of the particle $\bar{m} = n - ik$ relative to the index of the ambient medium taken to be air in this study. The functions π_v and τ_v are expressed in terms of the associated Legendre polynomials and depend only on the scattering angle θ. The function P(r) represents the size distribution of the particles with modal radius r_o and geometric width σ. For flame soot the distribution function P(r) is taken to be the zeroth order lognormal distribution function (ZOLD)[8] expressed as

$$P(r) = \frac{\exp\left(-\frac{1}{2}\ln^2\sigma\right)}{\sqrt{2\pi}\, r_o \ln\sigma} \exp\left[-\frac{\ln^2(r/r_o)}{2\ln^2\sigma}\right]. \qquad (6)$$

Assuming that the geometric pathlength transversed by the laser beam may be considered to be homogeneous and that multiple scattering is negligible the transmittance τ_λ of the particle suspension is given by

$$\tau_\lambda = I(L_o)/I_o$$
$$= \exp(-K_{ext} L_o), \qquad (7)$$

where L_o is the pathlength through the flame and K_{ext} (cm^{-1}) is the extinction coefficient, which for polydisperse spheres may be written as

$$K_{ext} = N\bar{C}_{ext}. \qquad (8)$$

The quantity $\bar{C}_{ext}(cm^2)$ is the mean extinction cross-section of the particles and is defined as

$$\bar{C}_{ext}=\int_{r=0}^{\infty} C_{ext}P(r)dr, \tag{9}$$

where C_{ext} represents the extinction cross-section of a homogeneous spherical particle and is given by the Mie theory as

$$C_{ext}=\frac{\lambda^2}{2\pi}\sum_{v=1}^{\infty}(2v+1)\ Re(a_v+b_v), \tag{10}$$

where $Re(a_V + b_V)$ denotes the real part of $(a_V + b_V)$.

In typical light scattering/absorption experiments the scattering cross section can be inferred from an internal calibration procedure[10-11] from the measured scattered fluxes from standard scatterers such as N_2 or CH_4 gas and the measured scattered flux from the particulates corresponding to the same scattering volume. On the other hand, K_{ext} can be calculated from Eq. (7). Note that the transmission is a relative measurement and thus requires no calibration. Defining the particle extinction efficiency as

$$Q_{ext}=\frac{C_{ext}}{\pi\ r^2}, \tag{11}$$

the particle radius may be determined from the relation

$$\frac{K_{vv}}{K_{ext}}=\frac{\lambda^2 i_{vv}}{4\pi^3 r^2 Q_{ext}}, \tag{12}$$

provided that the complex refractive index of the particle is known. For polydisperse system of particles, the right hand side of Eq. (12) takes the form

$$\frac{K_{vv}}{K_{ext}} = \frac{\lambda^2}{4\pi^3} \frac{\int_0^\infty i_{vv}\ P(r)dr}{\int_0^\infty Q_{ext}\ r^2\ P(r)dr}. \qquad (13)$$

The inferred size distribution parameters (r_o, σ) must satisfy simultaneously Eqs. (1) and (8). In this study the size distribution function was determined using the photocorrellation method[10-11] and the monodisperse results were utilized in the data analysis. It should be noted that the inferred volume fractions are independent of the type of P(r) used.

2.b. Inhomogeneous Particulates

From an optical standpoint a two component inhomogeneous particle may be treated, in the limiting cases, by two configurations: (i) as a coated sphere where the core consists entirely of one of the components and the second component constitutes the outer shell, and (ii) by a mixture in which one of the components is uniformly dispersed in a matrix of the second component. These two cases are discussed in the next sections treating the particles as spherical. It should be noted that in reacting systems the particles are not spherical but rather agglomerates of arbitrary structure. In this respect it has been shown that if the primary particles that constitute the agglomerate are small, typically 20 nm in diameter or less, and the total number of primary particles in the agglomerate is less than about 30 then the refractive index of the primary particle may be considered to be the same as the effective index of the agglomerate[11-12]. Thus, the treatment of the particles as

spherical in this study is justified. It should however be noted that soot is almost always characterized by primary particles in the diameter range of 10 nm to 60 nm, while the number of primaries per aggregate can reach the order of several hundred in overfire regions of leavity sooting systems. In such cases the sphericity assumption that is invoked in the present work would not be valid and further study is required to analyze such systems thoroughly.

2.b.1 Coated Sphere Model

Solutions for the scattering of electromagnetic radiation by two homogeneous concentric spheres embedded in air were developed by Aden and Kerker[8]. The form of the relations of the scattering and extinction of concentric spheres is the same as that of the homogeneous spheres (see Eqs. (4) and (5)) with the expressions for a_v and b_v modified accordingly. Specifically, assuming that the diameter of the inner spherical core is d_c and the diameter of the shell is d_s the electric and magnetic multiple coefficients may be expressed in terms of the complex refractive indices of the core $\overline{m}_1$ and shell $\overline{m}_2$ as well as the corresponding size parameters $\left(x=\frac{\pi d_c}{\lambda}\right)$ and $\left(y=\frac{\pi d_s}{\lambda}\right)$. A useful representation of the modified coefficients $\overline{a}_v$ and b_v for computational purposes is given by Bohren and Huffman[9] as

$$\overline{a}_v = \frac{\left[\overline{D}_v\sqrt{\overline{m}_2} + \frac{v}{y}\right]\psi_v(y) - \psi_{v-1}(y)}{\left[\overline{D}_v\sqrt{\overline{m}_2} + \frac{v}{y}\right]\xi_v(y) - \xi_{v-1}(y)} \tag{14}$$

and

$$\overline{b}_v = \frac{\left[\overline{m}_2/\overline{G}_v + \frac{v}{y}\right]\psi_v(y) - \psi_{v-1}(y)}{\left[\overline{m}_2/\overline{G}_v + \frac{v}{y}\right]\xi_v(y) - \xi_{v-1}(y)}, \tag{15}$$

where

$$\overline{D}_\nu = \frac{D_\nu(\overline{m}_2 y) - A_\nu X'_\nu(\overline{m}_2 y)/\psi_\nu(\overline{m}_2 y)}{1 - A_\nu X_\nu(\overline{m}_2 y)/\psi_\nu(\overline{m}_2 y)} \tag{16}$$

$$\overline{G}_\nu = \frac{D_\nu(\overline{m}_2 y) - B_\nu X'_\nu(\overline{m}_2 y)/\psi_\nu(\overline{m}_2 y)}{1 - B_\nu X_\nu(\overline{m}_2 y)/\psi_\nu(\overline{m}_2 y)}$$

$$A_\nu = \psi_\nu(\overline{m}_2 x)\frac{\overline{m}_r D_\nu(\overline{m}_1 x) - D_\nu(\overline{m}_2 x)}{\overline{m}_r D_\nu(\overline{m}_1 x) X_\nu(\overline{m}_2 x) - X'_\nu(\overline{m}_2 x)}$$

and

$$B_\nu = \psi_\nu(\overline{m}_2 x)\frac{\overline{m}_r D_\nu(\overline{m}_2 x) - D_\nu(\overline{m}_1 x)}{\overline{m}_r X'_\nu(\overline{m}_2 x) - D_\nu(\overline{m}_1 x) X_\nu(\overline{m}_2 x)}. \tag{17}$$

Here Ψ, ξ and X are the Ricatti Bessel functions, D_ν the logarithmic derivative defined as Ψ'_ν/Ψ_ν, and $\overline{m}_r$ is the refractive index of the shell relative to the refractive index of the core. Prime notation denotes differentiation with respect to the entire argument. Calculations of the scattering and extinction coefficients for coated and uncoated spheres as function of the core to shell ratio are presented in section 3.

2.b.2. Effective Medium Models

The coated sphere model is unlikely to apply for those conditions where agglomeration and dispersion of one component throughout the particle matrix dominate. However, in such cases, as Bohren and Huffman[9] point out the average dielectric function of an inhomogeneous particle may be determined by approximate methods provided that the properties of the constituent phases are known. The two most commonly used results for the effective optical properties of two component solid phase mixtures are the Maxwell-Garnett[13] and the Bruggerman[14] theories. The Maxwell-Garnett theory requires that a dominant phase (i.e matrix) in the mixture should always be present and the optical properties of each phase are defined with respect to vacuum. The Bruggerman theory, on the other hand, has the advantage of

being invariant with respect to the phase. The invariance is achieved by assuming that all phases are embedded in the effective medium itself and thus both phases are treated symmetrically. In this study the particles are assumed to conform to the Maxwell-Garnet theory since previous work has revealed iron oxide to be present within seeded particulates with volume percentages less than 25 percent.[6]

Thus if ε is the volume fraction of one component dispersed in the matrix of the second component the Maxwell-Garnett theory yields for the effective complex refractive index, m_e, the relation[9],

$$m_e = \overline{m}_2 \left[\frac{\overline{m}_1^2 + 2\overline{m}_2^2 + 2\varepsilon(\overline{m}_1^2 - \overline{m}_2^2)}{\overline{m}_1^2 + 2\overline{m}_2^2 - \varepsilon(\overline{m}_1^2 - \overline{m}_2^2)} \right]^{1/2} . \qquad (18)$$

where $\overline{m}_1$ and $\overline{m}_2$ are the refractive indices of the inclusion and matrix materials respectively. The parameter ε is determined from the known amounts of each component $\left(\varepsilon = \frac{\text{Volume of inclusion}}{\text{Volume (inclusions+matrix)}}\right)$. It should be noted that as the inclusion volume fraction tends to zero ($\varepsilon \to 0$) Eq. (18) yields the refractive index of the matrix material. Also for sufficiently large volume fractions ($\varepsilon \to 1$) the geometrical configuration becomes important since separated-grain microstructure of the two components cannot be maintained as the volume fraction approaches unity[15]. In the following sections calculations are presented for the scattering efficiency using both the Maxwell Garnett and coated sphere model and comparisons are made. In these calculations volume equivalency is defined by the relation

$$\frac{\text{Volume of inclusions}}{\text{Volume of (inclusions+matrix)}} = \left(\frac{r_c}{r_s}\right)^3 \qquad (19)$$

where r_c and r_s are the radius of the core and shell respectively. Note that schematics for the coated sphere model and the effective medium model are shown in Figure 1.

3. Scattering and extinction efficiencies

To assess the characteristics of the Maxwell Garnett effective medium model and the coated sphere the extinction and scattering efficiencies of two-component particles were calculated. For the case of coated spheres, the scattering cross sections are normalized using the cross sectional area corresponding to the shell radius. First, extinction and scattering efficiencies were calculated for coated spheres with a fixed shell refractive index $\overline{m}$ = 2.0 - 1.0i. The core refractive index was set equal to the index of the shell plus 50 percent, $\overline{m}$ = 3.0 - 1.5i, and plus 100 percent, $\overline{m}$ = 4.0 - 2.0i. The shell diameter was fixed to either 10, 50 or 100 nm, and the ratio of the core diameter to shell diameter was varied from 0.0 to 1.0. These ratios correspond to particles composed completely of the shell material for a core/shell diameter ratio of 0.0, and to homogeneous particles composed of the core material for a core/shell ratio of 1.0. The extinction efficiencies for the 50 nm particles with core indices enhanced 50 and 100 percent above the shell index are presented in Figure 2. The corresponding scattering efficiencies for the particles are presented in Figure 3.

To compare the coated sphere extinction and scattering efficiencies with the Maxwell Garnett model, the following calculations were also performed. For each [core/shell] diameter ratio, the equivalent inclusion volume percentage was determined from Eq. (19), namely ε = (radius core/radius shell)^3. The effective refractive indices were calculated by the Maxwell Garnett relation Eq. (18) assuming a matrix with refractive index $\overline{m}$ = 2.0 - 1.0i, and inclusions with refractive indices increased by 50 and 100 percent, and with volume percentages ε. The values of ε used vary from 0% to 100% as d_c/d_s varies from 0.0 to 1.0 and were calculated using Eq. (19). The Maxwell Garnett effective indices were then used to calculate the extinction and scattering efficiencies for 10, 50 and 100 nm diameter particles using the homogeneous Mie theory. The resulting Maxwell Garnett extinction and scattering

efficiencies for the 50 nm particles are also presented in Figures 2 and 3, respectively.

As it may be seen from Figures 2 and 3 the agreement between the coated sphere efficiencies and the corresponding Maxwell Garnett efficiencies is excellent. For the 50 percent enhanced core/inclusion indices, the average deviation between the coated sphere and Maxwell Garnett extinction and scattering efficiencies is 0.29 and 0.87 percent, respectively. For the 100 percent enhanced indices, the average difference between the coated sphere and Maxwell Garnett efficiencies is 0.91 and 1.45 percent for the extinction and scattering efficiencies, respectively.

In addition to particles with enhanced core/inclusion refractive indices, efficiencies were calculated for particles with reduced core and inclusion indices with respect to the shell/matrix indices. The extinction efficiencies were calculated for 50 nm particles with a shell/matrix refractive index $\overline{m}$ = 3.0 - 1.5i and a core/inclusion refractive index $\overline{m}$ = 2.0 - 1.0i, which corresponds to a 33.3 percent reduction in refractive index. The extinction efficiencies for the coated sphere and Maxwell Garnett models are presented in Figure 4. The agreement between the coated sphere and Maxwell Garnett efficiencies is again excellent, with the average difference being 0.26 percent. To investigate the influence of particle size on the observed trends, extinction efficiency calculations were also perfomed for 10 and 100 nm diameter particles for the case of shell/matrix index $\overline{m}$ = 2.0 - 1.0i, and core/inclusion index $\overline{m}$ = 4.0 - 2.0i (100% increase). The extinction efficiency profiles for the coated sphere and Maxwell Garnett models are presented in Figure 5. The agreement between the coated sphere and Maxwell Garnett efficiencies is found to decrease with increasing particle size, with the 10 nm diameter particle efficiencies yielding an average difference of only 0.03 percent and the 100 nm diameter particle efficiencies yielding an average difference of 4.45 percent.

Note that the extinction efficiency profiles for the particles presented in Figures 2, 3, 4 and 5 contain no extrema, but rather increase or decrease smoothly. However, thinly coated particles may be characterized by extinction efficiencies which are greater than those of homogeneous particles composed of either constituent material. Such maxima in efficiencies have been reported for water coated, soot particles,[16] and for a variety of soot and iron/iron oxide particles.[17] Peaks in extinction efficiency profiles of coated spheres occur as a result of the complex nature of light scattering and absorption by small particles. Since scattering is primarily a surface phenomenon while absorption takes place throughout a particle, the presence of a thin coating of a material with markedly different scattering characteristics may greatly affect the overall optical behavior. To assess the ability of the Maxwell Garnett model to predict such effects, the extinction efficiencies were calculated for 50 nm diameter particles using a shell/matrix refractive index $\overline{m}$ = 2.0 - 1.0i and a core/inclusion index $\overline{m}$ = 2.0 - 3.0i. The coated sphere and Maxwell Garnett extinction efficiencies for these particles are presented in Figure 6. The average difference between the predicted efficiencies by the two models is 0.99 percent. Furthermore, both the coated sphere and the Maxwell Garnett profiles exhibit a maximum. The coated sphere efficiency profile peaks at a core/shell diameter ratio of 0.738 while the Maxwell Garnett efficiency curve peaks at a core/shell ratio of 0.750, with a corresponding difference of 1.63 percent between peaks.

4. Flame Data Analysis

In addition to the extinction and scattering efficiency calculations presented above, data for scattering/extinction measurements from a flame were analyzed using the Eqs. (1) - (17), presented above employing both the coated sphere and Maxwell Garnett models. Extinction and differential scattering coefficients measured in a fuel rich, premixed propane and oxygen flame seeded with 0.32 percent by weight iron to fuel were analyzed. Complete details of the flame conditions, and experimental methods are presented elsewhere.[6,17] For convenience the measured scattering and extinction coefficients along with the percentage volume fractions ε of the iron species are presented in Table 1 as function of position above the burner surface. Since the intent of this paper is to examine the effects of optical inhomogeneities on the analysis of scattering/absorption, data analysis is based on particles composed of combinations of soot and either elemental iron or the iron oxide Fe_2O_3. Refractive indices used are representative of those in the visible spectrum, and are $\bar{m} = 2.4 - 3.5i$ for iron,[18] $\bar{m} = 1.6 - 0.3i$ for Fe_2O_3[6] and $\bar{m} = 1.9 - 0.4i$ for soot.[19].

To assess the effects of particle inhomogeneity due to the inclusion of iron species, the light scattering data was inverted as follows. For each data point, the metal volume percentage within the particles was calculated from a mass balance. Using the calculated metal volume percentages, the corresponding equivalent core/shell diameter ratios were also calculated at each point. The metal volume percentages ranged from 8.6 to 22.8 percent, with corresponding core/shell diameter ratios ranging from 0.44 to 0.61. Using the measured extinction and scattering coefficients, the calculated metal volume percentages and core/shell ratios, and the corresponding optical properties, the data was analyzed. First, the data was reduced using the homogeneous Mie scattering theory and an assumed refractive index for

soot $\overline{m} = 1.9 - 0.4i$. The data was then analyzed using the Maxwell Garnett effective medium model. For each data point, the effective refractive index was calculated using the index of soot as the matrix material, and either the refractive indices of Fe_2O_3 or Fe for the inclusion material. For the final case, the data was analyzed using the coated sphere theory. The core material was designated as either Fe_2O_3 or Fe with corresponding refractive indices, and the shell was designated as soot. The core/shell diameter ratios used were those equivalent to the metal volume fractions used for the Maxwell Garnett analysis see Eq. (19). The flame data (see Table 1) was inverted for all three schemes, designated as pure soot, Maxwell Garnett and coated sphere cases, and the resulting soot particle diameters, number densities and volume fractions were evaluated. The soot volume fraction profiles corresponding to the soot and Fe_2O_3 particle analysis are presented in Figure 7, and the volume fraction profiles for the soot and Fe analysis are presented in Figure 8. The inferred particle diameter profiles are presented in Figure 9 for the soot and Fe analysis.

The inferred volume fraction profiles presented in Figures 7 and 8 contain several interesting trends. For both the Fe_2O_3 and Fe analysis, the Maxwell Garnett and coated sphere theories yield nearly identical volume fraction profiles. For the Fe_2O_3 analysis, the average difference between the Maxwell Garnett and coated sphere volume fractions is 0.65 percent. Similarly, for the Fe analysis the average difference in volume fraction profiles between the Maxwell Garnett and coated sphere models is 1.4 percent. A second item to examine in Figures 7 and 8 is the degree of agreement between the pure soot (homogeneous) based analysis and the inhomogeneous analysis, either the Maxwell Garnett or coated sphere models. For the soot/Fe_2O_3 case, there is no significant difference between the homogeneous profile and the two inhomogeneous profiles. Specifically, the average difference between the pure soot based volume fractions and the coated sphere volume fractions is less than 0.1 percent. However, the difference between the pure soot based volume

fractions and the Fe based inhomogeneous analysis is significant, with the average difference between the pure soot and coated sphere volume fractions equal to 21.7 percent. This result clearly shows that the Maxwell Garnett and coated sphere models for the submicron particles (< 100 nm in diameter) may yield similar particle volume functions when used in inverting light scattering/absorption data. However, the importance of the corresponding values of the refractive indices of the core and shell is significant and must be evaluated on a case by case basis..

5. Discussion

The present comparisons of the Maxwell Garnett and coated sphere models for use in the evaluation of light scattering characteristics and data analysis for two-component particulate systems reveal two interesting aspects. The notable features are the degree of agreement between the Maxwell Garnett effective medium model and coated sphere scattering theory, and the difference between the two inhomogeneous models as compared with homogeneous analysis. The latter results can be addressed by considering the refractive indices of the two constituent materials and the relative volume contribution of each. When the core/inclusion volume percentage and/or the differences between the refractive indices of the two components became significant, the optical inhomogeneity of the particle must be considered. For the present data analysis cases, the differences between the real and imaginary parts of the refractive indices of soot and Fe are 26.3 and 775. percent, respectively. These differences yield significant changes in the inferred particle size and most notably in the volume fractions when compared with the homogeneous analysis. In contrast, the difference between the soot and Fe_2O_3 indices are 15.8 and 25.0 percent for the real and imaginary parts, respectively. Consequently, for the Fe_2O_3 case, the inhomogeneous analysis yielded no significant change in the inferred particle parameters as compared with the homogeneous analysis. It should be noted that there are no clear criteria other than scattering/extinction efficiency calculations to determine exactly when particle inhomogeneity becomes important. However the present calculations show that particle optical inhomogeneity becomes negligible for core/shell diameter ratios less than 0.30 for the range of refractive indices considered in this study. In terms of the percentage volume inclusion this corresponds to less than approximately 3.0 percent.

The second notable feature of the Maxwell Garnett and coated sphere model comparison is the degree of agreement found both for efficiency calculations and the flame data analysis. Furthermore, the maximum in the coated sphere extinction efficiency profile (see Figure 6) was also present in the Maxwell Garnett extinction profile. Prior to discussing the principles involved in the observed similarities of the two models, it is useful to elaborate on one identifiable trend in the present results. The differences between the Maxwell Garnett and coated sphere extinction efficiencies reveal a marked dependence on particle size. Specifically, for the cases of the $\overline{m}$ = 2.0 - 1.0i shell/matrix and $\overline{m}$ = 4.0 - 2.0i core/inclusion (+100%), three different diameters were examined, namely 10, 50 and 100 nm. These correspond to particle size parameters of 0.064, 0.32 and 0.64, respectively, at a wavelength of 488 nm. The average differences between the Maxwell Garnett and coated sphere extinction efficiencies are 0.03, 0.91 and 4.45 percent for the 10, 50 and 100 nm diameter particles, respectively.

It should be noted that the Maxwell Garnett effective medium model has been studied under various conditions since the original work by Garnett in 1904.[13] The present results regarding the agreement between the Maxwell Garnett and coated sphere calculations are perhaps best explained by considering the alternative derivation of the Maxwell Garnett model reported by Niklasson and co-workers.[15] In their particular model, the two-component microstructure consisting of inclusions with a given volume fraction dispersed in a continuous matrix is recast as an equivalent coated sphere with a core composed of the inclusion material, the shell composed of the matrix material, and the core to shell diameter ratio determined by the inclusion volume fraction. The Maxwell Garnett effective dielectric function is then calculated by setting the leading term in the series expansion of the forward direction scattering function equal to zero. This approach is based on one definition of an effective medium, namely that the random unit cell, embedded in the effective

medium, should not be detectable by scattering of electromagnetic radiation. In other words, this criterion dictates that extinction of the random unit cell should be the same if it is replaced within a material with the effective dielectric permeability. Several important features of the Maxwell Garnett model are elucidated from the physics of this treatment. Specifically, in the small particle limit, the Maxwell Garnett effective medium model and the coated sphere scattering solution are essentially equivalent. This appears to be the case for the present calculations in which the agreement between the Maxwell Garnett and coated sphere extinction efficiencies was found to significantly increase with decreasing particle size parameter.

6. Summary

The results of the present study may be summarized as follows.

a. The coated sphere model and effective medium model yield equivalent extinction and scattering efficiencies for submicron (< 100 nm in diameter) inhomogeneous particles for the range of refractive indices examined for core/shell diameter ratios varying from 0.0 to 1.0 with equivalent volume percentages from 0.0 to 100 percent.

b. The optical inhomogeneity of the particles may result in significant uncertainties in the inferred particle volume fractions (21 percent or higher) when compared with volume fractions inferred from the homogeneous analysis.

c. Scattering and extinction efficiency calculations using the Maxwell Garnett and coated sphere models may be used in determining the range of parameters over which particle inhomogeneity is unimportant and thus the data analysis may be simplified.

This work was supported in part by AFOSR/USA Grant under No. F49 620-92-J0447DEF under the technical monitoring of Dr. J.M. Tishkoff.

References

[1] Ulrich G D Aug. 6 1984 *Chem. Eng. News*

[2] Jones A R and Wong W 1975 *Comb Flame* 24 139-140

[3] Charalampopoulos T T and Chang H 1991 *Comb Flame* 87 89-99

[4] Charalampopoulos T T Hahn D W and Chang H 1992 *Appl Opt* 30 6519-6528

[5] Ritrievi K E Longwell J P and Sarofim A F 1987 *Comb Flame* 70 17-31 1987

[6] Hahn D W and Charalampopoulos T T 1992 *Twenty Fourth Symp. (Int'l) on Comb. The Comb. Institute* Pittsburgh PA 1007-1014

[7] Van de Hulst H C 1981 *Light Scattering by Small Particles* Dover Publications Inc

[8] Aden A L and Kerker M 1951 *J Appl Phys* 22 1242-1246

[9] Bohren C F and Huffman D R 1983 *Absorption and Scattering of Light by Small Particles* John Wiles and Sons

[10] Charalampopoulos T T 1992 *Prog in Energ and Comb Science* 18 13-45

[11] Charalampopoulos T T and Chang H 1988 *Combust Sci and Tech* 59 401-422

[12] Chang H and Charalampopoulos T T 1991 *Proc R Soc London* A430 577-591

[13] Garnett Maxwell J C 1904 *Phil Trans R Soc* A203 385-

[14] Bruggerman D A 1935 *Am Phys* 24 636-

[15] Niklasson G A Granqvist G C and Hunderi O 1981 *Appl Opt* 20 26-30

[16] Fenn R W and Oser H 1965 *Appl Opt* 4 1504-1509

[17] Hahn D W 1992 *Soot Suppressing Mechanisms of Iron in Premixed Hydrocarbon Flames* PhD Thesis LSU

[18] Landolt-Bornstein 1985 *Numerical Data and Functional Relationships in Science and Technology New Series* III/156:250

[19] Chippet S and Gray W A 1978 *Comb Flame* 31 149-159

Table 1. Measured Scattering (K_{vv}) and Extinction (K_{ext}) Coefficients as Functions of Position above the Burner Surface in a Premixed Propane-Oxygen Flame with Fuel Equivalence Ratio ϕ = 2.5. The Seeding Rate was 0.32 Percent by Weight Iron to Fuel. A'so shown are Percentage Volume Inclusions ε which were taken to be the same for Fe and Fe_2O_3 for comparison purposes.

Height Above the Burner Surface H(mm)	$K_{vv} \times 10^5$ $cm^{-1}sr^{-1}$	$K_{ext} \times 10^2 cm^{-1}$	ε	d_{core}/d_{shell}
3	0.0398	1.22	22.8	.611
4	0.300	1.80	15.9	.542
6	2.110	2.83	10.6	.473
8	5.930	3.67	9.1	.450
10	11.30	4.52	8.2	.434
12	16.9	5.13	8.0	.431
14	23.2	5.69	7.7	.425
16	29.0	5.98	7.6	.424
18	34.3	6.16	7.5	.422

*Average uncertainty over all heights: K_v (90°) ± 3.5%

**Average uncertainty over all heights: K_{ext} ± 2.3%

Figure Captions

Figure 1. Geometrical configurations for the (i) Maxwell Garnett effective medium model and (ii) coated sphere light scattering theory.

Figure 2. Extinction efficiency profiles for shell/matrix refractive index $\overline{m}$ = 2.0-1.0i, and for core/inclusion refractive indices $\overline{m}$ = 3.0-1.5i (+50%) and $\overline{m}$ = 4.0-3.0i (+100%). The particle diameter used is 50 nm.

Figure 3. Scattering efficiency profiles for shell/matrix refractive index $\overline{m}$ = 2.0-1.0i, and for core/inclusion refractive indices $\overline{m}$ = 3.0-1.5i (+50%) and $\overline{m}$ = 4.0-3.0i (+100%). The particle diameter used is 50 nm.

Figure 4. Extinction efficiency profiles for shell/matrix refractive index $\overline{m}$ = 3.0-1.5i, and for core/inclusion refractive index $\overline{m}$ = 2.0-1.0i. The particle diameter used is 50 nm.

Figure 5. Extinction efficiency profiles for shell/matrix refractive index $\overline{m}$ = 2.0-1.0i, and for core/inclusion refractive index $\overline{m}$ = 4.0-2.0i.

Figure 6. Extinction efficiency profiles for shell/matrix refractive index $\overline{m}$ = 2.0-1.0i, and for core/inclusion refractive index $\overline{m}$ = 2.0-3.0i.

Figure 7. Inferred volume fraction profiles for soot and Fe2O3 particle analysis.

Figure 8. Inferred volume fraction profiles for soot and Fe particle analysis.

Figure 9. Inferred particle diameter profiles for soot and Fe particle analysis.

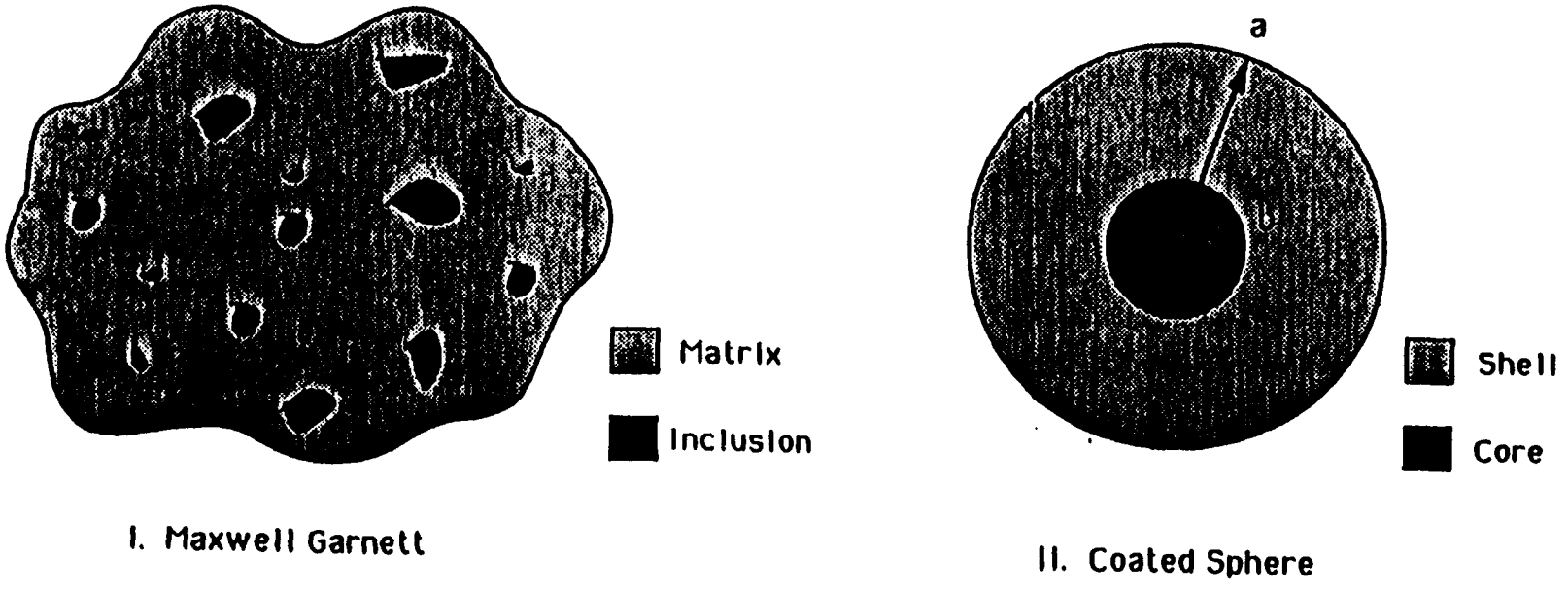

I. Maxwell Garnett

II. Coated Sphere

Figure 1

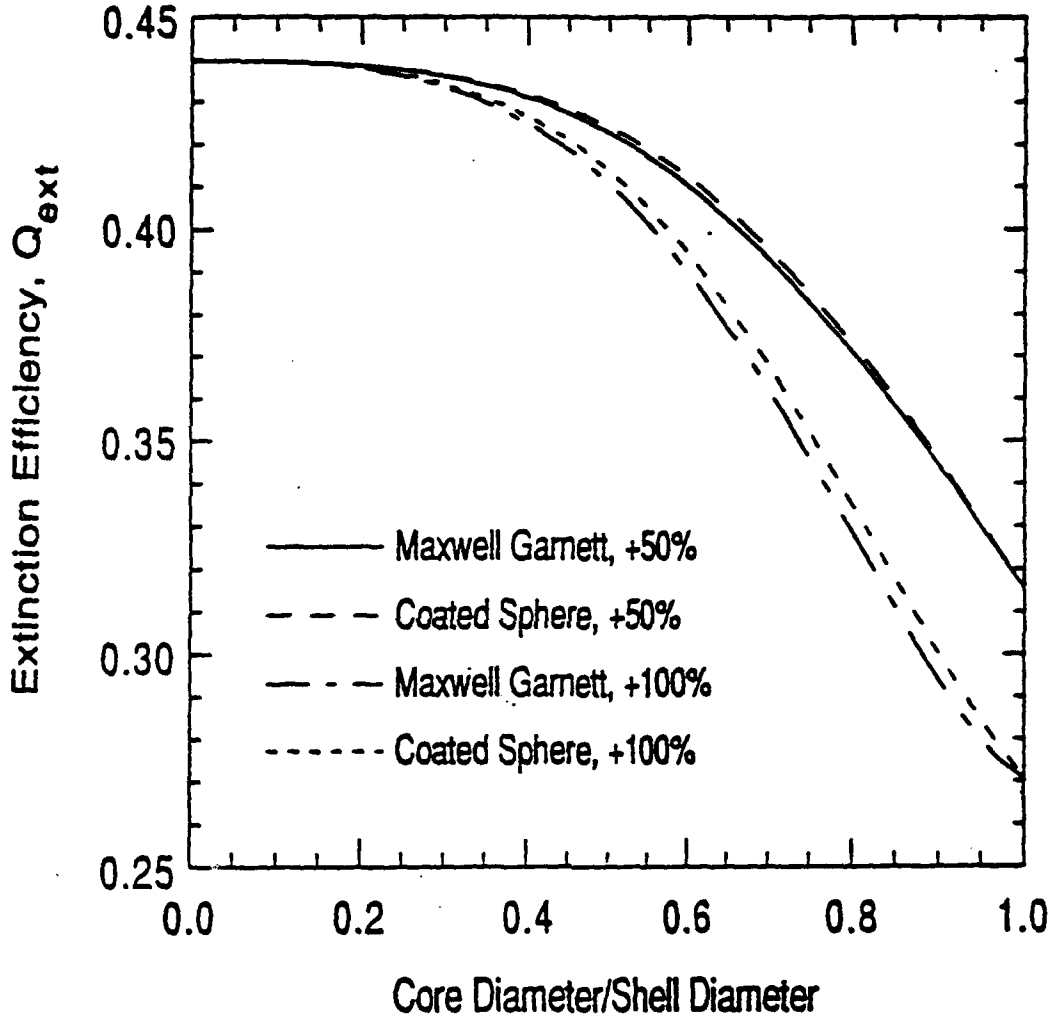
0.45
0.40
0.35
0.30
0.25
0.0
0.2
0.4
0.6
0.8
1.0
Extinction Efficiency, Q_{ext}
Core Diameter/Shell Diameter
Maxwell Garnett, +50%
Coated Sphere, +50%
Maxwell Garnett, +100%
Coated Sphere, +100%

Figure 2

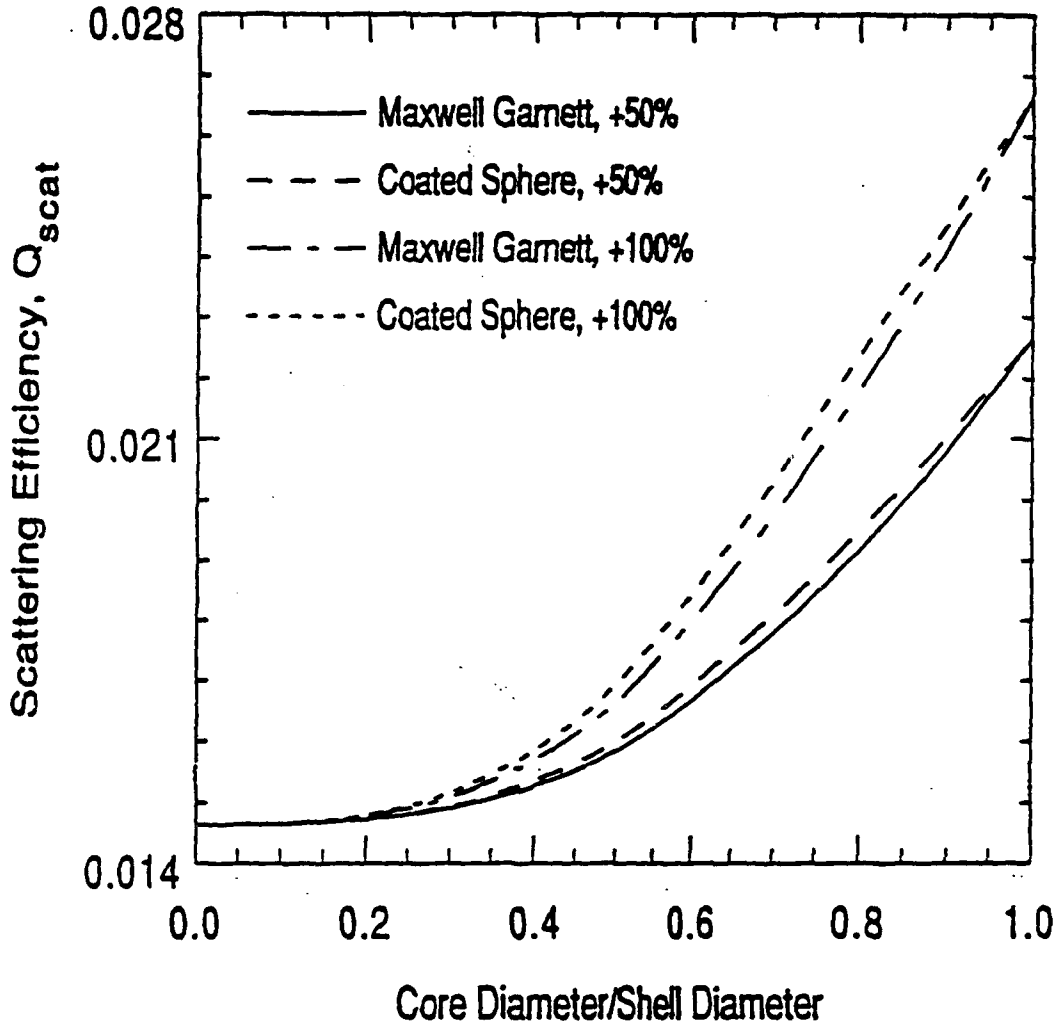
0.028
0.021
0.014
0.0
0.2
0.4
0.6
0.8
1.0
Scattering Efficiency, Q_{scat}
Core Diameter/Shell Diameter
Maxwell Garnett, +50%
Coated Sphere, +50%
Maxwell Garnett, +100%
Coated Sphere, +100%

Figure 3

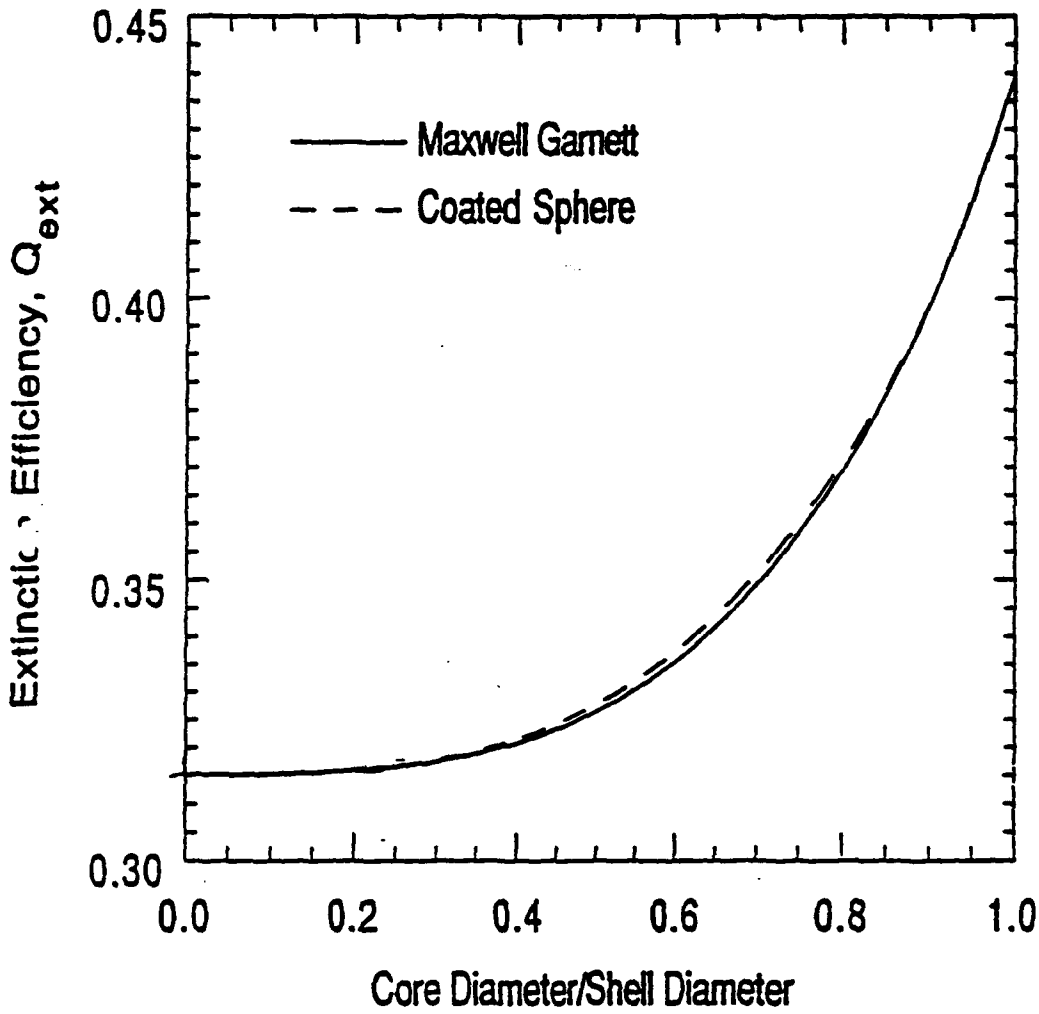
0.45
0.40
0.35
0.30
Extinction Efficiency, Q_{ext}
Maxwell Garnett
Coated Sphere
0.0
0.2
0.4
0.6
0.8
1.0
Core Diameter/Shell Diameter

Figure 4

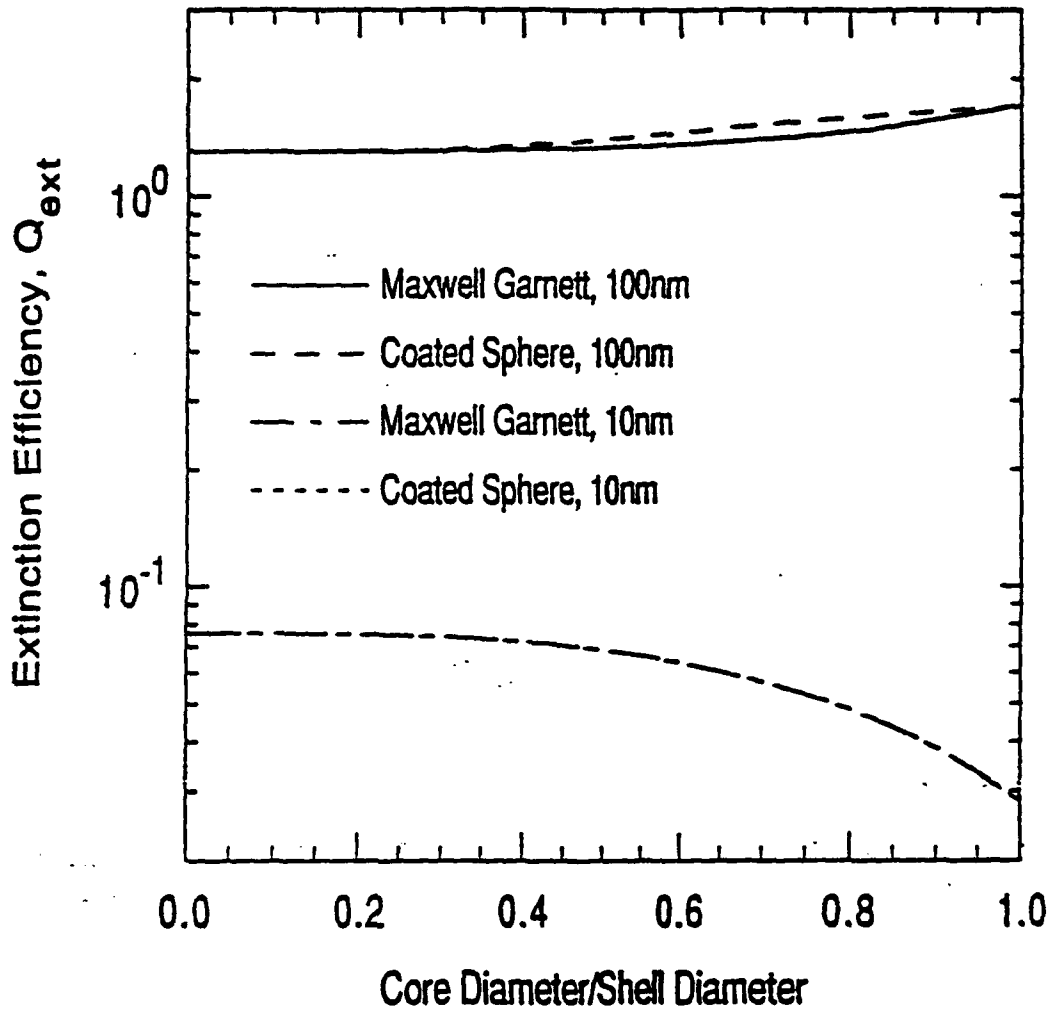
Extinction Efficiency, Q_{ext}
10^0
10^{-1}
Maxwell Garnett, 100nm
Coated Sphere, 100nm
Maxwell Garnett, 10nm
Coated Sphere, 10nm
0.0
0.2
0.4
0.6
0.8
1.0
Core Diameter/Shell Diameter

Figure 5

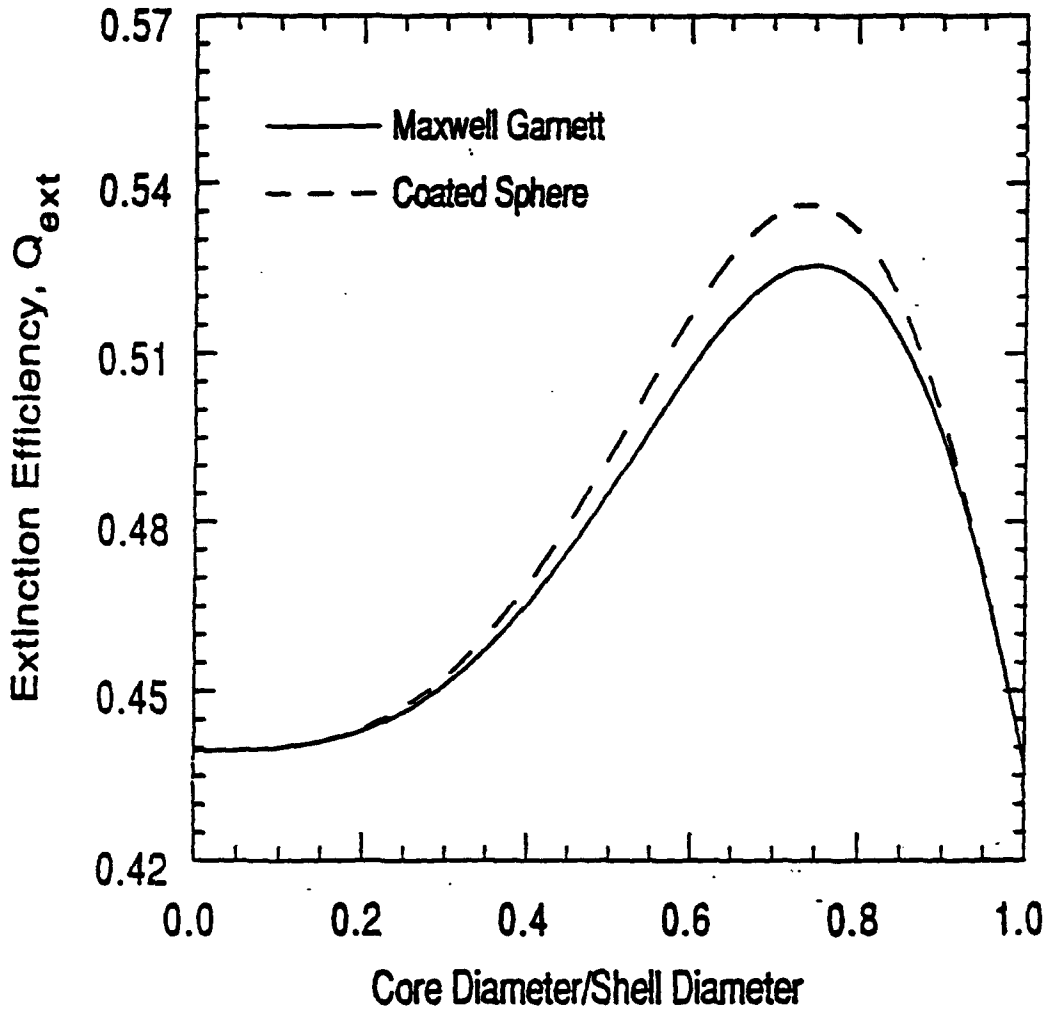
0.57
0.54
0.51
0.48
0.45
0.42
Maxwell Garnett
Coated Sphere
Extinction Efficiency, Q_{ext}
0.0
0.2
0.4
0.6
0.8
1.0
Core Diameter/Shell Diameter

Figure 6

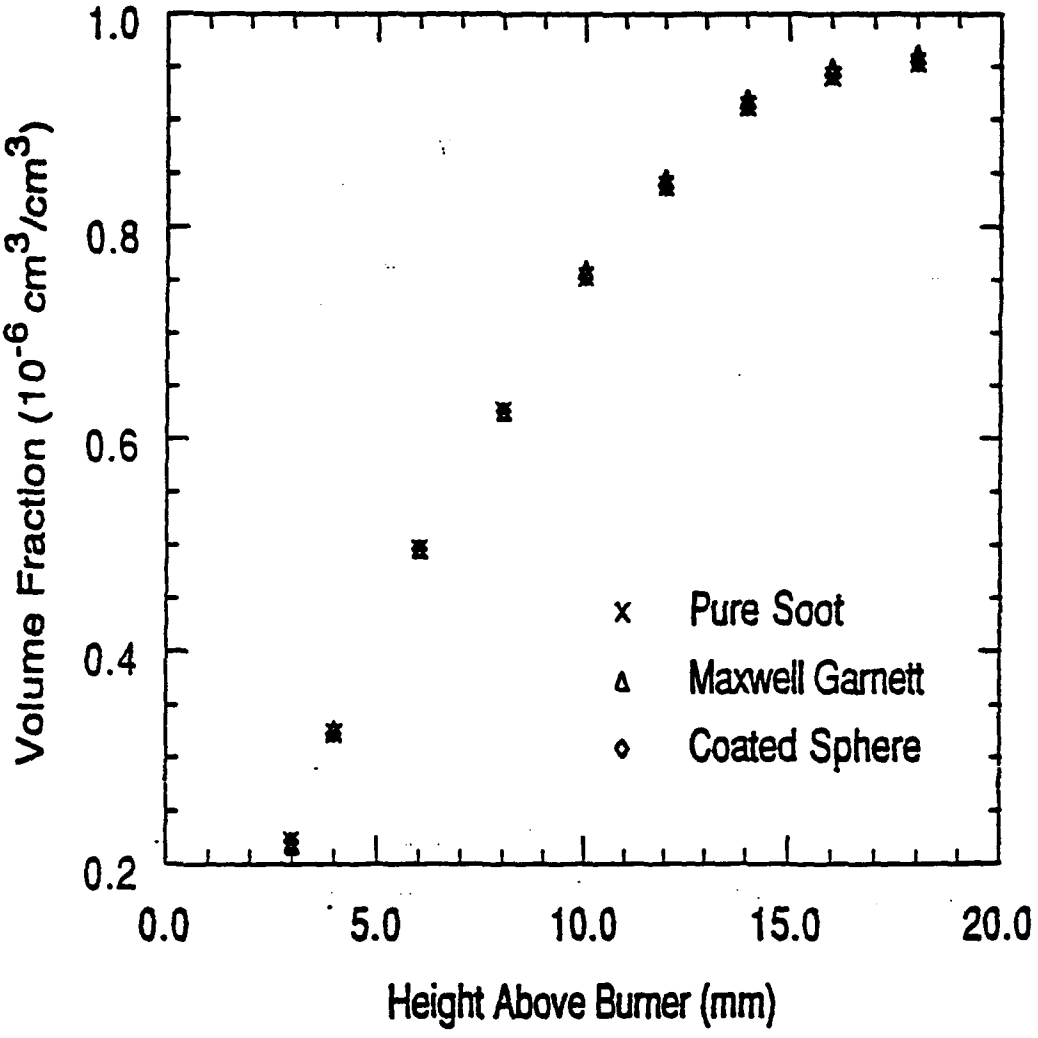
1.0
0.8
0.6
0.4
0.2
Volume Fraction (10^{-6} cm^3/cm^3)
0.0
5.0
10.0
15.0
20.0
Height Above Burner (mm)
Pure Soot
Maxwell Garnett
Coated Sphere

Figure 7

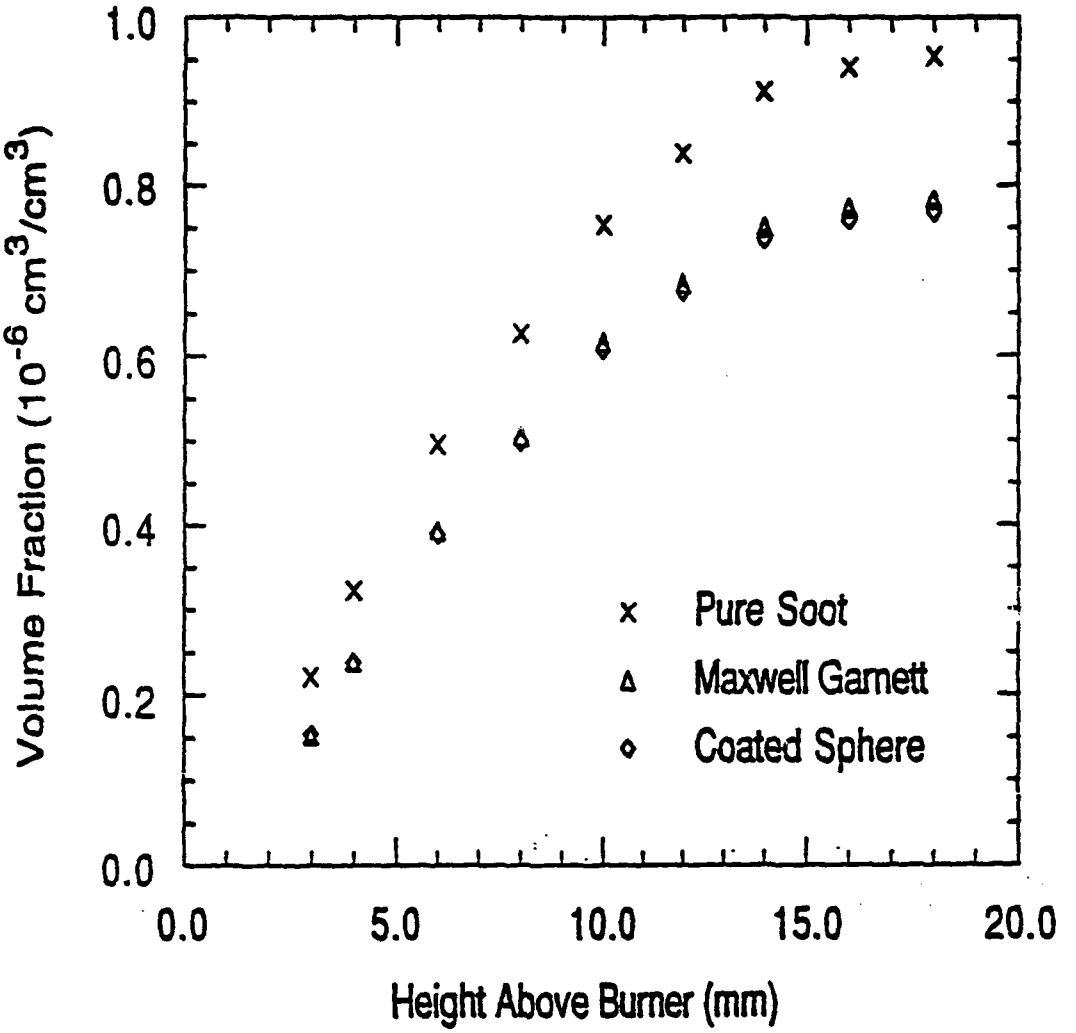
1.0
0.8
0.6
0.4
0.2
0.0
Volume Fraction (10^{-6} cm^3/cm^3)
0.0
5.0
10.0
15.0
20.0
Height Above Burner (mm)
Pure Soot
Maxwell Garnett
Coated Sphere

Figure 8

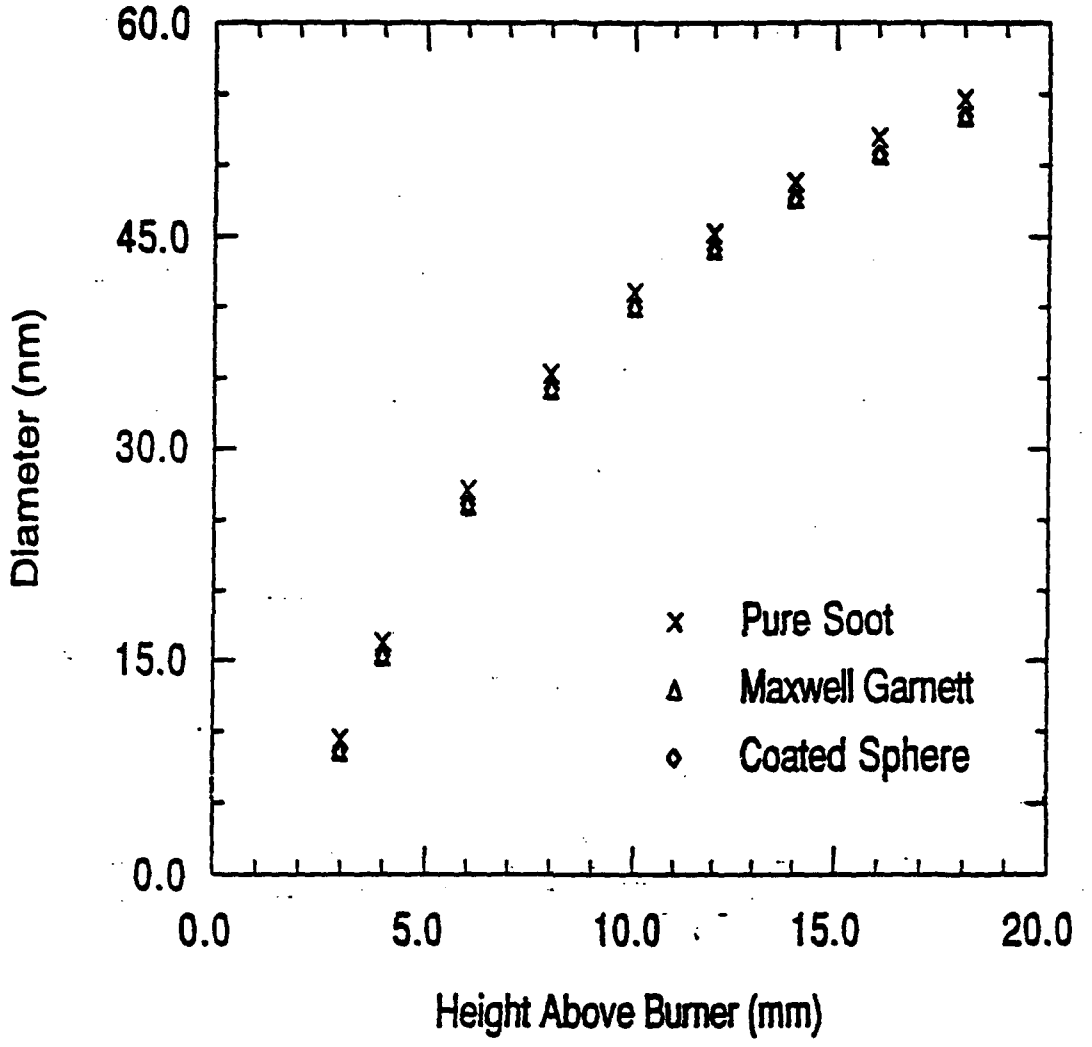
60.0
45.0
30.0
15.0
0.0
Diameter (nm)
0.0
5.0
10.0
15.0
20.0
Height Above Burner (mm)
Pure Soot
Maxwell Garnett
Coated Sphere

Figure 9

APPENDIX C

JOINT TECHNICAL MEETING
1993

CENTRAL AND EASTERN STATES SECTIONS
The Combustion Institute

COMBUSTION FUNDAMENTALS AND APPLICATIONS

March 15-17, 1993
Sheraton New Orleans
New Orleans, LA

Program Committee

R.W. Anderson	*K. Kailasanath*
D.W. Bahr	*F.C. Gouldin*
T.T. Charalampopoulos	*P.A. Tatem*

Refractive Indices of Carbonaceous Materials in the Temperature Range 25°C to 600°C

by

Barry J. Stagg
Columbian Chemicals Company
Operations and Technology Center
P.O. 96
Swartz, LA 71203

Tryfon T. Charalampopoulos
Mechanical Engineering Department
Louisiana State University
Baton Rouge, LA 70803

Abstract

A technique was developed that allows the determination of the temperature dependence of the refractive indices of carbonaceous materials from ellipsometric intensity measurements on bulk samples. The refractive indices of the carbonaceous samples pyrolytic graphite, amorphous carbon and flame soot were determined over the temperature range 25 - 600°C and the spectral region 400 - 700 nm. For all three samples it was found that the inferred refractive index shows insignificant variation with temperature for this range of temperature and wavelength. These results differ by 30 percent or more from the predictions of the Drude Lorentz dispersion model which has been used extensively to predict the variation of the optical properties of carbonaceous particulates.

Introduction

The complex refractive index (n - ik) of carbonaceous particulates such as soot is important in many areas of combustion research and in practical applications. This property characterizes the radiative transport in luminous flames and plays a key role in the interpretation of conventional light scattering measurements. Data for the refractive indices of soot have been obtained in both visible and infrared wavelengths [1-4]. However, the temperature dependence of the refractive index of soot or other carbonaceous materials has not been addressed.

Previous investigators have utilized the Drude-Lorentz model to predict the temperature dependence of the refractive index of soot by assuming that the damping constants of the free and bound electrons change with temperature. Lee and Tien [2] and Charalampopoulos et al. [5] assumed that the damping constants of the electrons were proportional to the square root of temperature. Calculations of the real part (n) of the refractive index using the dispersion model [5] in the temperature range 300 K to 1800 K have shown that the real part (n) of the complex refractive index is relatively insensitive to temperature change. Specifically, it was found that the real part (n) changes by less than five percent, whereas the imaginary part (k) of the refractive index may change by more than 50 percent when the temperature varies in this temperature range. Howarth et al. [6] assumed that the damping constants of the electrons were directly proportional to temperature and also assumed that the number density of free electrons increased with temperature. The assumption that the damping constants of the electrons are directly proportional to temperature is the extreme case corresponding to a perfect crystal and should therefore predict the maximum effect temperature can have on the refractive index. In this case, the real part of the refractive index was seen to change by as much as 20 percent as the temperature was varied from 300 K to 2000 K and the imaginary part of the refractive index was seen to vary as much as 300 percent for the same temperature change. Since most carbonaceous particulates occurring in combustion systems are not perfect crystals Howarth et al. [6] point out that their predicted temperature effects are too large.

Ideally, the temperature dependence of the index of refraction of combustion generated particulates should be evaluated under flame conditions. Nevertheless, since accurate knowledge of particle morphology [7], temperature and chemical composition under flame conditions is difficult, as a first step, an ex-situ study for this type of investigation was carried out.

The purpose of the present study is to determine the temperature dependence of the refractive indices of the carbonaceous samples, pyrolytic graphite, amorphous carbon and flame soot. This is accomplished by measuring the intensity of polarized light reflected from the surface of a bulk sample contained in a high temperature unit. Ellipsometric intensity measurements were carried out in the wavelength range 400 nm - 700 nm and as a function of the angular polarization state of the incident and

reflected light. On the other hand, due to sample oxidation, with the present system [8], the maximum temperature where reliable measurements could be carried out was 600°C [9].

Theory

The intensity of light through a simple Polarizer-Sample-Analyzer (PSA) ellipsometer system (see Fig. 1) may be written as [9-11]

$$I(P,A) = C_1 K_A K_P R_\perp [\rho^2 \cos^2(P) \cos^2(A) + \sin^2(P) \sin^2(A) + \frac{\rho}{2} \cos(\Delta) \sin(2P) \sin(2A)], \quad (1)$$

where K_A and K_P are the first principal transmittances of the analyzer and polarizer, $R_\perp$ is the perpendicularly polarized component of reflectivity, ρ and Δ the ellipsometric parameters of the sample [10,11], P and A are the polarizer and analyzer angles and C_1 is a constant. It can be shown from equation (1) that as the polarizer is rotated, the intensity through the PSA ellipsometer varies sinusoidally [12]. Therefore, equation (1) can be rewritten as a truncated Fourier series in the form

$$I(P,A) = a_0 [1 + a_2 \cos(2P) + b_2 \sin(2P)], \quad (2)$$

where the normalized coefficients, a_2 and b_2, are given as

$$a_2 = \frac{\rho^2 - \tan^2(A)}{\rho^2 + \tan^2(A)} \quad (3)$$

and

$$b_2 = \frac{2\rho \cos(\Delta) \tan(A)}{\rho^2 + \tan^2(A)}. \quad (4)$$

Solving equations (3) and (4), the ellipsometric parameters, ρ and Δ, are related to the normalized Fourier coefficients, a_2 and b_2, by the expression

$$\rho = \tan(A) \sqrt{\frac{1+a_2}{1-a_2}} \quad (5)$$

and

$$\cos(\Delta) = \frac{b_2}{\sqrt{1-a_2^2}}. \quad (6)$$

The Fourier coefficients may be determined from experimentally measured intensities by a discrete Fourier transform, given as

$$a_0 = \frac{1}{N} \sum_{i=1}^{N} I_i, \quad (7)$$

$$\tilde{a}_2 = \frac{2}{N} \sum_{i=1}^{N} I_i \cos(2P_i) \quad (8)$$

and

$$\tilde{b}_2 = \frac{2}{N} \sum_{i=1}^{N} I_i \sin(2P_i) , \qquad (9)$$

where I_i are the measured intensities at equally spaced azimuthal settings of the polarizer, P_i, N is the number of experimental measurements, and $a_2 = \tilde{a}_2/a_0$, $b_2 = \tilde{b}_2/a_0$. It is noted that if the sample surface is smooth and free of oxide films, the complex refractive index (n-ik) can be related to the complex ellipsometric parameter ($\rho e^{i\Delta}$) as [10]

$$n\text{-}ik = \sin(\theta)\left[\left(\frac{1-\rho e^{i\Delta}}{1+\rho e^{i\Delta}}\right)^2 \tan^2(\theta) + 1\right]^{1/2} , \qquad (10)$$

where θ is the angle of incidence of the incoming beam measured from the surface normal vector. Therefore, once the intensities are measured at equally spaced azimuthal settings of the polarizer, the complex refractive index can be evaluated through the application of equations (5) - (10).

Results

The refractive indices of three different carbonaceous samples were inferred from ellipsometric intensity measurements in the wavelength range 400 - 700 nm and in the temperature range 25°C - 600°C. The three carbonaceous samples include amorphous carbon (tradenamed POCO graphite), pyrolytic graphite and flame soot. For measurement purposes, the flame soot was compressed into a pellet yielding a surface suitable for reflection measurements [9]. Although it has been stated in the past that the surface generated from such a soot pellet is too rough for reflection measurements [13], the authors have shown that reflection measurements or ellipsometry measurements from a rough surface with specularity index as low as 0.07 can yield accurate refractive index values if the data are suitably inverted [9,14].

The experimentally determined values of the real and imaginary parts of the complex refractive index of the flame soot pellet are shown in Table 1 in the visible wavelengths for the temperatures 25°C, 300°C and 600°C. It is seen that the refractive index exhibits no measurable variation with respect to temperature, which is in contrast to the predictions of the Drude-Lorentz dispersion model. In Figure 2, the variation of the experimentally determined refractive index with respect to 25°C is compared to the predictions of the Drude-Lorentz dispersion model, which predicts variations in the index of up to 30 percent at 600°C.

Similar measurements were performed on the amorphous carbon and pyrolytic graphite samples. Although the overall magnitude of the refractive indices of each sample are different, no measurable variation in refractive index with respect to temperature is seen for any of the three carbonaceous samples for the wavelength and temperature range studied.

Discussion

The results of the present work show that the complex refractive index of the carbonaceous materials studied does not vary with temperature in the wavelength and temperature ranges considered. This does not imply that the refractive index of carbonaceous materials is completely independent of temperature at other values of wavelength and temperature. The temperature and spectral ranges evaluated in this study are 25-600oC and 400-700 nm, respectively. As pointed out by Bohren and Huffman [15], in general, temperature more greatly affects low-frequency than high-frequency absorption mechanisms. Therefore, the refractive indices of carbonaceous materials may be more greatly affected at infrared wavelengths than at the visible wavelengths studied. Measurements at the infrared wavelengths were not possible in this study because of the poor sensitivity of the ellipsometry technique at these wavelengths due to: (a) low polarizer quality available and (b) limitations of the ellipsometric facility used. It has also been pointed out [15] that absorption in amorphous solids tends to be independent of temperature, but that the far-infrared absorption in crystalline solids may change by several orders of magnitude as

temperature increases. Thus, it may be argued that the optical properties of amorphous carbon and flame soot (both amorphous materials) would be independent of temperature, but that the optical properties of pyrolytic graphite may be more sensitive to changes in temperature, since pyrolytic graphite approaches crystalline behavior [16]. Nevertheless, such conclusive inferences have yet to be established experimentally both for the amorphous and crystalline carbonaceous solids.

Conclusions

a. A technique for determining the temperature dependence of the refractive index of solid bulk samples was presented. The refractive index was determined from the measured Fourier coefficients of a polarizer-sample-analyzer (PSA) ellipsometer.
b. The refractive index of pyrolytic graphite, amorphous carbon and a flame soot pellet was inferred in the temperature range 25 - 600°C and the spectral range 400 - 700 nm.
c. For all three carbonaceous samples studied, the inferred refractive index showed insignificant temperature dependence.
d. The present results differ by 30% or more from the predictions of the Drude-Lorentz dispersion model using the, so far, assumed square-root temperature dependence of the electron damping constants for these type of amorphous or crystalline solids.

References

1. Daizell, W.H. and Sarofim, A.F. *J. Heat Transfer* 91:100 (1969).
2. Lee, S.C. and Tien, C.L. *Eighteenth Symposium (International) on Combustion, The Combustion Institute*, Pittsburgh, 1981, p. 1159.
3. Charalampopoulos, T.T. and Chang, H. *Combust. Sc. Technol.* 59:401 (1988).
4. Chang, H. and Charalampopoulos, T.T. *Proc. R. Soc. Lond.* A430:557 (1990).
5. Charalampopoulos, T.T., Chang, H. and Stagg, B. *Fuel* 68:1173 (1989).
6. Howarth, C.R., Foster, P.J. and Thrings, M.W. *Third International Heat Transfer Conf.* 5:122 (1966).
7. Charalampopoulos, T.T. *Prog. in Energy and Comb. Sci.* 18; 13 (1992).
8. Charalampopoulos, T.T. and Stagg, B.J. Submitted to Appl. Opt. (1992).
9. Stagg, B.J. PhD Dissertation, Mech. Eng. Dept., LSU, 1992.
10. Azzam, R.M.A. and Bashara, N.M. *Ellipsometry and Polarized Light* (North-Holland Publishing Company, Amsterdam 1977).
11. Stagg, B.J. and Charalampopoulos, T.T. *Appl. Opt.* 31:479 (1992).
12. Aspnes, D.E. *J. Opt. Soc. Amer.* 64:639 (1974).
13. Janzen, J. *J. Colloid Interface Sci.* 69:436 (1979).
14. Stagg, B.J. and Charalampopoulos, T.T. *Appl. Opt.* 30:4113 (1991).
15. Bohren, C.F. and Huffman, D.R. *Absorption and Scattering of Light by Small Particles*, John Wiley and Sons, New York, 1983.
16. Taft, E.A. and Philipp, H.R. *Phys. Rev.* 138:A197 (1965).

This work was supported by the National Science Foundation through grant CBT-8820480.

Table 1 .: Refractive index of propane soot pellet.

	T = 25°C		T = 300°C		T = 600°C	
λ (nm)	n	k	n	k	n	k
400	1.396	0.403	1.392	0.404	1.399	0.409
433	1.434	0.376	1.431	0.374	1.439	0.380
467	1.462	0.360	1.464	0.354	1.472	0.360
500	1.484	0.347	1.482	0.345	1.491	0.352
533	1.496	0.352	1.494	0.348	1.502	0.354
567	1.536	0.374	1.537	0.370	1.544	0.377
600	1.522	0.355	1.521	0.352	1.530	0.358
633	1.527	0.376	1.529	0.365	1.535	0.379
667	1.544	0.357	1.541	0.361	1.548	0.369
700	1.550	0.367	1.548	0.366	1.560	0.368

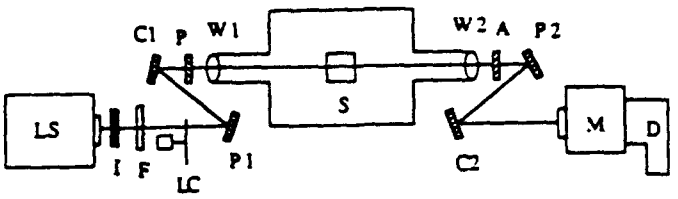

Figure 1: Schematic of PSA ellipsometer centered around a high temperature furnace. LS is the Xenon arc light source, C1 and C2 are curved first surface mirrors (200 mm focal length), P1 and P2 are plane first surface mirrors, W1 and W2 are quartz cell windows of the furnace, P and A are the polarizer and analyzer, M is the monochromator, D is the detector, S is the sample, I is the iris diaphragm, F is the cut-on filter, and LC is the light chopper.

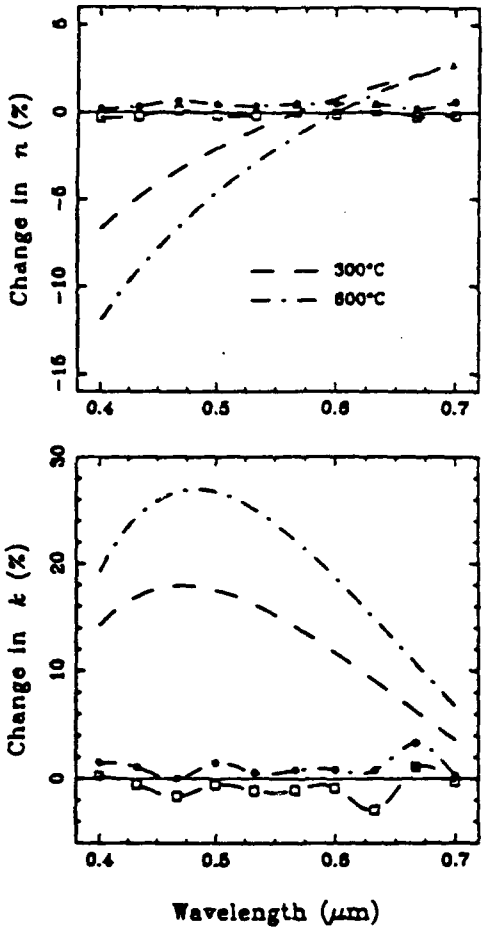

Figure 2: The percentage change of the real part (upper graph), n and imaginary part (lower graph), k, of the complex refractive index of flame soot with respect to room temperature (25°C) for the temperatures 300°C and 600°C. The smooth curves with no data points are predictions of the Drude–Lorentz model.

APPENDIX D

JOINT TECHNICAL MEETING
1 9 9 3

CENTRAL AND EASTERN STATES SECTIONS
The Combustion Institute

COMBUSTION FUNDAMENTALS AND APPLICATIONS

March 15-17, 1993
Sheraton New Orleans
New Orleans, LA

Program Committee

R.W. Anderson	*K. Kailasanath*
D.W. Bahr	*F.C. Gouldin*
T.T. Charalampopoulos	*P.A. Tatem*

JOINT TECHNICAL MEETING
1993

CENTRAL AND EASTERN STATES SECTIONS
The Combustion Institute

COMBUSTION FUNDAMENTALS AND APPLICATIONS

March 15-17, 1993
Sheraton New Orleans
New Orleans, LA

Program Committee

R.W. Anderson
D.W. Bahr
T.T. Charalampopoulos
K. Kailasanath
F.C. Gouldin
P.A. Tatem

Optical Properties of Two-Component Flame Particulates

D. W. Hahn and T.T. Charalampopoulos
Mechanical Engineering Department
Louisiana State University

This paper examines two models which are available to account for the optical inhomogeneity of two-component particles, namely the Maxwell Garnett effective medium model and coated sphere light scattering theory. The optical characteristics of both these model are examined and calculations are presented which correspond to two-component soot and iron particles. The application of the Maxwell Garnett and coated sphere theories is examined, and similarities between the two models within the small particle limit are discussed.

1. Introduction

Classical light scattering theory has many applications in the areas of flame and combustion science. Optical diagnostic techniques routinely employ light scattering and extinction measurements to infer soot particle sizes and number densities.[1] Additionally, scattering theory may also be applied to the calculation of flame emissivities and radiant heat transfer rates.[2] In these cases, knowledge of the optical properties of the particle of interest is of fundamental importance. For flame generated soot particles, the optical properties have been the subject of numerous studies.[3,4] Nevertheless, in many instances the flame particulates may not be optically homogeneous.[5] Particle inhomogeneities may result from inherent contaminants such as metallic species present in coal particles. Alternatively, inhomogeneities may be induced by the seeding of flames with metal based fuel additives, which may yield, due to differences in the nucleation rates of soot and metallic species, nuclei of one species coated by a second species, or a dispersion of one species within a matrix of the second species. Regardless of their origins, multicomponent or inhomogeneous soot particles may be characterized by optical properties significantly different from those of homogeneous particles. Consequently, when optical diagnostic techniques or heat flux calculations are to be applied to inhomogeneous particles, the effects of such inhomogeneities on the optical properties should be considered.

2. Models for Two-Component Particulates

One model available for two-component, inhomogeneous particles is the Maxwell Garnett effective medium model. The Maxwell Garnett theory provides the average dielectric function of a two-component mixture composed of inclusions of one material dispersed in an otherwise homogeneous matrix of a second material. The Maxwell Garnett effective dielectric function, ε_{MG}, may be expressed as

$$\varepsilon_{MG} = \varepsilon_m \frac{\varepsilon + 2\varepsilon_m + 2x(\varepsilon - \varepsilon_m)}{\varepsilon + 2\varepsilon_m - x(\varepsilon - \varepsilon_m)}, \qquad (1)$$

where ε and ε_m are the dielectric functions of the inclusion and matrix materials, respectively, and x is the volume fraction of the inclusions. The dielectric function is the square of the complex refractive index, $\varepsilon = (n\text{-}ik)^2$. The expression for the average

dielectric function described above was first derived by Maxwell Garnett,[6] and has been rederived under various conditions.[7,8] As will be discussed below, some of the derivations provide considerable insight into the optical behavior of two-component particles.

A special case of two-component particles exists when one component is concentrated entirely in the particle center. This configuration may be consequently described by the coated sphere model, where the inner sphere is designated as the core, and the outer, concentric sphere is designated as the shell. The formal solution to the scattering of light by a coated sphere has been developed by Aden and Kerker.[9]

3. Numerical Calculations

To assess the characteristics of the Maxwell Garnett effective medium model and the coated sphere scattering theory, a series of calculations were preformed. First, the extinction efficiencies of two-component particles were calculated using the Maxwell Garnett and coated sphere theories. In addition, actual light scattering data, collected under flame conditions which yield inhomogeneous particles, is analyzed using both the Maxwell Garnett and coated sphere models. The effects of iron addition on soot emissions has been the focus of recent research.[10-12] Furthermore, it is generally accepted that iron species are incorporated within soot particles, resulting in inhomogeneous particles. The authors have reported added iron to present in soot particles as the specific oxide Fe_2O_3 throughout the flame.[5,11] Other researchers have reported the presence of elemental iron in postflame zone particles.[10] Since the intent of this paper is to examine the optical characteristics of two-component particles, calculations will be based on particles composed of combinations of soot and either elemental iron or the iron oxide Fe_2O_3. Refractive indices used are representative of those in the visible spectrum, and are $\overline{m} = 1.9 - 0.4i$ for soot,[4] and $\overline{m} = 2.4 - 3.5i$ for iron,[13] and $\overline{m} = 1.6 - 0.3i$ for Fe_2O_3.[14]

The extinction efficiency Q_{ext} is defined as the extinction cross section of a particle divided by its cross sectional area, which becomes $Q_{ext} = C_{ext}/\pi r^2$ for spherical particles. For the case of coated spheres, the extinction cross section is normalized by the overall particle radius or shell radius. Extinction efficiencies were calculated for coated spheres by designating the shell as soot and the core as either Fe or Fe_2O_3. The shell diameter was fixed as 50 nm, and the ratio of the core diameter to shell diameter was varied from 0.0 to 1.0. These ratios correspond to solid soot particles for a ratio of 0.0, and to solid iron or iron oxide particles for a ratio of 1.0. The extinction efficiencies for the Fe_2O_3 and Fe cored, soot coated particles are presented in Figures 1 and 2, respectively. To compare the coated sphere extinction efficiencies with the Maxwell Garnett model, the following calculations were performed. For each core/shell ratio, the equivalent core material volume percentage was determined from the relation x = (radius core/radius shell)^3. The effective refractive indices were calculated using the Maxwell Garnett theory assuming inclusions of either Fe or Fe_2O_3 with volume percentages x, and with the matrix material being soot. The Maxwell Garnett effective indices were used to calculate the extinction efficiencies for 50 nm diameter particles with the homogeneous Mie theory. The equivalent Maxwell Garnett extinction efficiencies are also presented in Figures 1 and 2 for Fe_2O_3 and Fe inclusions, respectively.

The most interesting feature of Figures 1 and 2 is the excellent agreement between the coated sphere extinction efficiencies and the Maxwell Garnett efficiencies. For the soot/Fe_2O_3 particles, the maximum difference between the efficiencies is 0.25 percent. Similarly, the maximum deviation between the extinction efficiencies of the soot/Fe particles is 3.4 percent. Furthermore, the extinction profiles of the soot/Fe particles

possess a maximum, which occurs at a core/shell diameter ratio of 0.825 for the coated sphere efficiencies. The Maxwell Garnett extinction efficiency profile also possesses a maximum, which occurs at a core/shell ratio of 0.875, and differs form the coated sphere maximum by 6.1 percent.

In addition to the extinction efficiency calculations presented above, data reduction schemes employing the coated sphere and Maxwell Garnett theories were also evaluated. Extinction and differential scattering coefficients measured in a premixed propane and oxygen flame seeded with iron pentacarbonyl were analyzed. Complete details of the flame conditions and experimental methods and data are presented elsewhere.[5,11,14] To assess the effects of particle inhomogeneity due to the inclusion of iron species, the data was inverted as follows. For each data point, the volume percentage of iron within the particles was calculated from a mass balance. For the flame considered, the iron volume percentages are presented in Figure 3 along with the corresponding equivalent core/shell diameter ratio. The iron percentage varies from 22.8 to 7.5 percent, with a resulting core/shell ratio ranging from 0.61 to 0.42. Using the extinction and scattering coefficients and the estimated volume percentages and core/shell ratios, the data was analyzed as follows. First, the data was reduced using the homogeneous Mie scattering theory and the refractive index of soot, which corresponds to the neglecting of optical inhomogeneity. The data was then analyzed using the Maxwell Garnett effective medium model. For each data point, the effective refractive index was calculated using the index of soot as the matrix material, and either the indices of Fe_2O_3 or Fe for the inclusion material. The inclusion volume percentages used were those presented in Figure 3. For the final case, the data was analyzed using the coated sphere theory. The core material was designated as either Fe_2O_3 or Fe with corresponding refractive indices, and the shell was designated as soot. The core/shell diameter ratios used were also those in Figure 3. The flame data was inverted for all three cases, namely the homogeneous, Maxwell Garnett and coated sphere models, and the resulting soot particle diameters, number densities and volume fractions were evaluated. The soot volume fraction profiles corresponding to the soot and Fe_2O_3 particles are presented in Figure 4, and the volume fraction profiles for the soot and Fe particles are presented in Figure 5.

5. Discussion

The inferred volume fraction profiles presented in Figures 4 and 5 contain several interesting trends. For both the Fe_2O_3 and Fe analysis, the Maxwell Garnett and coated sphere theories yield nearly identical volume fraction profiles. For the Fe_2O_3 analysis, the average difference between the Maxwell Garnett and coated sphere volume fractions is 0.65 percent. Similarly, for the Fe analysis the average difference in volume fraction profiles between the Maxwell Garnett and coated sphere models is 1.4 percent. A second feature present in Figures 4 and 5 is the relative agreement between the soot based homogeneous analysis and the inhomogeneous analysis, either the Maxwell Garnett or coated sphere models. For the Fe_2O_3 analysis, there is no significant difference between the homogeneous profile and the two inhomogeneous cases. Specifically, the average difference between the solid soot based volume fractions and the coated sphere volume fractions is less than 0.1 percent. However, the difference between the soot based homogeneous volume fractions and the Fe based inhomogeneous analysis is significant, with the average difference between the pure soot and coated sphere volume fractions equal to 21.7 percent.

The differences between the homogeneous and two-component inhomogeneous analysis may be explained by the influence of the refractive indices on scattering characteristics. With reference to Figure 1, the extinction efficiency of a pure soot particle (core/shell ratio = 0.0) differs from the efficiency of a pure Fe_2O_3 particle

(core/shell ratio = 1.0) by only 7.8 percent. Furthermore, the extinction efficiency profile is nearly flat for core/shell ratios less than 0.5. Since there are no significant differences in the scattering characteristics of soot and Fe_2O_3 particles, nor any irregularities in two-component soot/Fe_2O_3 extinction efficiencies, the results presented in Figure 4 with respect to differences in homogeneous and inhomogeneous analysis are readily explained. However, the differences in the extinction efficiencies of solid soot and solid Fe particles is nearly 67 percent. Furthermore, the extinction efficiencies of soot/Fe particles may be enhanced by more than 83 percent over the solid soot particle efficiency. The large differences in refractive indices of soot and Fe and the resulting differences in light scattering characteristics, appear to be responsible for the differences between the homogeneous and inhomogeneous profiles in Figure 5.

The interesting result that there is no significant difference between the volume fraction profiles as determined with the Maxwell Garnett and coated sphere theories is perhaps best explained by examining an alternative derivation of the Maxwell Garnett effective medium model reported by Niklasson and co-workers.[8] In this model, the two-component microstructure consisting of inclusions with a given volume fraction dispersed in a continuous matrix is recast as an equivalent coated sphere with a core composed of the inclusion material, the shell composed of the matrix material, and the core to shell diameter ratio determined by the inclusion volume fraction. The Maxwell Garnett effective dielectric function is then calculated by setting the leading term in the series expansion of the forward direction scattering function equal to zero. Several important features of the Maxwell Garnett model are elucidated from the physics of this treatment. Specifically, in the small particle limit, the Maxwell Garnett effective medium model and the coated sphere scattering solution are essentially equivalent. This is the case for the present calculations, with particle size parameters on the order of 0.25. Additional insight is provided concerning the nature of the Maxwell Garnett theory. The Maxwell Garnett model is in general not invariant, with interchanging of the inclusion and matrix materials resulting in a different effective dielectric function. This phenomena may also be explained through the coated sphere analogy, since the scattering parameters of a coated sphere are altered if the core and shell are switched.

5. Conclusions

Several conclusions may be presented with respect to the behavior of two-component, inhomogeneous particles. The relative difference between the refractive indices of the two constituent materials and the percentage of each are important in assessing the effects of optical inhomogeneity. To this end, extinction efficiency calculations using the Maxwell Garnett and coated sphere models may be useful in evaluating the effects of inhomogeneity. This type of analysis will aid in determining cases in which the influence of particle inhomogeneity may be neglected, resulting in much simplified analysis. However, particle inhomogeneity may not in general be neglected during the analysis of light scattering data. In situations where a two-component model is required, however, neither the Maxwell Garnett nor the coated sphere theories may be applicable throughout the entire combustion system. Such ambiguities may be managed by selecting either theory as representative of particles throughout the flame. When the particles are in the small particle limit, the Maxwell Garnett and coated sphere theories yield equivalent solutions with respect to scattering and extinction calculations.

This work is supported in part by AFOSR grant no. F49 620-92-J0447DEF.

References

1. Charalampopoulos, T.T. and Chang, H., *Comb. Sci. Tech.*, 59:401-421 (1988).
2. Dalzell, W.H., and Sarofim, A.F., *J. Heat Transfer*, 91:100-104 (1969).
3. Chang, H. and Charalampopoulos, T.T., *Pro. R. Soc. London* A. 430: 577-591 (1990).
4. Chippett, S. and Gray, W.A., *Combust. Flame*, 31:149-159 (1978).
5. Charalampopoulos, T.T., Hahn, D.W., and Chang, H., *Appl. Optics*, 31:6519-6525 (1992).
6. Maxwell Garnett, J.C., *Philos. Trans. R. Soc. London* A. 203:385-420 (1904).
7. Bohren, C.F. and Huffman, D.R., *Absorption and Scanering of Light by Small Parncles*, Wiley, New York, 1983.
8. Niklasson, G.A., Granqvist, C.G., and Hunderi, O., *Appl. Optics*, 20: 26-30 (1981).
9. Aden, A.L. and Kerker, M., *J. Appl. Phys.*, 22:1242-1246 (1951).
10. Ritrievi, K.E., Longwell, J.P., and Sarofim, A.F., *Combust. Flame*, 70:17-31 (1987).
11. Hahn, D.W. and Charalampopoulos, T.T., *Twenty-Fourth (Int.) Symposium on Combustion*, Sidney, Australia, 5-10 July 1992.
12. Bonczyk, P.A., *Combust. Flame*, 87:233-244 (1991).
13. Landolt-Bornstein, *Numerical Data and Functional Relationships in Science and Technology*, New Series III/15b:250 (1985).
14. Hahn, D.W., *Soot Suppressing Mechanisms of Iron in Premixed Hydrocarbon Flames*, Ph.D. dissertation, Louisiana State University, 1992.

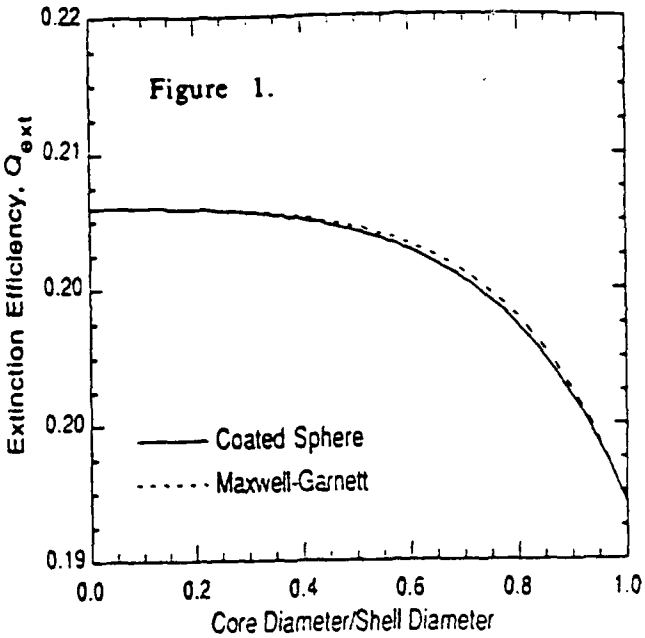

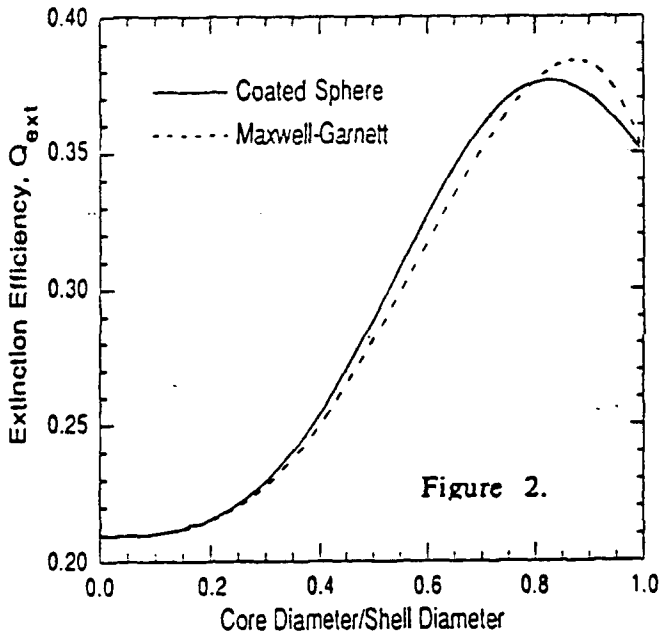

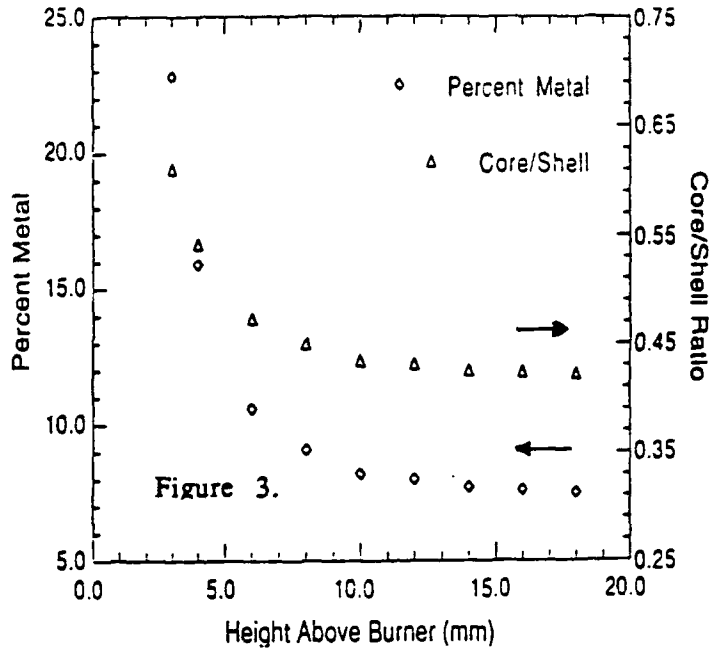

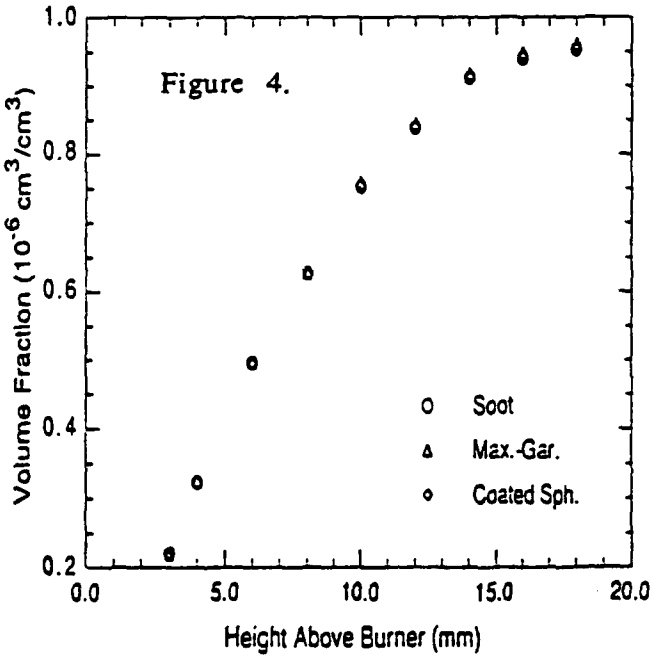

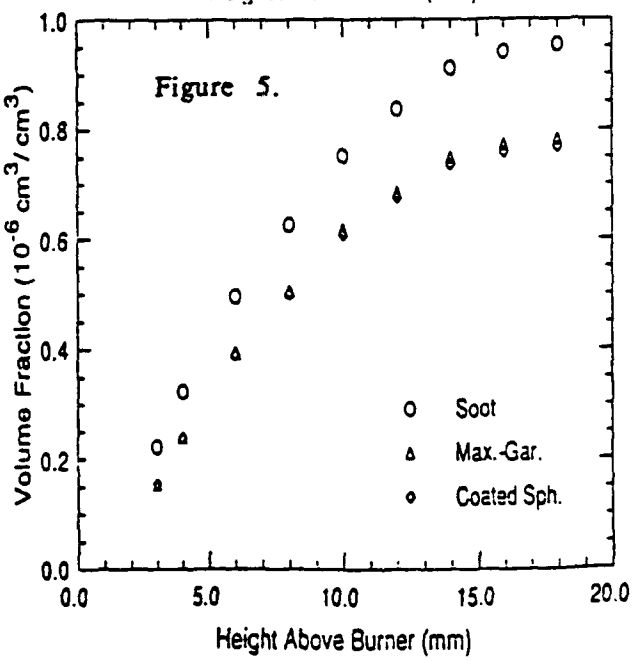

JOINT TECHNICAL MEETING
1993

CENTRAL AND EASTERN STATES SECTIONS
The Combustion Institute

COMBUSTION FUNDAMENTALS AND APPLICATIONS

March 15-17, 1993
Sheraton New Orleans
New Orleans, LA

Program Committee

R.W. Anderson
D.W. Bahr
T.T. Charalampopoulos
K. Kailasanath
F.C. Gouldin
P.A. Tatem

Extinction and Depolarization Characteristics of Agglomerated Flame Particulates

by

Pradipta Panigrahi, Demetris Venizelos and T.T. Charalampopoulos
Mechanical Engineering Department
Louisiana State University
Baton Rouge, LA 70808

ABSTRACT

A detailed analysis of the approximate expression for the extinction cross section of agglomerates of all particle size range, refractive indices and number of primary particles is presented. It is observed that the approximate extinction cross section is accurate to within 20%. The depolarized components of the scattered intensity are calculated for all types of agglomerates and are found to depend strongly on the agglomerate parameters. In addition the present calculations indicate that the reciprocity relation is not satisfied for agglomerates. Since multiple scattering may be the cause for the observed anomaly of the depolarized coefficients of the agglomerates preliminary experiments with dense polystyrene particle suspensions in water were carried out to better understand this phenomenon. Measurements are presented in the multiple scattering regime and the results are discussed.

INTRODUCTION

Electron micrographs of soot sample collected from flames demonstrate clearly the existence of agglomerated structures that depend on the flame conditions. Jones and Wong [1] determined the presence of soot agglomerates in flames from direct optical evidence. Several particle shapes are possible due to agglomeration such as clusters, straight chains or irregular random structures. Several investigators, see for example refs [2-4], have dealt with the development of theoretical models for the predictions of the absorption and scattering cross section of the agglomerated structures composed of two or more spherical monomers. More recently, Jones [5-6] developed an analytical model using the integral equation formulation for the scattering and absorption efficiencies of agglomerates consisting of spherical monomers with size parameter in the Rayleigh regime. Jone's expression for the extinction efficiency was recently modified by introducing a correction factor [7]. Since the expressions given in the Jone's formulation are computationally intensive other investigators [8-9] sought the development of simplified expressions for the scattering and absorption cross sections of the agglomerate. Charalampopoulos and Chang [10] inferred the primary particle diameter, number of the primary particles in the agglomerate and the number density of agglomerates using scattering, absorption and dissymmetry measurements in a premixed propane/oxygen flame. The data were analyzed using the scattering/absorption model for agglomerates and the refractive indices used were obtained, for the same flame system, using the Kramer-Krönig method of analysis in conjunction with spectral extinction data [11]. However, the anisotropic characteristics of the agglomerates and their implications in the interpretation of scattering measurements have not been fully explored. Recently, Charalampopoulos [12] observed that depolarized light scattering measurements in sooting flame possess the potential to yield particle morphology

information when combined with scattering/absorption and dissymmetry measurements .

The objective of this study is twofold: (a) To further investigate the accuracy of the approximate expressions for the extinction cross section of agglomerates for typical values of refractive indices, size parameter and number of primary particles and (b) To explore the possibility of using depolarization as a means for determining the type of soot agglomerate and the agglomerate parameters without knowing the index of refraction.

THEORY

Jones [6] developed the solution for electromagnetic wave scattering and absorption by agglomerates of small spheres with size parameter in the Rayleigh regime. Treating the incident field as a linearly polarized infinite plane wave and assuming that all small spheres have same complex refractive index (m = n+ik) but possibly a different diameter (dp), Jones derived an expression where the internal field of small spheres can be determined by solving a system of linear simultaneous equations. The scattered field at location (r, θ, ϕ) in space was described as a function of the incident field, the physical characteristics of the primary particles, their positions in the agglomerate and their internal fields. In addition limited calculations for the depolarized components of the scattering field were presented and it was inferred that the reciprocity theorem is valid for the agglomerated structures. It should be noted that the reciprocity theorem was stated originally by Krishnan [13]. Few years later Perrin [13] discussed the theorem more explicitly. Later Saxon [15] formulated mathematically the reciprocity theorem for a scattering object. According to reciprocity theorem, if we interchange the direction of the incident beam and the direction of observation, the component of the scattered wave in the direction of polarization remains unchanged; In other words, $H_v = V_h$ (See Figure 1). Here the subscripts represent the state of polarization of the incident light beam and the symbols V and H represent the state of polarization of the scattered beam. More specifically V or v and H or h represent the vertical and horizontal polarization orientation respectively. The approximate expression for the extinction cross section of the agglomerate is given by [5,7]:

$$C_{e,a} = N_p C_{e,s}, \qquad (1)$$

where N_p is the number of primary particles in an agglomerate and $C_{e,s}$ is the extinction cross section of a single spherical particle having same diameter and refractive index as the primary particles.

NUMERICAL CALCULATIONS

The percentage difference in extinction cross section using exact and approximate expression was calculated for different types of agglomerates and different ranges of agglomerate parameters. Results for straight chain agglomerate are shown in Figure 1 and 2. With reference to Figure 2 it may be seen that the percentage error is an increasing function of both real and imaginary part of refractive index, and is within 14.75%. In Figure 1 it is shown that the percentage error between the exact and approximate expression of extinction cross section is within 18%. It is also noted that the difference increases with increasing number of primary particles whereas it is a weak function of the size parameter. Similar trends of percentage error are observed for clusters. Specifically, the percentage

difference is below 5% for the range of refractive indices ($1.4 \leq n \leq 20$ and $0.4 \leq k \leq 1.0$), the number of primary particles ($3 \leq N_p \leq 30$) and the size parameter ($0.01 \leq x_p \leq 0.1$). For a random chain agglomerate the percentage difference is within 10% and varies randomly with the size parameter, the number of primary particles and the refractive index.

The depolarized scattered intensities H_v and V_h were calculated for straight chains, cluster and random structures using Jones' model as function of the diameter of primary particles, number of primary particles and refractive index. In Figure 3 the H_v to V_h ratio for straight chain is shown as a function of the scattering angle for conditions corresponding to different residence times in premixed propane/oxygen flame. The maximum deviation from the reciprocity theorem ($H_v/V_h = 1.0$) varies between -15% and 35%. For clusters the maximum deviation was between -15% to 335%. Calculations of H_v to V_h ratio for random chain as function of the scattering angle and of the primary particle number ($3 \leq N_p \leq 18$) (with $m = 1.6 + 0.53i$, and $d_p = 0.0156$ μm) resulted in a 20% deviation.

EXPERIMENTAL MEASUREMENTS

The results of the numerical calculations pointed to the need of experimental measurements to further study the validity of the reciprocity relations for agglomerates. It should be noted that in the agglomerate model multiple scattering between the primary particles was accounted for. Extinction and multiangle light scattering measurements of polystyrene particles (0.22 micron diameter) dispersed in purified deionized water were used in the present study. The differential scattering coefficient of the vertical-vertical polarization at 90°, the transmission and the depolarized scattering coefficient at different angles were measured. The differential scattering coefficient was determined by an internal calibration procedure using propane gas [16]. In order to test the light scattering set-up the ratio of the measured propane and methane differential scattering cross-sections at 90° were compared to previous results [17] before each experimental run.

RESULTS AND DISCUSSION

The measured scattered intensity from the polystyrene suspension normalized with the scattered intensity at 90°, was compared with the Mie theory prediction at different scattering angles for dilute suspensions. It was observed that reflections from the scattering cell contributed to the scattered intensities in the forward and backward scattering directions. The best agreement with the Mie theory predictions was in the angular range of 60° to 130°.

In order to simulate the effects of multiple scattering, high particle number densities were used to measure the H_v and V_h components of the scattered intensities at different scattering angles. Figure 4 shows the measured depolarized scattering coefficients for H_v and V_h orientation and their ratio as a function of scattering angle at transmission level of 19.8%. It was observed that the H_v and V_h intensities increase with decrease in transmission or increase in number density. Their ratio is also seen to be function of transmission

SUMMARY

1. The approximate expression for extinction cross section of an agglomerate was found to be accurate to within 20% irrespective of the type of agglomerate, size range and number of primary particles.
2. The ratio of the depolarized scattering components (H_v/V_h) was found to depend strongly on agglomerate parameters and the type of agglomerate.
3. The preliminary experimental results indicate that there is a need for further investigation of the validity of the reciprocity relations in dense particle dispersions.

This work is supported by the Air Force Office of Scientific Research (AFSOR) under the direction of Dr. Julian Tishkoff.

REFERENCES

1. Jones, A.R. and Wong, W. *Comb. Flame* **24**:139 (1975).
2. Lips, A. and Levine, S. *J. Colloid Interf. Sci.* **46**:139 (1974)
3. Ravey, J.C. *J. Colloid Interf. Sci.* **1**:139 (1974).
4. Ravey, J.C. *J. Colloid Interf. Sci.* **50**:545 (1975).
5. Jones, A.R. J. Phys. D.: *Appl. Phys.* **12**:1661 (1979).
6. Jones, A.R. *Proc. R. Soc. London* A **366**:111 (1979).
7. Ku, J.C. *J. Phys. D.: Appl. Phys.* :71 (1990).
8. Felske, J.D., Hsu P.F. and Ku, J.C. *J. Quant. Spect. Radiat. Transf.* **35**:447 (1986).
9. Kumar, S. and Tien C.L. *Comb. Sc. Technol.* **66**:199 (1989).
10. Charalampopoulos, T.T. and Chang, H. *Comb. Flame* **87**:89 (1991).
11. Chang, H. and Charalampopoulos, T.T. *Proc. R. Soc. London* **430**:577 (1991).
12. Charalampopoulos, T.T. *Prog. Energy and Comb. Sci.* **18**:13 (1992).
13. Krishnan, R.S. *Indian Acad. Sci.* **11**:21 (1938).
14. Perrin, F. J. Chem. Phys. **10**:415 (1942).
15. Saxon, D.V. Phys. Rev. **100**:1771 (1955).
16. Charalampopoulos, T.T. and Chang, H. *Comb. Sc. Technol.* **59**:401 (1988).
17. Rudder, R.R. and Bach, D.R. *J. Opt. Soc. Amer.* **58**:1260 (1968).

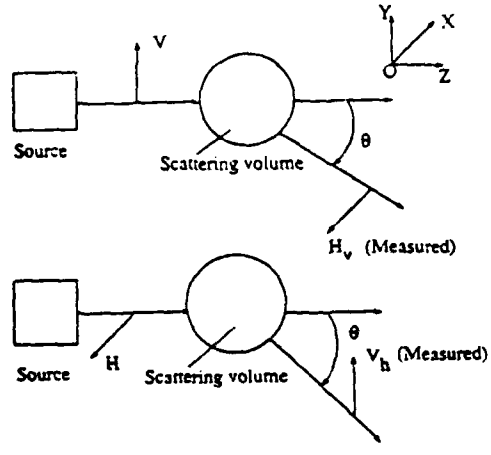

RECIPROCITY THEOREM

$$H_v = V_h$$

Figure 1. Depolarized scattering coordinate system.

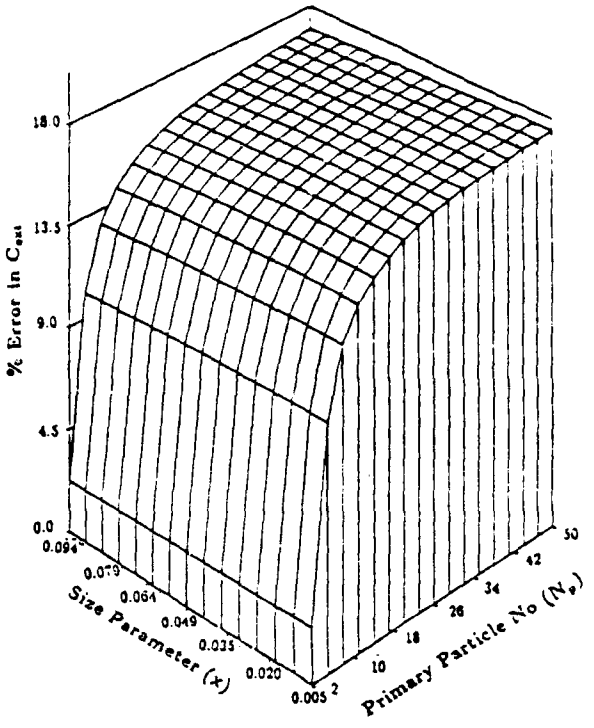

Figure 2. Percentage error in extinction cross section of straight chain with $\bar{m}$ = 2.0 - 1.0 i with correction.

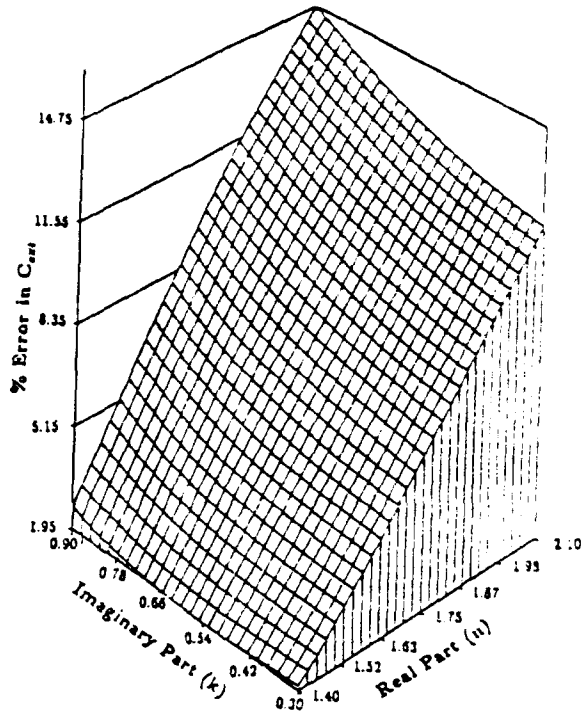

Figure 3. Percentage error in extinction cross-section of straight chain with N_p = 10 and size parameter of 0.01 with correction

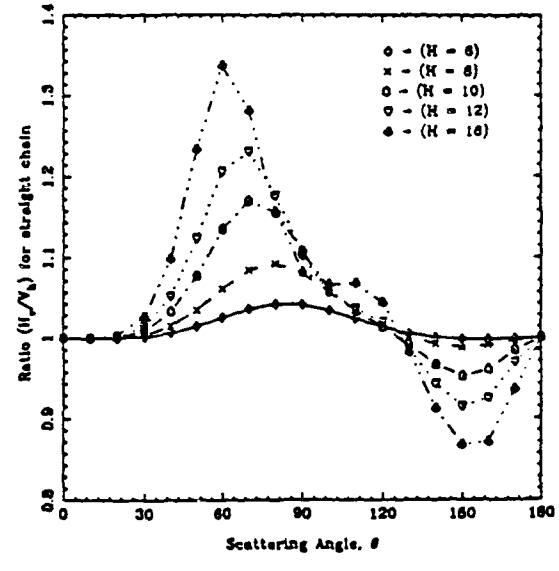

Figure 4. H_v to V_h ratio with respect to scattering angle for straight chain at different positions in the flame.

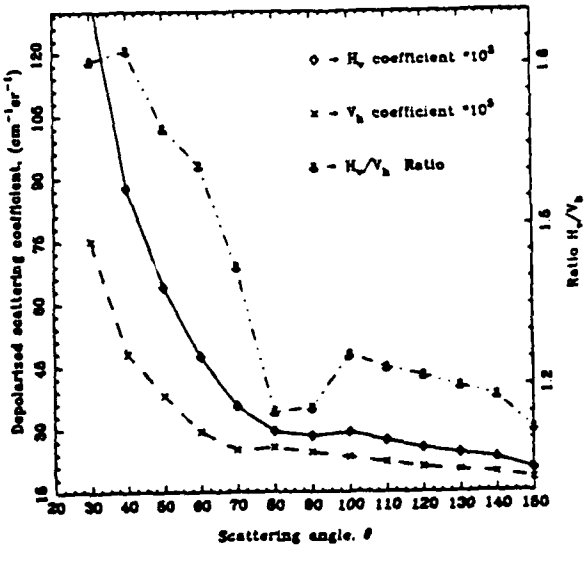

Figure 5. Depolarised scattering coefficients and their ratio versus scattering angle for polystyrene sphere 0.22 μm in diameter at 19.8% transmission.